ELECTRON-INDUCED ELECTRON SPECTROSCOPIC MEASUREMENTS ON A Sb (100) CRYSTAL SURFACE

A thesis presented for the degree of Doctor of Philosophy at the University of Keele

by

GHASSEM KAVEI, B. Sc., M. Phil.

Physics Department
Keele University
Staffordshire

February, 1981

The following has been redacted from this digital copy of the original thesis at the request of the awarding university:

Fig.1-3

Fig.1-4(a)

Fig.1-6

Fig.1.7

Fig.1-8

Fig.1-9

Fig.1-10

Fig.2-3

Fig.4-23

Appendix 4

عزیز آنالا را

قوچـــاق ایگیـدلـــر د وغـــان آنـــــالا را

جوانلاری گالخیب ایقا وطـــن سس‌لئین آنـــالا را

وطـــن یـــولونـــدا جـــوانلار ورن آنـــــالا را

جـــوانلار د اغنـــــد ان جـــان ورن آنـــالا را

To: Beloved mothers,

for conceiving a loyal, brave generation
whose young arose to defend our Country's freedom
whose young were dedicated to our fatherland
who died of broken hearts for her youth,
we give you our gratitude for love.

CONTENTS

CONTENTS continued

CONTENTS continued

Acknowledgement

I wish to acknowledge Professor W. Fuller for the use of the laboratory facilities.

Many thanks to Dr. E.B. Pattinson for constructive criticism during the study. Without his unrefusing and gracious help it would have been too difficult for me to continue the work, and impossible to finish, I owe him too much. His excellent supervision was appreciated.

The greatest debt of gratitude goes to my colleague Mr. R. Moran, who helped me in many ways to express my ideas in the thesis. His kindly comments suggestions and corrections of English will not be forgotten.

Also, I am grateful to my colleagues Mr. M. Davies, Mr. J. Minshull and Mrs. M. Fadavi for their help and cooperation throughout the research, and Mr. M. Daniels for his kind photographic work.

This work could not have been completed without the cooperation of many colleagues, in particular in departmental mechanical and electrical workshops, who helped me with open hearts. My thanks to all of them.

Finally, I am indebted to my nation for awarding me a grant for 1½ years through Ormia University. My ambition is to have committed obedience to my nation to repay my debt. My family for their continuous support should always be remembered.

Abstract

Observations and experimental techniques of Auger, characteristic energy loss, and secondary emission yield electron spectroscopy are reported. Data from the latter has been used in the observation and calculation of electronic surface resonances on a Sb (100) crystal.

Auger and energy loss electrons from the Sb (100) crystal were detected by means of an AES system operating in the derivative mode. The purpose of the Auger studies was largely limited to determining the surface atomic species, and hence as a monitor to assist in obtaining a clean surface characteristic of Sb for the other measurements.

Secondary electron emission yield spectroscopy was obtained consecutively with AES, simply by operating the external detection system in one of the two relevent modes available. The operating aim was to monitor the particular surface system and then to measure the secondary electron emission reflection coefficient of the surface as a function of energy in the low-energy region for a series of angles of incidence of the primary beam.

A method of determining the surface band structure of a crystal surface is presented. The method is based on the pioneering work of McRae and Caldwell (1978), who showed the existence of surfaces resonances in the elastic scattering of low-energy electrons at a crystal surface. That is, electrons incident on a crystal surface can be temporarily

trapped in surface states at energies above the vacuum level. The method consists of; observation of the narrow fluctuations of the elastic scattering intensity with respect to a variation of electron energy and incident direction. The fluctuations are superimposed on the SEE reflection coefficient and suitable manipulation of the data enables a measurement of the surface resonance band structure $E(k_{||})$ to be made, where E and $k_{||}$ respectively denote the electron energy and surface-parallel momentum for which resonances occur. Thus, the surface resonance band structure is measured by a net current reflection method, and has been interpreted by two dimensional nearly free electron scheme. Experimental and calculated surface resonance band structure for a Sb (100) surface are presented for E in the range 0-50 eV and $k_{||}$ running half way from $\bar{\Gamma}$ towards $\bar{H}$ in the surface Brillouin zone for Sb (100). There is reasonable agreement between experiment and theory, although the experimental data must be regarded at this stage as preliminary, since the data analysis system was not finalised or fully operational at the time of writing.

Chapter 1

Introduction

1-1 Surface Science

The importance of surface science arises from the fact that solids interact with their surrounding through their surfaces, the properties of which depend on specific atomic arrangements with specific electronic properties. Many important physical and chemical processes in solids such as catalysis, optical reflection, adhesion, corrosion, thermionic and photoelectric emission, depend critically on the nature and condition of the surface. The term surface is used here to denote the top atomic layer or the top layer along with a few atomic layers beneath. Scientific interest in surfaces also stems from the fact that quite often surfaces have properties with no counterpart in bulk solid state physics. With the development of new techniques for observing these surface properties, and of theoretical models that translate observations into quantitative measures of the condition of the outermost layers of a solid, the study of surfaces is rapidly becoming a quantitative science.

A complete description of a solid surface may be achieved if the following can be answered:

1. What atomic species are present on the surface?
2. How are they arranged?
3. How are their valence electrons distributed?
4. What describes their atomic motions?

These questions may be answered only by fitting

together the results of many experiments in a consistent fashion.

For the purpose of the present thesis, the subject of low energy electron spectroscopy includes those research techniques, which are concerned with the measurement and analysis of electron-induced electron spectra. The nature of the interaction of the electrons giving rise to these spectra varies quite considerably.

Several of these effects (e.g. the Auger process and the various characteristic energy losses) were under investigation for many years. Others have gained in interest or come to be investigated seriously for the first time only in recent years, for example automatically recorded yield spectra and the study of surface resonance band structure.

Recently, very rapid development and improvement of electrostatic spectrometers has made it possible to investigate electron spectra at low energies down to a few electron volts. There has been both an improvement in established methods, and the development of new methods of analysis for spectroscopic data.

The techniques for surface analysis which were employed in the present work are introduced together with a brief outline of the mechanism of the process. The spectrographic methods carried out include:

1. Auger electron spectroscopy (AES)
2. Characteristic electron energy loss (CEEL) spectroscopy
3. Secondary electron emission (SEE) yield spectroscopy.

The methods rely on the fact that when the surface of a solid is bombarded with charged particles of sufficient kinetic energy, several processes, resulting in electron emission by the solid, may occur. If the incident radiation is in the form of photons, the emitted electrons are termed photo-electrons. When electrons or other particles, e.g. positive ions, form the incident radiation, then the products are secondary electrons. When a beam of a primary electron strikes the surface of a solid, a certain fraction is elastically reflected, (elastically reflected primaries) and the remainder penetrates into the solid. The primaries that enter the solid will dissipate their energy by exciting lattice electrons into higher energy levels within the solid, or exciting plasmons in the valence electrons. The excited electrons may then move towards the surface and a certain fraction will escape from the solid as secondaries "true secondaries". It is also possible that the primaries which have lost part of their energy inside the solid, return to, and escape from the surface as a result of Rutherford scattering; such electrons are called "inelastically reflected primaries".

Thus, the need to monitor electron emission leads to a study of the secondary electron energy distribution, N(E), i.e. the number of electrons emitted with energy E recorded as a function of incident excitation energy E, (in the following text, N(E) is referred to as the ordinary mode). For the purpose of this research, high sensitivity is important, and often the differential mode, $\frac{dN(E)}{dE}$, is recorded as a function of incident excitation energy, since weak structure present on the N(E) spectrum is enhanced by differentiation. Typical

N(E) and $\frac{dN(E)}{dE}$ curves of the electrons emitted by Be upon bombardment by electrons with primary energy of E_p are shown in Fig. 1-1. In this figure the N(E) curves show three major features:

a) A sharp peak at the primary energy E_p termed the elastic peak. Close to this peak there are a few small maxima, the positions of which, relative to the elastic peak, are characteristic of the material and independent of the primary electron energy. These maxima evidently correspond to inelastically reflected primaries which have lost discrete amounts of energy before escaping from the surface, the so-called characteristic energy loss electron.

b) A relatively flat region, sometimes called the region of rediffused primary and back scattered electrons.

c) A broader peak at low energies ($<$ 50 eV) with a half width of $\sim$10 eV, the so-called true secondary region.

The region (b) contains inelastically scattered primary electrons and the more energetic of the secondary electrons. This is the region where most of the Auger peaks occur, Harris (1968). In the N(E) versus E plot, these peaks are often only just resolved. They are superimposed on a variable background where the total secondary current is much larger than the Auger current, and therefore, before any quantitative information can be gained the peaks need to be accentuated. This is usually accomplished by differentiating the energy distribution, so as to get the $\frac{dN(E)}{dE}$ curve shown in Fig. 1-1.

One of the main objectives of the present work was the use of SEE yield spectroscopy in an attempt to obtain the

Seoondary Electron Emission distribution curve

Fig.1-1

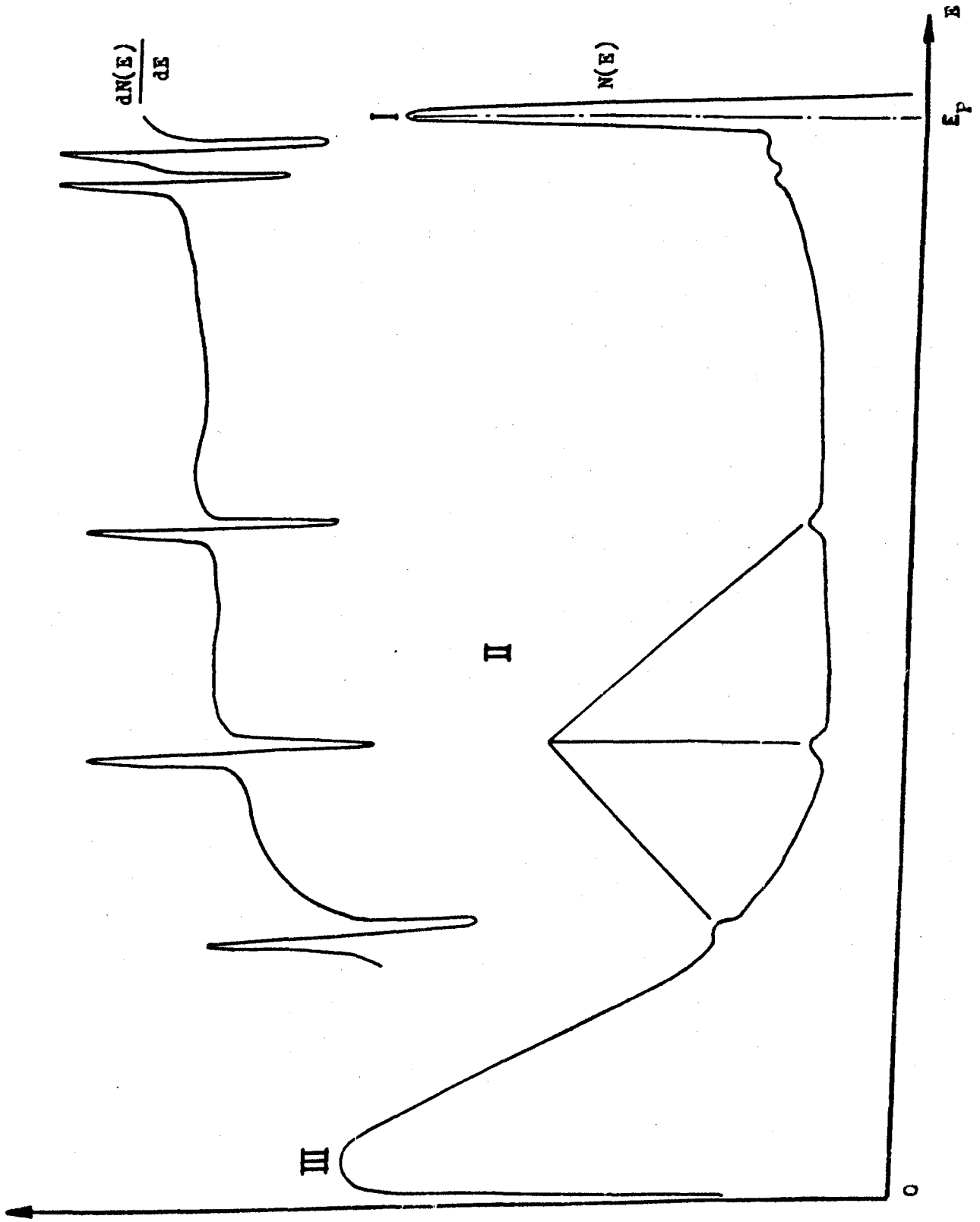

surface band structure of a clean Sb crystal (100) surface. To obtain accurate and acceptable data, obviously the degree of surface contamination had to be monitored, and therefore the techniques of AES and CEEL spectroscopy were also necessary.

In the following sections of this chapter, some of the relevent processes occuring on surfaces, and the techniques used in their investigation, are described and reviewed, including some recent work and developments. In Chapter 2, the theory of the processes is detailed; Chapter 3 is devoted to a description of the apparatus used and in Chapter 4, the results of the present studies are analysed and discussed.

1-2 Auger Electron Spectroscopy

1-2.1 Auger Effect

When a neutral atom is ionized in an inner shell W, the system may be considered as consisting of the ionized atom and the ejected electron at infinity. The ejected electron may be characterised by a positive energy E_W, and is measured with respect to the ground state energy of the neutral atom. A transition in the atom may occur in which the inner vacancy is filled by an electron from an outer shell X, with the excess energy appearing as radiation, i.e. "photo-emission" of frequency ν given by,

$$\hbar\nu = E_W - E_X$$

Alternatively, the excess energy may be passed on to yet another electron of the same atom belonging to a shell Y, which is subsequently ejected. If the ionized energy of this electron is E_Y, it will leave the atom with positive kinetic energy

E_A, given approximately by

$$E_A = E_W - E_X - E_Y$$

This latter process of radiationless reorganisation of an atom ionized in an inner shell is known as the Auger effect, and the electron ejected with energy E_A is known as the Auger electron.

The Auger effect therefore consists of three principal stages:

1. Initial production of the ionized atom.
2. Decay of this excited state by Auger emission.
3. Escape and collection of these Auger electrons.

The effect was discovered by Auger (1925), who first interpreted this transition, since he observed pairs of tracks in a cloud chamber containing inert gases ionized by an X-ray beam. The paired tracks have a common origin; one of the tracks is that of a photo electron ejected from an inner shell of the atom by the incident radiation; the second is that of an Auger electron, ejected during a radiationless reorganisation of the atom.

Auger transitions are usually designated according to the three levels participating in the process, denoted by the X-ray level notation , K - 1s; L_1 - 2s; $L_{2,3}$ - 2p; M - 3s; $M_{2,3}$ - 3p; $M_{4,5}$ - 3d , and so on. Also, V is used to represent the valence band electrons.

A schematic diagram of a general Auger transition is shown in Fig. 1-2a, (in the case given in Fig. 1-2, the final two hole state will be relaxed immediately by valence band

Fig. 1-2

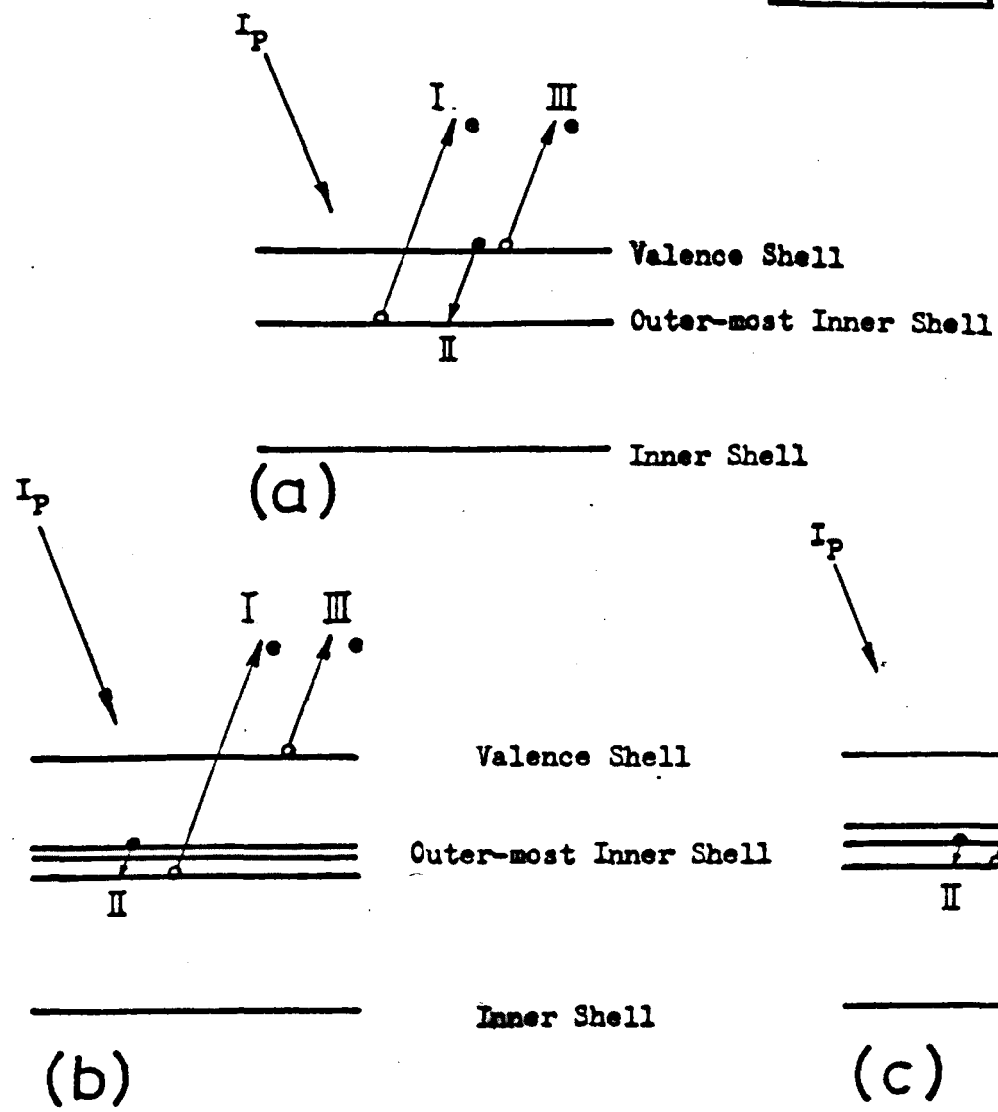

Schematic Representation for Processes that Form the Basis of:

a) Auger Transition.

b) Coster - Kronig Transition.

c) Super Coster - Kronig.

Open Circles Correspond to Ejected Electrons.

Solid Circles Correspond to Transfered Electrons.

I, II, III, are the Transition Sequences Shown on the Figures.

electrons). Thus, the Auger process consists of a higher level electron moving down into the core hole and giving its energy to a second outer lying electron which is then emitted.

As an indicator of the transition probability of a particular Auger transition, the free atom line-width proves valuable and is determined by the life time of the vacancies involved, i.e. by the transition rates. According to the uncertainty principle

$$\Gamma_A = \frac{\hbar}{\tau_A} = \Sigma\Gamma_{WXY}$$

where τ_A is the lifetime of the vacancy A, and Γ_A represents the total width corresponding to all Auger transitions resulting from this vacancy. Typically, τ_A is of the order of 10^{-15} seconds, so that $\Gamma_A \approx 0.5$ eV. For example, Γ_K for Mg is about 0.5 eV, while the L_2 and L_3 levels have a width of less than 0.05 eV, corresponding to the low transition probability for Auger transitions to these levels, Chattarji (1976).

For elements lying in certain defined Z-value regions of the Periodic Table, the Auger transitions described above can occur with an initial vacancy in the inner subshell; e.g. the M_3 subshell may become filled by an electron from an outer M_4 subshell, the energy difference freeing another electron from a shell lying beyond the M shell. This process is a particular type of Auger transition and was first described by Coster and Kronig (1935). Therefore, the Coster-Kronig transition is an Auger transition where the initial hole and one of the two initial electrons involved in the transition have the same principal quantum number. A schematic diagram of a typical Coster-Kronig transition is illustrated in Fig.1-2b.

McGuire (1972) observed another type of Auger transition, again in certain Z value regions of the Periodic Table, and termed the Super-Coster-Kronig transition. Both electrons involved in the transition have the same principal quantum number as the initially ejected electrons. A schematic diagram of this transition is shown in Fig. 1-2c, the Super-Coster-Kronig transition occuring when both of the participating electrons have the same quantum number as the initial hole. This transition is not possible for initial K and L shell holes but allowed for M shell holes, McGuire (1972a).

The hypothesis of Super-Coster-Kronig transitions predicts that there should be a large number of low energy secondary electrons. The consequent band width broadening due to Super-Coster-Kronig transitions is to some extent expected to mask the structures.

The weakness of certain specific Auger transitions as observed in the Auger investigation is attributed to large Coster-Kronig transition probabilities. From this, one would expect very strong spectral electron lines lying at low energies.

1-2.2 Three Important Aspects of AES

1) The intensity of the Auger transition.

The intensity of a transition is tentatively equal to:

rate of production of the particular core hole involved x

$$x \quad \frac{\delta(\text{Auger line})}{\delta(\text{total})} \qquad \text{Singh (1976)}$$

where δ(Auger line) is the specific Auger transition probability, and δ(total) is the total Auger transition

probability, for Auger processes involving that core level.

The observed intensity will depend on:

a) primary energy; the strength of an observed Auger peak depends on the primary electron energy, E_p, due to the ionization cross-section being energy dependent, Neave et al. (1972).

b) Coster-Kronig and Super-Coster-Kronig transitions effect, see previous section.

c) back scattering, (see Section 1-3) effect; Gallon (1972), Neave et al. (1972), and Meyer and Vrakking (1975) have studied the role played by back scattered electrons in the production of Auger peaks. They concluded that a sizable fraction of the Auger electrons usually observed came, not from ionization created by the primary beam of impact electrons, but from back scattered electrons. Neave et al. also pointed out the particular importance that back scattered electrons play in the production of Auger electrons as a function of glancing incidence of the initial beam.

d) Staib (1972) has compared relative intensities of KLL Auger lines of O, Al, and Si and the LMM lines from potassium under the controlled conditions of looking at only the top layers of a cleaved mica sample where the positions of the different atoms are known from crystallography. Results are compared with the semi-empirical formula of Drawin (1961).

e) As pointed out by Coglan and Clausing (1971), the Auger line intensity is not calculable because the line intensities will be influenced by many unknown factors, see Section 1-2.4. However, a line intensity estimate can be obtained from the "normalised multiplicity", based on a summation of the number of electrons present in the particular transition subshells.

The principal error is then due to the assumption that all transitions are equally probable, see Section 4-1.

2) Electron beam characteristics; incident electron beams used in AES may have energies up to 3 kV, a beam current of 10 to 50 μA, and a spot size of ~1 mm. Such a beam represents a considerable energy input (~15 watts/cm^2), on the surface under investigation. Such a load can introduce electron beam induced anomalies because it will cause local heating of the target if it is a poor thermal conductor. Consequently, induced effects such as dissociation of compound surfaces, surface diffusion within the region of bombardment, and electron induced desorption and adsorption can occur. In some circumstances, to reduce the surface load, low currents and a diffused beam may be used, but this gives a low resolution spectrum. Numerous investigations of these effects have been reported; typical of which are Musket and Ferrante (1970) and Florio and Robertson (1969).

3) Inter-atomic Auger or "cross" transitions: such transitions can occur when two atoms are in close proximity or chemical combination with one another. A hole created in a core level of one atom is relaxed by an Auger transition in which the electrons from the neighbouring atoms participate by a tunnelling mechanism. This was originally proposed for an effect observed in X-ray emission spectra where Gallon and Matthew (1970) interpreted them as inter-atomic Auger transitions. Further useful information has been obtained by Medvedev and Smereka, (1975), Citrin (1975) and Kobayashi et al. (1979).

1-2.3 Sources of Auger Electrons

As has been stated, an Auger electron may be emitted as a result of the filling of an ionized internal atomic shell. There are a number of possible ways of forming the initial vacancy, each with its own particular advantages and disadvantages with respect to the investigation of the resulting Auger spectra. The main ones may be enumerated as follows:

1 - Electron bombardment.

2 - Bombardment by photons.

3 - Ion bombardment.

4 - Internal conversion in a radioactive element.

Investigations can also be carried out using other particles as an excitation source e.g. protons (Musket and Bauer (1972)).

The present interest lies in surface excitation by electron bombardment, this being the easiest and least expensive method for exciting Auger electrons. Atomic ionization using an electron beam has a greater cross-section than for a photon beam, often exceeding 10^{-19} cm^2, Wright (1972), and is reasonably independent of primary energy over a wide range from three to six times the binding energy of the initial core hole. Moreover, an electron beam is readily electrostatically focussed, and positioned, by simple deflection plates at various points on the sample. An appraisal of AES (e.g. X-ray and electron induced Auger electrons) has been carried out by Alford et al. (1979).

The impinging electron will most probably lose only a part of its energy in the ionization of a bound atomic electron, may ionise further atoms and then subsequently be

emitted, thus the electron spectrum will then be in effect a continuum upon which the specific Auger spectra are superimposed. Since the incident beam can cause multiple atomic ionization, or excitation, the resulting complete Auger spectrum will be due to the superimposition of Auger electrons originating from atoms in a variety of atomic excitation and ionization states. The resultant complexity of the Auger spectrum may well hinder its subsequent analysis.

Photon beam (X-ray) induced ionization also has some disadvantages, for example, long scanning time, and low ionization cross-section. However, one important advantage of photon beam excitation is that the strong rediffused primary electron (continuum) background is absent. An article describing a photon impact system has been published by Fraser et al. (1973).

Discussion and experimental technique of the other two methods of the excitation i.e. ion bombardment and internal conversion can be found in [Haas et al. (1974), Prospst and Luscher (1963)], and Dionisio and Viev (1975) respectively.

1-2.4 AES and its Application to Surface Science

The earlier sections provide a background in explanation of the Auger process. The basis so far has been predominantly for single or free atoms. It happens, however, that the Auger effect is far from being a phenomenon of interest only to the atomic scientist. The main use of Auger spectra is as a tool in the investigation of solid surfaces, and was first suggested by Lander (1953). The necessity of preparing solid surfaces of known chemical purity in materials science and industry

cannot be overemphasized. Obviously, this requires sensitive techniques for the detection of impurities.

The importance of AES stems from the fact that atoms present on a surface can be identified, and hence the surface can be characterised for other measurements. The technique is convenient for the investigation of extremely thin layers on the surface of a sample, the sensitivity can be as good as 1/100 of a monolayer.

As mentioned previously, Auger electrons emitted by a material under electron bombardment may be detected as small peaks in the secondary-electron distribution, (see Fig. 1-1). The excitance of such peaks indicate the presence of the elements associated with the observed peak energies. The energy distribution curve in the normal mode is not generally too informative, because Auger peaks on the curve are very small and are superimposed on a relatively large background. For this reason, the earliest attempts to use Auger electron spectroscopy were not too successful.

AES of atoms involves three stages (see Page 6) and in the solid these stages are influenced by the solid-state environment of the atom in question. The resulting Auger peaks contain information about this environment as well as the atom itself. The physical situation is, of course, more complicated than in free atoms, having a seriously adverse effect on simple detection methods employed to analyse data.

The choice of an analyser to be used in Auger studies with low energy electron diffraction (LEED) was dictated by

the needs for simplicity and high transmission and the limitations placed by the desire for surface cleanliness. Thus, a retarding grid device was chosen. The energy resolution of such a device is usually from 3% to almost 0.3%, Huchital and Rigden (1972). One of the biggest handicaps of taking data by the retarding grid method is that the signal is received in the integral mode. Even modulation of the signal or differentiation does not aid analysis of the lower-energy lines. The secondary spectrum even in a homogeneous solid contains, in addition to specific Auger peaks, plasma loss peaks associated with both the elastic peak and the more pronounced Auger peaks. Since an Auger electron may excite a plasmon before being emitted, it may also contain other Auger satellites for example those due to double ionization. Furthermore, there may be ionized loss peaks due to an incident electron losing an amount of energy slightly greater than the binding energy of the electrons. Interband transitions may also occur, and additional information for loss phenomena will be given in Section 1-3. However, because of the above complications, and many other known (see Section 1-2.2) and unknown factors, much of the theoretical formulation of the Auger effect is still empirical.

1-2.5 History

The first use of AES as a method of surface chemical analysis was made by Lander (1953), who studied various surfaces with low-energy electrons (500-1000 eV) and measured the resultant Auger electrons that were emitted, using a 90° spherical electrostatic analyser. His work was followed, to a certain extent, by Harrower (1956), who tried to use the "energy loss peaks" due to primary electrons that have lost

discrete amounts of energy to the electron gas through plasma excitations, to supplement the characteristic X-ray tables at low energies. Recent interest, however, was engendered by Thorp and Scheibner (1967), and Weber and Peria (1967), who coupled Auger spectra measurements to a conventional LEED system.

Since the use of Auger spectroscopy for studying surfaces has come primarily from the work of surface scientists, much attention has been paid to optimising the sensitivity of the technique. Differentiation was employed to separate the Auger peaks from the background, and a major contribution in this direction was made by Harris (1968, 1968a). It should be noted, however, that the idea of electrical differentiation of the retarding field plot has been suggested earlier by Leder and Simpson (1958). Harris first achieved enhancement in the detectability of the Auger peak through electronic differentiation of the measured energy distribution function, and demonstrated the application of this technique in a large number of cases, using a cylindrical electrostatic sector analyser.

Palmberg et al. (1969), have shown that the cylindrical mirror analyser can be used to measure Auger spectra so as to increase the sensitivity by one or two orders of magnitude relative to other analysers previously used. To achieve higher sensitivity, Palmberg (1975) in his ESCA and AES combined system, used a double pass cylindrical mirror analyser. This type of analyser was also used by Singh (1976). This increased sensitivity can be traded, if desired, for much greater scan speeds.

Grant et al. (1973, 1974) have suggested processing the data electronically by first differentiating and then integrating back the spectrum. The background, which can usually be represented by a polynomial, is removed by such a procedure, while the signal is restored to its original form.

Comprehensive tables based on atomic binding energies have been prepared by Coghlan and Clausing (1971) for all Auger transitions for energies between 10 and 3000 eV for elements up to Z = 103. Also, experimental data for most of the elements has been published by Palmberg et al. (1972).

Payling et al. (1979) detected Auger electrons using the integral rather than derivative mode, in conjunction with dynamic background subtraction. Advanced techniques in surface characterisation using combined LEED and AES have been used by Tracy and Burkstrand (1974), and with high performance by Namba et al. (1979). Also studies of material surfaces by means of a combined AES, ESCA, and SIMS systems were carried out by Marcus (1977). Michel et al. (1980) developed AES in conjunction with LEED and work function (Kelvin probe) measurements. They studied the initial interaction of clean Al (111), (100) and (110) surfaces with oxygen at room temperature. The oxidation process was found to be surface orientation dependent.

The quantitative aspects of Auger spectroscopy have been discussed by Seah (1979) and Oda and Rhead (1980). Meyer and Varkking (1972) have studied C, N, O, P, S and Cl for quantitative analysis, combining AES with ellipsometry.

In conclusion, it may be said that AES is now a routine part of most surface investigations and a vast amount of published material exists (too numerous to give here) which details its use in a wide variety of circumstances and studies. Two recent reviews of Auger related publications are given by Chang (1974), who gives a comprehensive bibliography of material published up to 1972, and Alford et al. (1979) who reviewed and made comparisons with other methods of Auger spectroscopy.

1-2.6 Recent AES on Antimony

There has been considerable interest and activity in the AES of Sb, because of its interesting physical properties. Coghlan and Clausing (1971) calculated the energy of Auger transitions by means of empirical expressions, see Section 2-2, for the energy of an Auger transition. Harris (1972) produced the AES of Sb in the 300-500 eV energy range and the result was compared with those of Strausser and Uebbing (1970), Aksela (1971). Later, Wright (1974) extended Harris's work on antimony, and improved results were achieved. Palmberg (1972) obtained Auger electron spectra for most of the elements including Sb, and these are often used as initial reference spectra.

With the improvement of experimental apparatus and techniques, research by AES on antimony was extended to increasingly detailed investigations and Singh (1976) has produced some significant results from antimony and its components.

1-3 Characteristic Electron Energy Loss

Characteristic electron energy losses are experienced by incident electrons when they impinge on an atom and interact with it. Measurement of the various losses (ΔE) of the incident beam reveals atomic and other characteristics. CEEL spectroscopy gives an important insight into the variety of excitations of a solid being closely dependent on both the individual atomic nature of the sample and the electron band structure of the material. The information is obtained by measuring the energy losses which the electrons suffer after reflection or transmission. Incoming electrons impinging on the solid interact with the free and bound electrons of the solid, and this 'electronic' excitation covers the energy range of 0 to several 100 eV. Energy losses are also produced by coupling of the incident electron with the electromagnetic field so that photons are created.

Consideration is now given briefly to describing electronic excitations (where the energy (ΔE) and momentum q, is transferred to the electrons of the solid). The process can be approximately described as follows:-

1. In the case of a metal, the beam can interact collectively with the essentially free valence electrons which have a density amounting to 10^{22} - 10^{23} cm^{-3}, Kittel (1976) (plasmons).
   a) For low values of q momentum transfer, q_c (cut off vector: when the electron loss intensity drops quickly to zero with angle, Watanabe (1956)), or low values of scattering angle $\theta < \theta_c$ $\theta_c = q_c/k_{el}$ (k_{el} is the wave vector of the incident electron)collective oscillations of the electrons (plasmons) can be excited.

These oscillations run as longitudinal charge density fluctuations through the volume of the crystal (volume plasmons) and along its surface (surface plasmons). The energy is $\hbar\omega_p$ (ω_p is frequency of oscillation), and is of the order of 15 eV and depends on the density of the valence or loosely bound electrons. The loosely bound electrons are those for which $\hbar\omega_p$ is larger than their binding energy, e.g. in metals, the electrons in the conduction band; in semiconductors the electrons in the valence band, the frequency in the volume wave is higher than that of the surface wave.

b) If the momentum transfer $q < q_c$; the incoming electrons collide with a nearly unscreened plasma electron which can result in a single electron excitation. The transferred energy values vary from zero to high energies.

2. In large band gap (insulators) the conditions are not favourable for the excitation of plasmons. Here inter band transitions are observed in the energy region of the valence band 10 eV, and excitations are detectable for the deeper levels, e.g. for L and K edges, at some 10^2 eV. The deeper the shells, the more the excitation can be regarded as that of a single particle; in general the probability of excitation can therefore be calculated assuming an interaction of the incoming electrons with isolated atoms or ions.

The characteristic losses can be used to identify the chemical nature of the irradiated atom of the solid. In the region of low-energy losses of about 10 eV (plasmon and inter

band transitions) the results of the experiments are described by the dielectric theory,(Kittel (1976)). It should be noted that real plasmons move in a periodic potential and not in a free electron gas, as do ideal plasmcns, so that the dielectric function is used for the calculation of energy. CEEL spectroscopy with fast electrons has given detailed information of the properties of the real plasmons, and contributed considerably to the development of the physics of plasmons.

In the following text a more exhaustive survey of the dielectric function, plasmons and inter band transitions is given. A short history of experimental and theoretical methods in general, and more specifically to Sb, is also presented.

1-3.1 Plasmons Peaks

These peaks are due to primary electrons that have lost discrete amounts of energy by exciting collective density fluctuations in the valence electrons of solid metals (the plasmons). A physical picture of these excitations was given by Pines and Bohm (1952, 1953), who developed the theory using a many body approach, where the electron gas displays both collective and particle aspects. In a collective oscillation, the system oscillates as a whole, as a consequence of each individual electron suffering a small periodic perturbation of its velocity and position due to the combined Coulomb interaction of all the other particles. Because of the long range of this interaction, a very large number of electrons contribute to the potential at a given point. The energy of the plasmons can be calculated using a simple classical picture which gives the same result as the sophisticated many body theory of Pines and Bohm, by considering the motion of

a homogeneous mixture of electrons and positive cores, as in the Sommerfield model of a metal. Classically, this is carried out as follows; Raether (1965), taking into account the Coulomb interaction between the electrons, (Raimes (1961)), shows that a plasmon oscillation of the electron density can take place. Let the electron gas momentarily expand radially outward from some origin, $\delta(r)$ being the radial displacement at r. the number of electrons leaving a sphere of radius r is $4\pi\, nr^2\delta\,(r)$, where n is the electron density. This gives rise to a radial electric field

$$E(r) \quad = \quad \frac{4\pi ner^2\ \delta(r)}{r^2} \quad = 4\pi ne\ \delta(r)$$

and a force on the other electrons, $F = -4\pi ne^2\delta\ (r)$, where e is the electric charge. Equating this to the force of restoration $m\ \delta(r)$,

$$\frac{d^2\,\delta(r)}{dr^2} \quad + \quad \frac{4\pi ne^2}{m} \quad \delta(r) \quad = \quad 0$$

This gives a simple harmonic motion with oscillation frequency

$$\omega_p \quad = \quad \left(\frac{4\pi ne^2}{m}\right)^{\frac{1}{2}}$$

and energy

$$E \quad = \quad \hbar\omega_p$$

In metals $\hbar\omega_p$ is about 15 eV, and therefore ω_p is of the order of 10^{16} radians/second. In a crystal, m may be replaced by the effective mass m*, Kittel (1976).

As noted, $\delta(r)$ being the radial displacement also represents harmonic density fluctuations; they osicllate with a frequency which is the dispersion relation of the plasma oscillation based on the free electron theory of Bohm and Pines (1953), and given by:

$$\omega_p^2 \quad = \quad \omega_{p,o}^2 \quad + \quad K^2\ \bar{v}^2$$

where $\omega_{p,o}$ is the Longmuir frequency, $K = \frac{2\pi}{\lambda}$ is the wave vector of the oscillations and $\bar{\nu}^2$ is the mean square of the velocity of the plasma electrons. When $\bar{\nu}^2$ becomes zero, ω_p reduced to $\omega_{p,o}$. In the case of the Fermi gas velocity

$$\bar{\nu}^2 = {}^3/_5\, \nu_F^2$$

The wave length of the oscillations λ has a lower limit (the value of K an upper one $= K_c$, K_c is the so-called cut-off wave vector), since the concept of organised oscillations of electrons becomes meaningless if the wave length of these oscillations decreases and becomes comparable with the mean distance of electrons $\lambda_{min} \approx \left(\sqrt[3]{n}\right)^{-1}$. A more exact definition is given by Raether (1965).

Other useful properties of plasma losses, such as angular dependence of the intensity, cut-off scattering angle, dispersion relation (i.e. the dependence of energy loss value on the scattering angle), angular dependence of the half breadth, the total cross-section of excitation of plasmon were described by Sueoka (1969) for the elements Be, Mg, Al, Si, Ge, Sn, Sb and Bi.

The plasmon as discussed above is the volume plasmon, or three dimensional fluctuation in the bulk of the crystal. At the surface of a solid the electric field is weaker, because of charge density oscillations, and the ideal surface plasmon or two dimensional fluctuation has a smaller energy, Pines (1964).

$$\hbar\omega_s = \frac{1}{\sqrt{2}}\, \hbar\omega_p \quad \text{or} \quad \omega_s = \frac{1}{\sqrt{2}}\, \omega_p$$

In the bulk of a solid, the real part of the dielectric

constant has a value of ϵ_1, (see page 24). At the solid surface this quantity changes to that of the adjoining medium ϵ_1'. Assuming that there is a plasma oscillation in the first medium, the necessary continuity of the normal component of the electric displacement requires that for a charge oscillation at the surface, Stern and Ferrell (1960)),

$$\epsilon_1 = -\epsilon_1'$$

Then for a free electron gas with surface plasmon frequency ω_s,

$$1 - \frac{\omega_p^2}{\omega_s^2} = \epsilon_1$$

or

$$\omega_s = \frac{1}{\sqrt{1 + \epsilon_1'}} \omega_p$$

Hence, if the surface is covered by a dielectric constant ϵ the surface plasmon energy becomes,

$$\omega_s = \frac{1}{\sqrt{1 + \epsilon}} \omega_p$$

The energy of plasmons in general are quantised in the range 10 – 15 eV, the energy depending upon the density of the electron gas and whether or not they are bulk or surface plasmons.

The exciting particle may generate more than one plasmon as it passes through the solid and so suffer multiple plasmon losses. Al or Mg are perhaps the best known examples exhibiting multiple plasmon losses where, for Al up to twelve loss peaks may be seen which are made up of the combination of surface plasmon (10.3 eV) and the volume plasmon (15.3 eV) losses, Powell and Swan (1959).

1-3.2 Inter/Intra-Band Transitions and Ionization Losses

In addition to plasmon excitation, various single- and double-particle excitations can occur. Thus an electron may lose energy by raising a second electron from its ground

state to an empty state in the solid (e.g. inter-band transition or a transition from a core level to an impurity state). Inter-band transitions are a single particle excitation, in contrast to the excitations of collective density fluctuations in the electron gas in a solid which are known as plasmon transitions, which have just been discussed. In inter-band transitions, electrons from lower bands are excited to some higher partially filled band. Intra-band transitions have much lower energies and involve the excitation of electrons from the lower regions of a band to upper regions of the same band. Pines (1964) has pointed out that the probability of a fast moving charge losing energy whilst moving through and electron gas is proportional to $-I_m\left(\frac{1}{\epsilon}\right)$, where $-I_m\left(\frac{1}{\epsilon}\right) = \frac{\epsilon_2}{\epsilon_1^2 + \epsilon_2^2}$ and ϵ_1, ϵ_2 are the real and imaginary parts of the complex dialectric constant ϵ, defined as

$$\varepsilon = (n + jk)^2$$
$$= \varepsilon_1 + j\varepsilon_2$$

Inter-band transitions contribute to the make up of ϵ_1 and ϵ_2 components, and can strongly influence the energy at which the plasmon oscillation of the valence electron is observed. Raether (1965) has shown that the presence of a strong inter-band transition, whose energy is less than the calculated free electron like plasmon energy, shifts the observed value of plasmon to higher energies, whereas a strong interband transition of energy greater than the calculated plasmon energy has the opposite effect. This is a simplified picture, as normally several interband transitions can be excited in a solid and the situation is particularly confusing for the noble elements in which strong interband transitions are excited with energies close to the plasmon energy.

An ionization loss peak arises when the primary electron causes ionization of a core level (as might precede an Auger de-excitation). The energy distributions appear at $E = E_p - E_b$ where E_b is the binding energy of the level which has been ionized.

1-3.4 History

The phenomenon of energy loss has received considerable attention in the past 50 years, because of its analytical applications. In 1924, Langmuir demonstrated that in an electric discharge in a gas vapour the primary electrons suffer scattering resulting in a redistribution of energies considerably in excess of the original value. Energy loss interaction of electrons with matter were first investigated by Rudberg (1930), who analysed the energy distributions of 50-400 eV electrons. The energy spectra, after reflection from the surface of a material were observed, and he concluded that the primary electron beam had been degraded in multiples or combinations of certain discrete amounts of energy loss. The distribution peaks occured at fixed energy displacements from the elastically scattered electron peaks, irrespective of the primary bombarding energy or scattering angle, and Rudberg and Slater (1936) proposed that the energy losses were due to excitation of conduction electrons to higher allowed energy levels. These authors also reported the origin of some losses line in Al which may be due to inter-band transitions.

Pines and co-workers (1952, 1956) and Noziéres and Pines (1958, 1966) have shown theoretically that the prominent energy loss in metals is due to the collective excitation of

the conduction electrons, (in a conduction electron-ion core plasma). The fundamental bulk energy loss is given by $\hbar\omega_p$, where ω_p, the free electron plasma frequency, is equal to $\left(\frac{4\pi ne^2}{m} \right)^{\frac{1}{2}}$, and n is the free electron density.

Besides the volume plasma oscillations, surface plasmons have been found which occur in the boundary of the crystal. The lowered plasma loss has been proposed by Ritchie (1957). The measurements, made with very thin evaporated targets, show that low lying losses changed considerably in position, as well as in intensity relative to the volume plasmon. These changes, which were interpreted in terms of Ritchie's theory, definitely indicate that the low-lying loss is influenced by the surface layers of the specimen. Since that time, many papers have appeared using CEEL spectroscopy as a tool for surface analysis of different materials: Powell (1960), Suleman and Pattinson (1971), Singh (1976). Wright (1974) has presented a comprehensive review of CEEL publications.

Since the use of CEEL spectroscopy for studying surfaces has come primarily from the work of surface physicists, more theoretical work has been undertaken. Chung and Everhart (1977), investigated the role of plasmon decay in secondary electron emission in the nearly-free-electron model applicable to Al and comparison with experimental work shows good agreement. Pellerin and Le Gressus (1979) measured the characteristic energy loss, and secondary electron emission ($0 < E < 50$), of a clean Al surface after carbon contamination, and a rapid decrease of surface and bulk plasmon losses were observed, whereas a main characteristic energy loss peak and a secondary electron peak at 20 eV appeared.

Advances in the field, both experimental and theoretical, together with electron spectroscopy improvements are described by Thomas and Weinberg (1979). Their spectrometer was designed to measure a variety of electron spectra of solid surfaces in ultra high vacuum, and was capable of high-energy resolution (10 -15 meV). It was also capable of angle resolved photo-emission measurements, AES and CEEL measurements of electronic excitation.

Raether (1965, 1980) and Daniels et al. (1970), have presented a theoretical analysis of CEEL spectroscopy, augmented by comparison with the experimental results of numerous authors. Consideration of their studies proves useful for any investigation in the field of CEEL spectroscopy.

1-3.5 Recent Work on Antimony in this Field

Although Auger spectroscopy on antimony is quite recent, the original characteristic energy losses have been investigated since 1949, Soezima (1949). Leder and Martin (1954) measured the characteristic energy loss of 30 keV incident electrons impinged onto a Sb surface. A thin film (50 to 100 Å thick) of Sb was deposited onto a salt crystal surface, floated off in water, and mounted on a 200-mesh screen. Leder (1956) obtained an improved result over that of the previous work, and described different ways of preparing the thin foil sample. In Leder's study, a similarity was found between the electron energy loss spectra in some metals and their oxides or sulphides. He concluded that a slightly higher energy loss value occured in inter-metallic compounds as compared to that in the less electro-negative (i.e. more metallic) compound. Watanabe (1954), by using a transmission

technique, observed three energy loss peaks at 6.3, 13 and 19.5 eV when an antimony foil was bombarded with 22 keV electrons. Energy losses at 15 and 29.8 eV were also identified by Gauthé (1959). Powell (1960) in his study of various pure metals (Be, Sb, Bi, Ge, Sn, Cd, Cu, Pt, Pb, Ca and Li) revealed some new characteristic losses. Geiger (1962) measured and calculated the volume plasmon loss and dispersion coefficient ($\alpha = {}^{3}/_{5} \frac{E_f}{\hbar\omega_p}$). The dispersion coeffiecient was corrected for the so-called exchange correction proposed by Bohm and Pines (1953) and Pines (1960). Sueoka (1965), in his transmission method of CEEL analysis, studied the plasma oscillation of electrons in several metals (Be, Mg, Al, Si, Ge, Sn, Bi and Sb). He also introduced other effects that can influence CEEL, e.g. dispersion relation, half breadth. Bartning (1972) measured the volume loss, and its band width, with fast electrons on a thin film of Sb by the transmission method and comparison was made with the reflection method. Measurement of the dispersion coefficient on poly-crystalline and crystalline Sb was also reported.

In our laboratory, considerable work has been carried out to investigate CEEL on Sb by Harris (1971), Wright (1974) and Singh (1976). Singh's work improving upon that of Wright and Harris.

1-4 Secondary Electron Emission Yield Spectroscopy

The SEE yield δ is the number of secondary electrons i_s per incident primary electron, thus if i_p is the number of primary electrons, $\delta = i_s/i_p$. According to this definition the yield includes all three catagories of emitted electrons

discussed in Section 1-1. The plot of δ against E_p, known as the "yield curve", has in general the same shape for all materials. A typical yield curve for Ge is illustrated in Fig. 1-3; δ increases with primary energy up to a maximum, (δ_{max}). As the primary energy is raised beyond the maximum, electrons are excited increasingly deeper within the material, so that many of them are unable to diffuse to the surface and surmount the potential barrier to escape.

The two primary electron energies at which the yield is unity are denoted the first and second cross overs (E_I and E_{II} in Fig. 1-3). Indeed, there are a few materials for which the secondary emission ratio is less than unity for all primary energies. The SEE ratio depends also on various other factors, which will be discussed later.

It is useful sometimes to distinguish between low-energy secondary electrons that are produced inside the material and have undergone a diffusion process to the surface, and those higher energy electrons which have suffered only a few collisions in being scattered back from the target. Such a distinction is often necessary when making comparisons of experimental data with theory. The high-energy electrons are denoted backscattered electrons. The energy that is generally taken as the dividing line between the low-energy secondary electrons and the backscattered electrons is 50 eV. This energy is quite arbitrary, but most of the electrons usually have either much lower energy (true secondaries), or much greater energies, (see Fig. 1-1). The division is mostly not very sensitive to the exact position of the dividing line.

According to the above definition, the total yield,

Fig. 1-3

δ_{tot} is equal to

$\delta_{tot} = \delta_{true\ secondaries} + \delta_{elas.} + \delta_{inelas.}$ where $\delta_{true\ sec.} = \delta_s$

$= \delta_s + \eta$

where η (backscattered fraction) is the ratio of the number of secondary electrons having energy in excess of 50 eV (including elastic electrons) to the number of incident primaries. The backscattered fraction generally increases with the atomic number, being nearly constant with energy for low-atomic number materials, and increasing with primary energy for high atomic number elements.

Kanter (1961a) considered the true secondary electrons, and concluded that backscattered electrons can contribute considerably to secondary formation. Thus, it is convenient to consider δ_s to be composed of two parts, those directly produced by the incoming primaries, δ_o, and those produced by the backscattered electrons δ_1, so that

$$\delta_s = \delta_o + \delta_1$$

Dobretsov and Matskevich (1957) derived a relationship for δ_o in terms of δ_{tot} and η as:

$$\delta_o = \frac{\delta_{tot} + \eta}{(1 + \beta\eta)}$$

where β denoted the increased efficiency (on the average) in secondary production of the backscattered electrons over the primaries. They suggested that the extreme values of β under normal incidence of primaries were 1 and π. The above calculation was made for a two dimensional model. An analogous calculation for the three dimensional model leads to a value for β of 4. The experimental value of β for different materials ranged between 3 and 8, Bronshtein and Dolinin (1968). Thomas and Pattinson (1970) found β for Al to be dependent on the primary energy and substrate and varies from 6.8 at 800 eV

to 3.8 at 2 keV for Al film on the gold, and 5.8 at 1 keV to 3.2 at 2 keV on the silver.

1-4.1 Measurements of Secondary Electron Emission Yield

A number of methods have been used to determine δ, Bruining (1954), and [Goto and Ishikowa (1972), Henrich (1973), and Suleman and Pattinson (1980)]. These latter authors used a progressively more sophisticated electronic circuit to measure δ. Two direct conventional methods are described here:

Method I. In this method, the primary and secondary electron currents are both measured directly. The circuit and more details are given in Section 3-2.11a.

Method II. A second method for measuring secondary emission yield involves making all of the current measurements in the target circuit. This may be a considerable advantage, particularly when using pulse measurement technique, [see Section 3-2.11 and Henrich (1973), and Suleman and Pattinson (1980)].

1-4.2 Secondary Electron Emission Yield Dependence

The SEE yield of a solid is influenced by many known and unknown factors, and some of the former may be classified as follows:

1) Correlation of δ_{max} and work function: The dependence of δ on the work function as treated in Baroody (1950) where the relation between work function and maximum yield is reported as $\delta_{max} = (0.35\phi)^{\frac{1}{2}}$, where ϕ is the work function. From this it appears probable that materials with a high work function will have a high yield. A number of authors [Thomas and Pattinson (1970), Suleman and

Pattinson (1980)], have shown the effect of work function on the yield without varying any other parameters, which might effect yield. As a consequence of deposition and surface oxidisation respectively, these authors obtained different work functions, although it was not their intention to investigate the relationship between δ_{max} and ϕ. Suleman and Pattinsons' result indicates that as oxide coverage thickness increases, the maximum yield and primary energy maximum increases and the first cross over decreases. The authors pointed out that at an oxygen coverage corresponding to an Auger peak-to-peak height of 30 cm the maximum yield subsequently increases very rapidly. This may be because the oxide layer has reached a thickness sufficient to cause band bending as suggested initially by Simon and Willimas (1968) and Kortov and Slesarev (1975). Further confirmation is indicated in a different study carried out by Dionne (1975).

2) The effect of temperature on yield: Dekker (1958) introduced a theory to explain the variation in yield as a function of temperature. He showed that while the production of secondaries in a metal is well understood, the escape problem for metals is rather complicated, because of the interaction of secondaries with conduction electrons. However, when the temperature is raised the average energy loss suffered by the secondaries per collision decreases [e.g. for $M_g o$ $\alpha(298\ ^{\circ}K) = 0.108$ eV and $\alpha(1013\ ^{\circ}K) = 0.063$ eV].

The decrease of the yield with increasing temperature is thus a consequence of the reduction in the mean free path and indeed the path of secondaries is curled up. For low primary energies, corresponding to the rising part

of the yield curve, the influence of temperature on the yield is very slight, because most secondaries are then produced close to the surface and the energy losses resulting from scattering become less important.

3) Angular dependence of the yield: The SEE ratio depends also on the angle of incidence of the primary electron beam with respect to the surface. This is illustrated in Fig. 1-4a. According to this figure, the variation in angle for the illustrated metal gives a yield that is almost exactly constant up to $\pm 15^{\circ}$. When the beam impinges on the surface at less than normal incidence, the path of the beam inside the solid lies closer to the surface, (see Fig. 1-4b). More electrons excited by the primary beam are thus able to reach the surface and escape. The dependence of yield on the incident beam angle was measured for several metals by Thomas and Pattinson (1969).

4) Surface effect: The most important surface properties which effect the escape of internal secondary electrons, in addition to those mentioned above, are the surface roughness, and crystal surface structure.

a) Surface roughness: Experimental evidence shows that a rough or porous surface has a lower secondary emission yield than a smooth one. This is qualitatively explained by Bruining (1954) by postulating that a rough surface can be thought of as consisting of a number of "holes" or "wells" which form miniature Faraday cages out of which the secondaries cannot escape, as shown in Fig. 1-5. An investigation in this area was carried out by Rashovskii (1958)

b) The dependence of δ on surface structure is most

Fig.1-4

(a) Variation of δ with angle of incidence (after Müller). 0° corresponds to normal incidence. The primary electron energy was 2500 ev.

H. O. Müller, *Z. Physik* 104, 475 (1937).

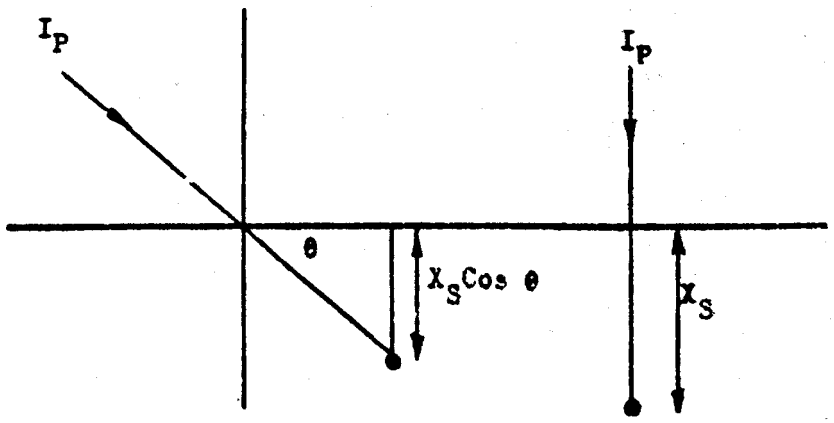

(b)

Fig. 4b Dependence of the Mean Depth of Origin of Secondaries With Angle of Incidence of Primaries.

Fig.1-5

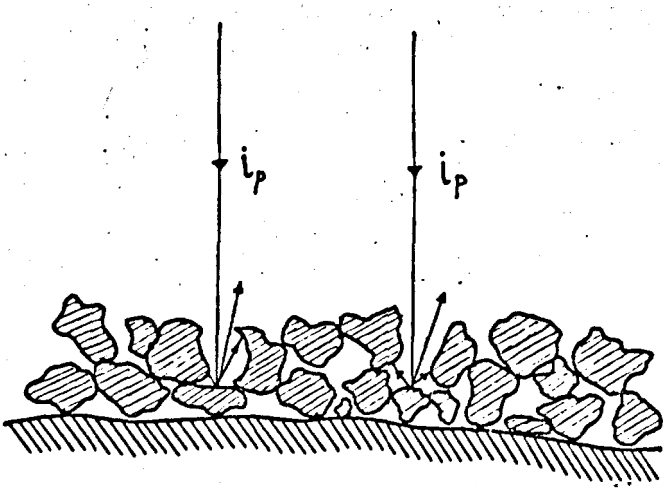

Diagram showing the nature of a 'rough' surface and its influence on the escape of secondaries

clearly shown by a consideration of the variation of work function with crystal surface direction. Since the yield is dependent on work function, variation in crystal direction will directly effect δ. For example, ϕ for tungsten varies from 4.35 eV for the (111) crystal direction, to 4.65 eV for the (110) direction, Bruining (1954), which will give a corresponding variation in δ.

1-4.3 History

Secondary electron emission was first noticed by Austin and Strake (1902). Although, at first, little attention was paid to SEE, interest was renewed with the advent of electronic tubes.

Gehrts (1911), and many others, investigated the SEE yield from various metals using primary energies of 0 to several keV. The apparatus was very simple compared with contemporary equipment. The secondary emissions and primary current was measured by means of a galvanometer and the resultant, $\delta = \frac{i_s}{i_p}$ was plotted versus V_p manually.

Ahearn (1931) measured the SEE yield from tungsten which was cleaned by heating it until bright red, thus introducing heating as a cleaning technique.

Bruining (1954) compiled information from empirical studies and published known SEE yield results for the period up to 1954.

Thomas and Pattinson (1969) recorded SEE yield curves automatically, using an I.C. operational amplifier. This method speeds up the measurements (to a few minutes) which

is a primary requirement for reactive elements. Goto and Ishikawa (1972, 1973) developed a circuit in which the SEE yield can be measured in both the ordinary and differentiated modes. They reported fine structures on the total yield curve which were assigned to surface structures. Henrich (1973,1975) studied the total SEE yield as a function of incident beam energy in the region ($E_p \leqslant 50$ eV), where some fine structures due to elastically scattered or diffracted electrons are superimposed on the generally smooth yield curve. Suleman and Pattinson (1980) have obtained the SEE yield of a clean and slowly oxidised Be surface. The surface composition changes were monitored simultaneously by AES, and changes in the yield were measured as a function of oxygen coverage of the Be surface.

From the theoretical viewpoint, Fröhlich (1932) studied SEE. Wooldridge (1939) concluded that there were some errors in Fröhlich's calculations, and carried out calculations on the production of secondaries using quantum theory. Studies were continued by Marshall (1952), van der Ziel (1953) and Baroody (1956). In addition, semi-empirical theories based on the electron range-energy power-law have been presented by Jonker (1954) and Dekker (1958a).

Kanaya and Kawakatsu (1972) and Dionne (1975) have developed the theory of secondaries by the generalised power law concerning the energy loss of electrons penetrating into a solid target making use of range measurements by Holliday and Sternglass (1959) and Cosslett and Thomas (1964). Ono and Kanaya (1979), in the energy dependence of secondary emission based on range-energy retardation power studies, derived the

δ_m, (maximum yield), and primary energy E_m, (energy related to δ_m), function for the parameters, atomic number Z first ionization energy I, plasmon loss ϵ and backscattering coefficient r. To find the relation between δ_m and E_m, the function $\frac{\delta_m}{E_m}$ was plotted against Z, and was found to be essentially constant for $Z \leq 90$, where Z is the atomic number, with a value of $\frac{\delta_m}{E_m}$ of approximately 2.

1-4.4 Recent Secondary Electron Emission Yield Studies of Sb

In the article of Kaneff (1960), static secondary emission measurements were reported on polycrystalline layers of antimony and antimony-rubidium with different proportions of the metals. The yield maximum lies at higher primary electron energies as the rubidium content is increased. Enrichment of the Rb atom, by additions of pure antimony, increases the number of slow electrons and the energy distribution peak shifts to lower values. The yield for $RbSb_2$ and Rb_3Sb is almost independent of temperature, as indicated from measurements made on the SEE yield reported by Appelt and Hachenberg (1960). Its temperature dependence and its energy distribution are studied for Sb, Sb-Cs, Bi and Bi-Cs layers. The antimony compound CsSb (with high yield) was studied, showing little temperature dependence, and a yield not much greater than antimony's yield. Change in emission with composition can be related to a change in work function. Because of the importance of the Sb compounds, (e.g. Cs, Rb which have high yield), they have been widely studied; for example, Tinofeew and Lunkowa (1940), Morgulisu and Djatowitzkaja (1940) and Kunze (1960). Characteristics of secondary emission of Sb are tabulated in Kolloth (1956), Ono and Kanaya (1979), C.R.C. (1979), Dieke (1963) and Frederikse (1963).

1-5 Fine Structure Superimposed on the Yield

The presence of fine structure in the energy distribution of secondary electrons backscattered into the vacuum from a crystal surface under bombardment by fast primaries can be partially accounted for by excited Bloch states (surface states) lying above the vacuum level. A discussion of these states will be given, with only a passing reference to the other effects (e.g. ionization) that possibly contribute to any other fine structure.

SEE yield spectra provide an excellent medium for observation of such structure. Further, it is possible to use digital filtering and other computational methods to eliminate the large background due to elastic and inelastic collisions. These methods were first used in connection with this application by McRae and Caldwell (1978), and the filtering methods were based on Finite Impulse Response Digital filters, a design for which has been developed by McClellan et al. (1973).

As mentioned above, fine structure superimposed on the yield curve can be due to surface states above the vacuum level, where an incident electron captured by such a state, is elastically reflected after a life time in the state of, typically, 10^{-12} seconds. Investigation of these surface states is significant, since the relation between state energy (dispersion of the surface state) and surface parallel momentum becomes obtainable (i.e. one can get the surface band structure). Unlike surface states below the vacuum level, surface resonances are accessible through direct observation of elastic scattering experiments. The mechanism

of excitation is that an electron, (from the incident beam) gains parallel momentum at the expense of normal momentum, see Section 2-3.1 .

In elastic scattering at the crystal surface, both the energy and surface parallel momentum of the electron are conserved. Consequently, surface resonance band structure can be determined by mapping the positions of resonance fluctuations observed in any electron scattering experiment, where both the electron energy and momentum are resolved.

Fine structures are observed as narrow fluctuations of the elastic scattering intensity with respect to variation of electron energy and incident direction. Willis et al. (1974) have observed highly resolved fluctuations in the low energy range $\leqslant$ 50 eV, in SEE energy distributions. The spectral density provides information on the density of the unfilled or "final" state profile.

A more detailed study of surface states necessitates further information on surface structure and related phenomena, and will be discussed in the following sections.

1-5.1 Electronic Structure of Solid Surfaces

The concept of the volume of space containing the first few atomic layers and the nearby vacuum, where the atomic geometry may differ from that of the bulk, is central to surface electronic structure. From experimental observations, the surface density and, from this, the local density of states becomes a well defined concept. That is, the total density of states weighted by the squared energy range at a particular

spatial point. Integration over the surface region with a weighting factor that decays towards the bulk, then gives the surface density of states.

Electron eigenstates can be classified by a unique three dimensional wave vector $\underline{k}$, but since the presence of a surface destroys periodicity in the surface normal direction, this vector can be reduced by a two dimensional Bloch wave vector $\underline{k}_{||}$, unique in the surface Brillouin zone. For every $\underline{k}_{||}$ continuous energy ranges and gaps appear where bulk band states exist and disappear respectively. Further, symmetry operations possessed by the solid are not wholly lost through the imposition of a surface.

Periodic, surface normal (Z direction) solutions of Schrödinger's equation for a bulk potential combined with $\underline{k}_{||}$, energy and symmetry type, form a basis for the investigation of band structure from the viewpoint of the classification of surface states. If the energy occurs in one of the allowed ranges mentioned above, then one or two pairs of Bloch states, with vectors $\underline{k}_z^{\pm}(E)$, exist For complex $\underline{k}_z$, an infinite number of evanescent Bloch waves exist, but since their amplitudes diverge as z goes to $+\infty$ or $-\infty$, they are neglected when considering the bulk. However, at a surface, such waves that decay into the bulk, are permissable components of a wave function. The situation is simplified by the fact that, in certain energy ranges, $\underline{k}_z(E)$ becomes real and is thus associated with a band of propagating waves; only evanescent waves associated with bands near a given energy need therefore be considered. In the vacuum region, electron wave functions are decaying exponentials with surface parallel periodic

modulation, whereas in the surface region the two dimensional periodic potential defies any simple description, (see Section 2-2).

Two different types of wave function are connected with surface electronic structure, and for a given $\underline{k}_{||}$ and any E in an allowed band, one or more scattering states exist, the specification depends on the fact that, in the bulk they consist of a single current carrying Bloch wave and one or more reflected Bloch waves. The density of states is then calculated from the incident Bloch waves after normalisation (one electron/bulk unit cell), summation over occupied bands, integration over the three dimensional bulk Brillouin zones, with equal weighting assigned to equal volume elements for the Bloch vector $\underline{k}$. The second type of wave functions are surface state functions, which occur in energies that coincide with the gaps, for a given $\underline{k}_{||}$.

The existence of one or more surface state in a gap depends on the nature of the potential and so cannot generally be predicted, but once confirmed for a given $\underline{k}_{||}$, its dispersion relation $E(\underline{k}_{||})$ can be defined, as a function of $\underline{k}_{||}$. A number of effects may occur; the gap and surface state may exist over the whole surface Brillouin zone; the gap may close up and "squeeze out" the surface state, or the surface state may overlap a band at the edge of the gap and so disappear. The extent of charge localisation will also effect the surface state behaviour, with a state in a wide gap displaying high localisation. Conversely, a state in a small gap will have much of its charge content in the slowly decaying evanescent component. Consequently, a state merging into the edge of a gap may gradually fade away, rather than suddenly vanish

A further situation may exist, involving scattering states and this is termed the surface resonance. If the amplitude squared of the scattering state, integrated over the surface, is plotted as a function of the energy E across an allowed band, it will generally vary smoothly and go to zero at the band edges. However, sharp peaks may appear at particular energies with the integrated charge under a peak equal to a large fraction of an electron in the surface region. This effect may occur, for example, at the edge of a band if the disturbance is not sufficiently strong to separate the surface state from the band. Resonances also occur when a surface state, split well below one minimum in the band structure, overlaps another band, and here the state would not disappear, but would keep its charge intact and acquire a small energy width, Appelbaum and Hamann (1976). Finally, sharp resonances can occur when a well-localised surface state at a Brillouin zone symmetry point is overlapped by a band of different symmetry. Away from the symmetry point, the state, and the band, will be mixed by the symmetry breaking component of $\underline{k}_{||}$. Given "weak" mixing, it is valid to assign a surface state with the resonance even though the mixing is over a considerable region (a true surface state exists at a point or on a line).

In conclusion, the most interesting and observable features of the surface density of states are those arising from the surface state. The structure due to the two dimensional dispersion relation "$E(\underline{k}_{||})$" is sharper than that derived from the bulk density of states, and the appearance of surface-states structure provides a convenient test for theories of geometric and chemical band changes at the surface. Non-resonant scattering states also reflect such

information, but their contributions are probably gradual modulations of the bulk density of states and so difficult to characterise and interpret.

1-5.2 Electronic Surface Resonance of Crystals

Resonance scattering at crystal surfaces is a physical mechanism, in which an incident electron on the crystal is temporarily trapped in a quasi-stationary, or "non stationary" surface state lying above the vacuum level. This will subsequently be released without change of energy or $\underline{k}_{||}$ (reduced parallel momentum), or it may undergo inelastic scattering. Generally the resonances are observed as narrow fluctuations of elastic scattering intensities with respect to the variation of incident electron energy and direction. The scattering process is called electronic surface resonance scattering. The temporary surface states that are intermediate states in resonance scattering are called electronic surface resonances. Surface resonance applies to any non-stationary surface state, but in the present text it is applied exclusively to temporary but long-lived surface states that exist at energies above the vacuum level in the absence of an externally applied field.

Willis and Christensen (1978) in the theory of resonance scattering at crystal surfaces have pointed out that an elastic scattering process, where both energy and $\underline{k}_{||}$ are conserved may account for the excitation or decay of the surface state. The interpretation of the surface resonance band structure can be understood by analogy with three dimensional band theory. In a nearly free-electron scheme the interaction elements responsible for the splitting of degenerate levels

are Fourier coefficients of a pseudo-potential. In principle at least, these Fourier coefficients may be determined empirically by fitting to observed band structure. In the case of the surface resonance band structure, the analogous statements apply to a scheme in which the electron motion is treated as nearly free in two dimensions parallel to the surface. The interaction elements are coefficients of a two dimensional Fourier transform of an effective potential which is an average of the effective scattering potential of the crystal a "pseudo-potential", acting with respect to the depth distribution of electron density in a surface resonance "the surface weighted pseudo-potential".

Crystal surface characterisation may be interpreted by the dispersion $E(\underline{k}_{||})$ of electronic surface resonances. The lateral variation of the potential acting on electrons at the surface is related to the lateral geometrical arrangement of surface atoms. The dispersion is determined by entering the locations of the surface resonance fluctuations on a plot of energy E against reduced parallel momentum $\underline{k}_{||}$, of the incident electrons. However, to date, resonances have been observed most commonly in LEED, McRae and Caldwell (1967), and SEE experiments, Willis et al. (1977). A cross-check of SEE and LEED is needed because in both methods, resonance features are usually weak and difficult to locate precisely.

Agreement between the observation in both experiments is good at some values of $\underline{k}_{||}$, but differences are encountered at some other values, McRae (1978). This discrepancy may be part due to the uncertainty in location of the resonance centre in the electron reflection method. Unless special attention

is given to the line shape, the resonance positions cannot be located to an accuracy better than about half the line width.

SEE measurement is better suited than LEED to observation of the resonance features. In total electron reflection, the structure associated with elastic scattering is observed against a smooth background due to the inelastic scattering. In LEED, if more than one LEED beam (e.g. 01, 02) is present, the structure in the elastic-scattering contribution (the sum of LEED beam intensities) is usually smoother than that due to any individual beam. However, the finer detail associated with resonances is retained because all LEED beams have resonances in common.

In total reflection experiments, resonance features may be identified through a correlation between their positions and those of the beam thresholds (grazing emergence of diffracted beam). The binding energy of an isolated resonance is nearly independent of incident conditions. If there are neighbouring resonances there may be interactions between them as has been observed in one instance by McRae (1971), and Louzier et al. (1971), but a correlation between resonance positions or intensities and beam thresholds is still present. The positions of resonances and beam thresholds shift for the most part much more rapidly under varying incidence conditions than do the peaks comprising the coarse structure of LEED or total reflection intensity curves. The effect is that if, for example, the angle of incidence is varied, the resonances shift comparitively slowly varying background.

1-5.3 Resonance Scattering

Resonance scattering means that an electron incident on the crystal surface is captured by the surface to form a compound state which subsequently decays with the release of the electron. Existing compound states can generally decay by several paths (channels), which are characterised individually by the final quantum states of the target and of the scattered particles. Resonance scattering occurs with appreciable probability only in a narrow range of incidence energy and momentum characteristic of the compound state. It always occurs at the same time as "direct", or non-resonance scattering, whose probability varies relatively slowly with respect to the incidence conditions, and does not involve a surface state. The coherent superposition of the resonance and direct contributions to the scattering amplitude results in a fluctuation of scattering intensity centred at values of incidence energy and momentum for which the magnitude of the resonance contribution is at a maximum, i.e. energy and momentum values match the corresponding values for a quasi-stationary surface state. The width in energy Γ of the fluctuation is related inversely to the life time Δt of the compound state, through the uncertainty relation $\Gamma \cdot \Delta t \approx \hbar$.

Each of the general properties of resonance scattering has particular realisation in scattering at crystal surfaces. In surface resonance scattering the intermediate compound state is a surface state. In an electron scattering experiment, a resonance is observed as a fluctuation of scattering intensity centred at values of incidence electron energy E, and reduced parallel momentum $\underline{k}_{||}$ characteristic of the surface state. The fluctuations intensity may have various

line shapes, peaks and dips and asymmetric line shapes are possible.

The mechanism underlying such observations is indicated schematically in Fig. 1-6. In the case of elastic reflection (Fig. 1-6a), the direct process shown schematically (right) is a multiple ion-core scattering. In the resonance process (left), the electron first undergoes an elastic scattering in which it gains parallel momentum $2\pi g$, leaving it insufficient normal momentum to surmount the surface potential barrier. This means that the electron is trapped in the crystal. If in addition there is a bulk band gap preventing the electron from penetrating the crystal and a phase or matching condition is satisfied, then a surface state exists. This is not a stationary surface state, however, as it can decay either by inelastic scattering or, as indicated in Fig. 1-6a (left), by a second elastic scattering event in which the electron gains sufficient normal mementum to escape from the crystal. However, the intermediate surface state may be excited by an electron incident from the vacuum [reflection case, Fig. 1-6(a), (b)] or from the bulk crystal [emission case, Fig. 1-6(c), (d)]. The surface state may decay by an elastic channel [Fig. 1-6(a), (c)] or an inelastic one [Fig. 1-6(b), (d)]. Resonance may be observed in either elastic or inelastic scattering experiments, depending on the decay channel monitored.

The E and $\underline{k}_{||}$ values derived from observation of a narrow resonance intensity fluctuation are independent of the scattering mechanism responsible for it. However, the line shape of the fluctuation depends critically on the

Fig.1-6

Resonance and direct mechanisms of electron scattering at a crystal surface: (a) elastic reflection; (b) inelastic reflection; (c) elastic emission; (d) inelastic emission. Straight arrows indicate incident or elastically scattered electron waves, wavy arrows indicated surface states, open circles denote elastic scattering with change of surface parallel momentum, filled circles denote elastic scattering with or without change of surface parallel momentum, open squares denote inelastic scattering., McRae (1979)

mechanism. This is so because the scattering amplitude is the superposition of two contributions, namely the resonance and direct contributions as indicated in Fig. 1-6. The line shape is the sum of the squared modulus of the resonance amplitude contribution and the cross-term due to the interference between the resonance and direct terms.

An example of resonance intensity fluctuation is provided by LEED results for an Ni (100)C(2 x 2)S surface, shown in Fig. 1-7. All of the circled features have been identified as resonances. The resonances have widths of about 1 eV, and are observed at electron energies up to and above 50 eV. Metal surfaces exhibit such resonances.

1-5.4 Review of Recent Work

The study of electronic structure of solid surface has become an active area in the last few years. Advances in experimental techniques (e.g. photo-emission, LEED and SEE) have produced an abundance of information from clean and well-ordered single crystal surfaces, Plummer et al. (1975), Park (1975), and Eastman et al. (1978). Theoretical calculations of the electronic structure of crystalline semi-conductor surfaces have been used successfully to interpret some of the experimental results, Chelikowsky and Cohen (1976), and recently a fully self consistent technique has been applied to d-band metal surfaces by Smith et al. (1980).

Although the phenomenon of emission of secondary electrons has been the subject of considerable experimental research during several decades, it has only recently been possible to achieve an energy resolution which is sufficient

Fig. 1-7

LEED intensity curve for Ni(001)$c(2 \times 2)$S surface showing resonance fine structure (circled). Colatitude incidence angle $\theta = 58°$, [11] azimuth. The curve is not normalized to constant primary current (McRae, Aberdam, Baudoing, and Gauthier).

to reveal fine structure modulation of the otherwise rather featureless background distribution curve . It appears that this fine structure can be related to the one-electron density of states for energies above the vacuum level [Burns (1960) , Christensen and Feuerbacher (1974), Feuerbacher and Christensen (1974), Willis and Christensen (1978) and Christensen and Willis (1979)] . The experimental work of Willis and Christensen (1978) provides spectra, recorded in a number of off-normal directions for each of the three low-index crystal planes of tungsten. Christensen and Willis (1979) have investigated whether the correspondence between the electronic band structure and measured SEE spectra which they carried out for W in the earlier work, Willis et al. (1978) is valid in general.

The existence of surface resonances in the elastic scattering of low energy electrons at crystal surfaces have been detected in experiment using methods of LEED by [Hayakawa and Miyaka (1974), Lauzier et al. (1971), and McRae and Wheatley (1972)], using methods of net current electron reflection by,[Henrich (1975), McRae and Caldwell (1976)], and angle-resolved secondary emission, Best (1975).

A method for the determination of the lateral structure of a crystal surface has been presented by McRae and Caldwell (1978). The method involves measurement of the surface resonances and structure of a Ni (100) crystal and its oxide compounds. The raw reflection data, (shown in Fig. 1-8) were subsequently filtered, (see Fig. 1-9) to emphasise the band structure on the smooth background. Comparison was made between the theoretical and filtered data by means of plotting

Fig. 1-8

V (VOLTS)

Raw electron-reflection data for Ni(001),

McRae & Caldwell(1978)

Fig.1-9

V(VOLTS)

Filtered data (filter29HP) derived from raw data in Fig. 1-8 for Ni(001), McRae & Caldwell(1978).

$E(k_{||})$ vs. $k_{||}$, and good agreement was achieved (see Fig. 1-10). However, because in the present work the results were not filtered, (see Section 4-4), McRae's raw and filtered data is displayed on the theoretically plotted $E(K_{||})$ vs. $k_{||}$, shown in Fig. 1-11, to show the deviation between the raw and filtered data, and the practicality of using raw data to obtain a less accurate correspondance between theory and experiment, (such as is the case for the present work where the digital filter has not been completed, see Section 4-1).

Perhaps the most significant publication in the area of electronic surface resonance is the paper by McRae (1979).

No reports of any experiments on surface band structure of Sb have been found in the literature, but Jona (1967), Lemonier et al. (1973), Lin and Phillips (1966), and Falicov and Lin (1966) have carried out theoretical Sb bulk band structure calculations.

Fig.1-10

Surface resonance band structure for Ni(001). The experimental points refer to maxima (crosses) and minima (open circles) taken from filtered data of fig. 3. E denotes electron energy, $k_{\parallel}$ denotes reduced parallel momentum, and a denotes the unit mesh side for Ni(001) (a = 2.491 A). The full lines are free-electron resonance energies $E_g^0(k_{\parallel})$ (eq. (4)). The inset at upper left shows the first two-dimensional Brillouin zone (square), reciprocal-net points (crosses) and symmetry points (filled circles) for Ni(001) surface. The arrows indicate approximately the range of $k_{\parallel}$, relative to the Brillouin zone, represented by the width of the figure.

McRae and Caldwell (1978)

Fig.1-11

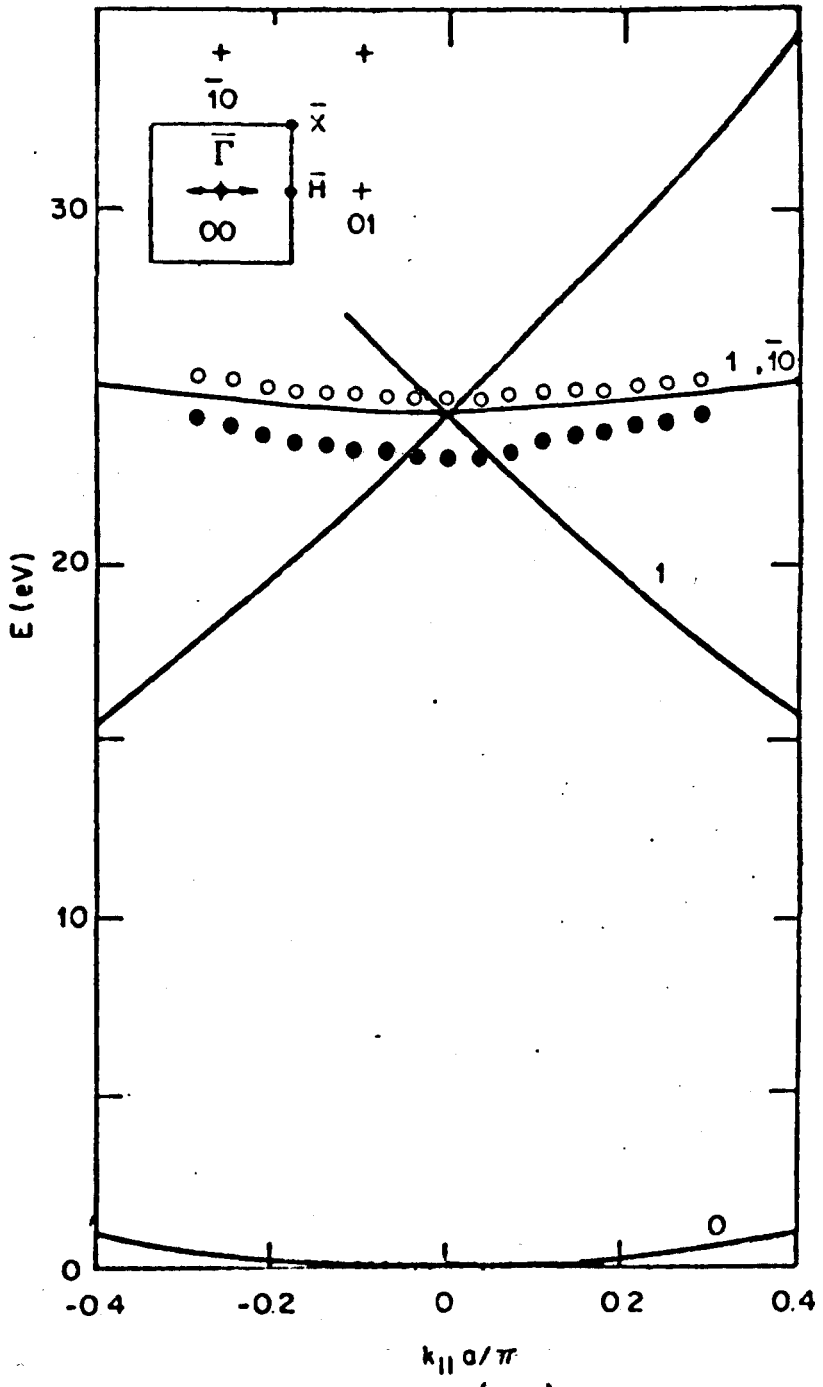

Surface resonance band structure for Ni(001). The experimental points refer to minima taken from unfiltered data of Fig. 1-8. The positions of the observed resonances are fitted by the 2D-free electron approxi-mation with a binding energy of 3.5 eV. For notations see Fig. 1-8 caption.

o Filtered data.

● Unfiltered data

Chapter 2

Theory

2-1 Introduction

One of the main aims of the present work is to provide a discussion of the use of SEE yield spectroscopy and its use to find the surface band structure. In addition to this, it is clear that a study of other surface phenomena must also be included since the detection and subsequent analysis of reproducable and unambiguous surface structure features are inseparable related to these effects. Thus, the mechanisms of AES, CEEL spectroscopy, and SEE yield fit naturally into the overall framework of this thesis. However, due to the extensive development of both the practical and theoretical aspects of these fields of study, a complete discussion has not been attempted. More, the aim has been to develop certain practical and theoretical aspects dictated by their relevence to the experimental work carried out. Thus, only a concise treatment of the mechanism of AES has been given. With regard to CEEL spectroscopy, and SEE yield, a more comprehensive discussion can be found in Wright (1974), Pines (1964), Servier (1972) for the former, and Dekker (1958), Hachenberg and Brauer (1959) for the latter.

2-2 Theory of Auger Transitions

A complete analysis of the theory of Auger transitions is the exclusive subject of many texts, notably Burhop (1952), Chang (1974), and Cattarji (1976). Also Palmberg and Rhodin (1968) and Suleman (1971), have fully expressed the method of derivative mode measurement by which the sensitivity of the

technique is notably enhanced. Since the technique was used here only as a probe to monitor surface contamination, a discussion of the empirical assignment of Auger peaks is all that is required. An empirical calculation for Auger transition energy level is therefore introduced.

When atoms combine to form a solid, perturbations in the energy levels of an atom are caused by the presence of its neighbours in the crystal lattice array. The binding energy of inner (i.e. X-ray) electronic levels are then slightly affected with respect to the outer, or optical, levels. The energy shifts may constitute a great number of levels (valence bands) characteristic of the crystal as a whole, rather than the individual atoms composing it. The energy range of the levels is of the order of only a few electron volts so that they form an effectively continuous band (valence band) within the crystal.

Where valence bands are involved in the Auger transitions, particularly in the conduction band of metals, the two holes in the conduction band may not interact very strongly owing to screening by the electron gas comprised of the free electrons in this band. The condition for energy conservation is:

$$E_A(Z) = E_W(Z) - 2E_V(Z), \text{ (metal)}$$

where $E_A(Z)$ is the Auger electron energy, $E_W(Z)$ is the binding energy of the ejected primary from the atom, and $E_V(Z)$,(metal) is the most prominent conduction band energy measured relative to thevacuum level.

In general, for given initial and final state configurations in which parity and angular momentum are conserved,

only those transitions which are energetically possible actually take place.

$$E_A(Z) = E_W(Z) - E_X'(Z) - E_Y'(Z) > 0$$

where $E_X'(Z)$ and $E_Y'(Z)$ are the binding energies of the two participating electrons, i.e. corresponding to the two final vacancies in bound states. Assuming that the electron with energy $E_X'(Z)$ in the vacancy, the usual practice is to correct for the binding energy of the other electron with energy $E_Y'(Z)$, which is ejected into the continuum and, therefore, supposed to "feel" the reduced screening due to the inner shell ionization. The correction is made by taking $E_X'(Z)$ and $E_Y'(Z)$ corresponding to an atom of the next higher atomic number, $(Z + 1)$. This is a rough approximation, and from the viewpoint of quantum electrodynamics, no statement can be made about which electron jumps in "first" and which one is ejected "later", and so on.

To satisfy the above correction an empirical expression for the energy of an Auger transition has been derived by Chung and Jenkins (1970).

$$E_A(Z) = E_W(Z) - \tfrac{1}{2}\left[E_X(Z) + E_X(Z+1)\right] - \tfrac{1}{2}\left[E_Y(Z) + E_Y(Z+1)\right] \quad \text{Eq.2-1}$$

where $E_X(Z)$ and $E_X(Z+1)$ are the atomic binding energies for the X electron in atoms having atomic number Z and Z + 1, respectively, $E_Y(Z)$ and $E_Y(Z+1)$ are the same for the Y electron. A relation of this form is based on the fact that the binding energies of the X and Y electrons will exchange when one of their inner electrons is removed from an atom. The remaining electrons can be thought to behave as if the nucleus has more charge (i.e. appear to the electron as a nucleus of higher atomic number). Taking the energy half way between the value it would have for an atom having

atomic number (Z+1) is arbitrary, but seems to give good results when the energy of the Auger transitions are compared to experimental values. Further, Hartree-Fock electron calculations, especially on atoms with missing electrons, might give better information on what the binding energies of the X and Y electrons really are.

Further modification was made by Chung and Jenkins (1970) as:

$$E_A(Z) = E_W(Z) - \tfrac{1}{2}\left[E_X(Z) + E_X(Z+1) + E_Y(Z) + E_Y(Z+1)\right] - \varphi$$

where φ is the work function of the crystal. In fact, if the energy of the electron passing through the analyser is measured relative to the Fermi level of the analyser material, this introduces an additional term $-(\varphi_A - \varphi)$, the work function of the analyser measured relative to the material under investigation.

Therefore:

$$E_Z(Z) = E_W(Z) - \tfrac{1}{2}\left[E_X(Z) + E_X(Z+1) + E_Y(Z) + E_Y(Z+1)\right] - \varphi_A$$

2.3 Electronic Surface Band Structure Theory

2-3.1 Mechanism of Resonance Electron Reflection

As discussed in Section 1-4.2, the resonance is associated with a process in which the incident electron with a well-defined value of energy E, and reduced parallel momentum, $\underline{k}_{||}$, is trapped by the target to form a quasi-stationary compound surface state (surface resonance). After a delay, equal to the surface resonance life time, the electron may be released without change of E or $\underline{k}_{||}$ (elastic decay) or it may undergo inelastic scattering.

The mechanism of excitation and of elastic decay of surface resonances is one of diffraction, McRae (1971). The result of the diffraction decay event is either a plane wave propagating in the vacuum, or a Bloch wave propagating in the crystal. In either case, an electron gains parallel momentum $\underline{k}_{||}$ at the expense of normal momentum $\underline{k}_{\perp}$, in amounts $2\pi\underline{g}$, where $\underline{g}$ is a reciprocal-net vector. Therefore, in the excitation of a surface resonance, an electron can be trapped with respect to the outwards surface normal component of its motion by the surface potential barrier. With respect to the inward surface-normal component of its motion, the trapping of the electron depends on the existence of "forbidden gaps" in the band structure, Jones (1975). However, only those surface states with nearly the same energy (within the width of the surface state) and $\underline{k}_{||}$ as the incident electron can take part in resonance electron reflection, because of the conserved value of E and $\underline{k}_{||}$ in the elastic excitation of surface resonances.

The non-resonance contribution to the amplitude varies relatively slowly with respect to incident electron energy and momentum. The resonance fluctuation of the reflection intensity results from the interference between the resonance and non-resonance amplitude contributions. The interference is centred at those values of E and $\underline{k}_{||}$ for the incident beam that match the corresponding values for a surface resonance.

2-3.2 Tightly Bound Electron Approximation

For a free atom, V(z) gives the potential energy of an electron in the field of the atom plus that of other atomic electrons, z being the distance from the nucleus. The

potential for a free electron is a constant, V_o, and for an electron in a free atom is an exponential function $V(z) = V_o e^{\pm ikz}$, where k is a constant. The potential energy of the electron in a crystal, then looks like Fig. 2-1a and b; in the zero order approximation it can be determined by:

$$U_o(z) = A^{-1} \int U(z,r)dr \qquad \text{Eq. 1}$$

where z is the inward surface normal coordinate and r the parallel coordinate and $U_o(z)$ its lateral average. The integration is over one unit mesh, and A is the unit mesh area, the equation can be defined by Bloch function. In the zeroth order, (two dimensional (2D) free electron) description, the effective scattering potential of the crystal (a pseudopotential) is replaced by a potential that retains the 2D periodicity of the surface structure, it approaches indefinitely closely to the average of the actual potential with respect to the directions parallel to the surface, a schematic representation of this laterally-averaged potential $U_o(z)$ for a crystal is shown in Figs. 2-1c and 2-3.

2-3.3 Energy Bands in the Free Electron Limit

In the zero approximation the periodic potential of the lattice structure becomes arbitrarily weak while the symmetry properties of the wave function are preserved. Any U_k of the form $e^{ik.r}$ is acceptable, and the energy of the state of wave vector $\underline{k}$ is just:

$$E(k) = \frac{\hbar}{2m} K^2$$

here $$\underline{K} = \underline{k} + \underline{G}$$

and $\underline{G}$ is any reciprocal lattice vector. This simple expression allows the energy band of electrons in many metals to be reasonably well approximated.

Fig. 2-1

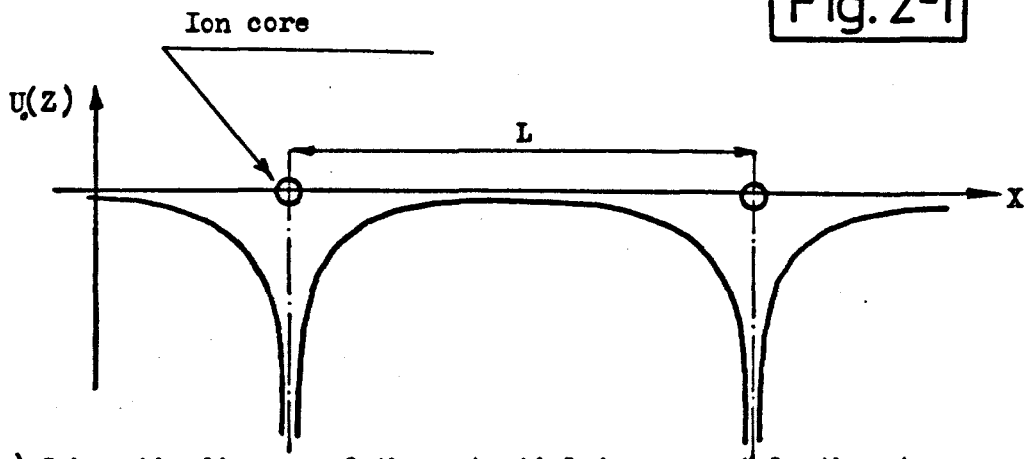

a) Schematic diagram of the potential in a crystal, the atoms are widely separated.

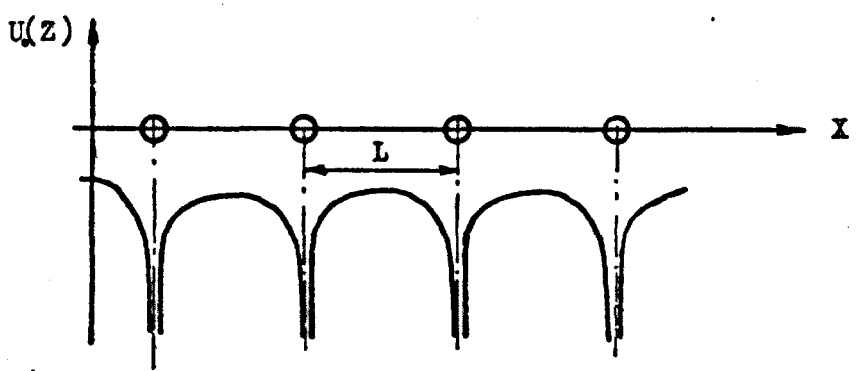

b) Schematic diagram of the potential in a crystal, the atoms are close to each other.

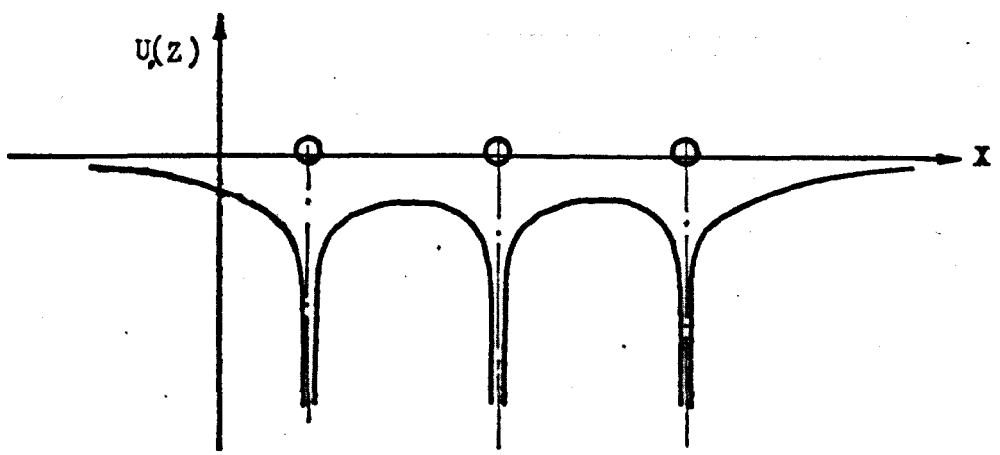

c) Laterally averaged potential U(Z) for a crystal.

Fig. 2-3

Laterally averaged potential $U_0(z)$ for a crystal, together with energy levels pertaining to resonances according to the 2-D free-electron description (schematic). z is the inward surface-normal coordinate. $E_{\infty g}(\mathbf{k}_{\parallel})$ denotes the threshold energy for the diffraction beam indexed by reciprocal-net vector $\mathbf{g}$, e_n denotes the nth bound-state energy eigenvalue for potential $U_0(z)$ and $e_n + E_{\infty g}(\mathbf{k}_{\parallel})$ denotes the resonance energy. $\mathbf{k}_{\parallel}$ is the reduced parallel momentum. Broken lines indicate an idealized form of potential adopted for an approximate calculation of the eigenvalues e_n.

McRae (1979a)

Actual band structures are usually shown in the first Brillouin zone, along with free electron energies that approximate band energies.

In

$$E = \frac{\hbar^2}{2m} K^2$$

there is no restriction on the wave vector $\underline{K}$, but it can always be written in terms of $\underline{k}$ restricted to the first Brillouin zone. For any $\underline{k}$ there exists a reciprocal lattice vector $\underline{K}$ for which $\underline{K} = \underline{k} + \underline{G}$, with $\underline{k}$ in the first Brillouin zone. The energy is written

$$E(k_x, k_y, k_z) = \frac{\hbar^2}{2m} (k + G)^2 = \frac{\hbar^2}{2m} \left[(k_x + G_x)^2 + (k_y + G_y)^2 + (k_z + G_z)^2 \right]$$

For clarification, it is useful to consider the low lying free electron bands of a simple cubic lattice.

It is often convenient to use the Hartree-Fock atomic units in an energy band problem. The units are such that $m = e = \hbar = 1$. With this choice the unit of length turns out to be the Bohr radius a_o. The energy is expressed in Rydbergs

$$a_o = 0.52917 \text{ Å} \qquad 1\text{Ry} = 13.6049 \text{ eV}$$

Several low lying bands with energies at $\underline{k} = 0$ and along the k_x in the first zone are written and illustrated in Fig. 2-2.

Band	$G.a/2\pi$	$E(k_x 00)$	$E(000)$
1	000	k_x^2	0
2,3	100, $\bar{1}00$	$\left(k_x \pm \frac{2\pi}{a}\right)^2$	$\left(\frac{2\pi}{a}\right)^2$
4.5.6.7	010,0$\bar{1}$0,001,00$\bar{1}$	$k_x^2 + \left(\frac{2\pi}{a}\right)^2$	$\left(\frac{2\pi}{a}\right)^2$

The degeneracy of the bands (e.g. 4,5,6,7) were shown by calculation, are plotted by Harrison (1966) for Al in

Low lying energy bands in the free electron limit of the simple cubic lattice as transformed to first Brillouin zone, plotted versus $(k_x 00)$.

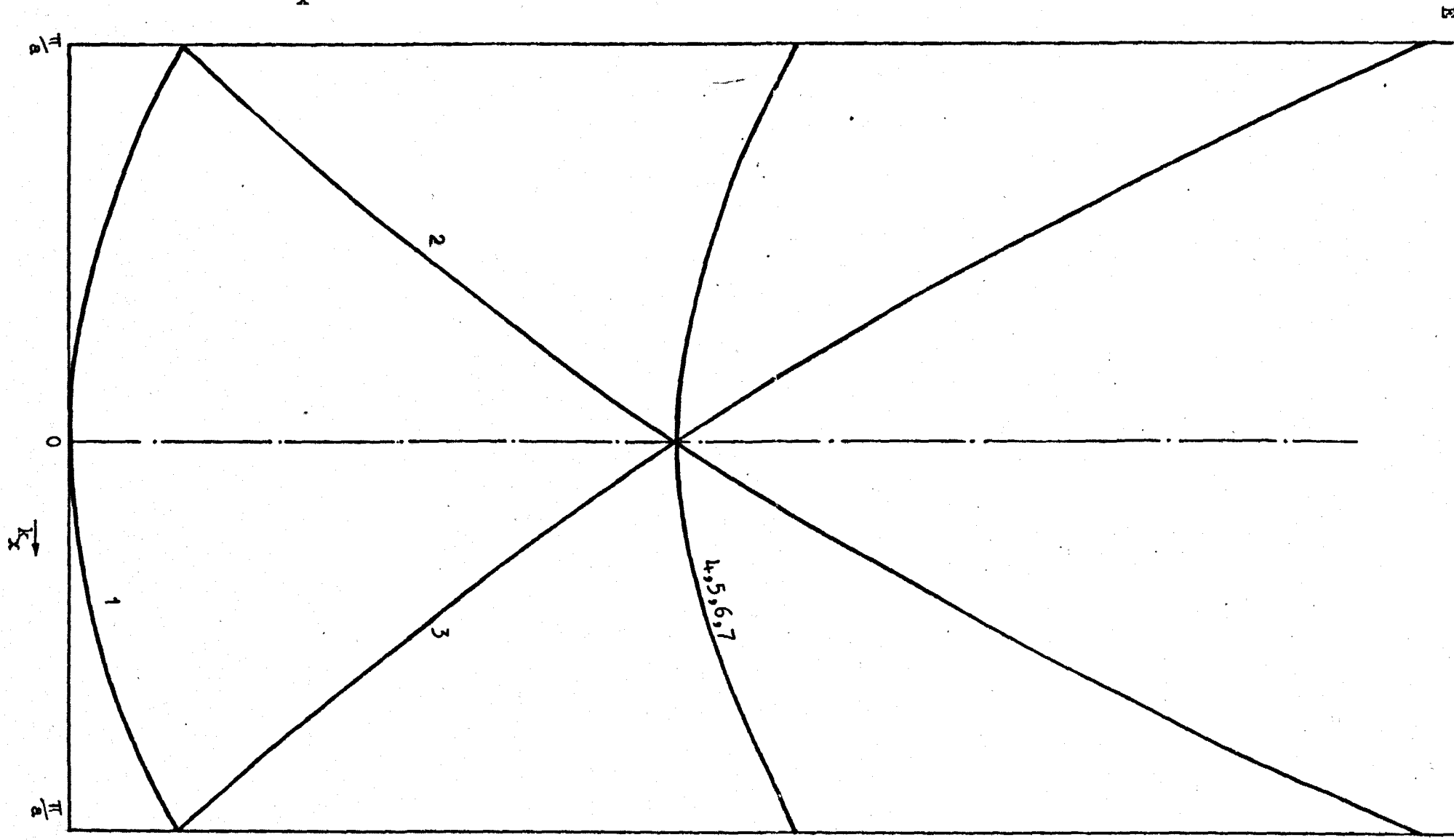

Fig. 2-2

Brillouin zone.

2-3.4 Two-Dimensional Nearly Free Electron Distribution of Surface Resonance

The surface resonance band structure may be calculated approximately by a perturbation scheme based on the zero-description functions. This is called the 2-D nearly free electron scheme. The surface state wave functions are separable into two components representing electron motion normal and parallel to the surface, respectively. Therefore,

$$\psi_{ng} = |ng\rangle = \psi_n(z)\exp\left[i(k_{||} + 2\pi g)\cdot r)\right] \qquad \text{Eq. 2}$$

where $\psi_n(z)$ is the nth bound-state solution of the Schroedinger equation for the potential $U_o(z)$ that vanish for $z \longrightarrow -\infty$ and $\exp\left[i(\underline{k}_{||} + 2\pi g).r\right]$ represents free electron motion parallel to the surface with momentum $\underline{k}_{||} + 2\pi\underline{g}$. In the elastic scattering of electrons at crystal surfaces, the projection of electron momentum parallel to the surface is conserved by $2\pi\underline{g}$, where $\underline{g}$ is the reciprocal lattice vector, $\underline{k}_{||}$ is the reduced parallel momentum and $2\pi\underline{g}$ is the parallel momentum transfer.

The electron energies corresponding to the wave functions of Equation 2. are

$$\bullet\ E_{ng} = e_n + E_g^{\circ}(k_{||}) \qquad \text{Eq. 3}$$

where e_n is the energy eigenvalue corresponding to ψ_n, and $E_g^{\circ}(k_{||})$ is the kinetic energy of electron motion parallel to the surface.

$$-\frac{\hbar^2}{2m}\nabla^2\psi = E\psi$$

$$-\frac{\hbar^2}{2m}\frac{\partial^2}{\partial r^2}\exp\left[ik_{||} + 2\pi g.r\right]\psi_z = E_g^{\circ}(k_{||})\psi_z$$

$$-\frac{\hbar^2}{2m}|(k_{||} + 2\pi g)^2|\psi_z = E_g^{\circ}(k_{||})\ \psi_z$$

$$E_g^{\circ}(k_{||}) = -\frac{\hbar^2}{2m}|(k_{||} + 2\pi g)^2| \qquad \text{Eq. 4}$$

In Hartree-Fock (atomic unit)

$$E_g^{\circ}(k_{||}) = E(k_{||}) = |k_{||} + 2\pi g|^2$$

$E_g^{\circ}(k_{||})$ is the threshold energy (grazing emergence energy) for the diffracted beam indexed by reciprocal-lattice vector $\underline{g}$. The energy level separation from Equation 3:

$$E_g^{\circ} - E_{ng} = -e_n$$

describes the binding energy of the nth surface state associated with a given threshold, relative to the threshold. The threshold energy functions, (Equation 4) collectively make up the surface band structure in the free-electron limit $U(z,r) \longrightarrow 0$. In the 2D free electron description, the surface band structure for a given level index n is displaced to lower energies from the free electron limit by a fixed amount equal to the binding energy $-e_n$. The pattern of energy levels presented is presented in Fig. 2-3.

The Hamiltonian which leads to the wave function in Equation 2 is:

$$H = T_{||} + T_{\perp} + U(z,r)$$

$T_{||}$ is the surface parallel kinetic energy operator, the energy matrix

$$\langle ng|H|n'g'\rangle = \int_{-\infty}^{+\infty} \psi_{n'}^{*}(z) H_{gg'} \psi_n(z)\, d(z) \qquad \text{Eq. 5}$$

where $H_{gg'}$ results from integration over surface-parallel coordinates, McRae (1979). The eigenvalues of energy matrix Equation 5, are resonance energies calculated neglecting interaction with continuum.

A useful approximation to the energy matrix may be found from the following gross properties of the function $\psi_n(z)$.

These functions are bound state eigenfunctions of the Hamiltonian $T_\perp + U_o(z)$. $\psi_n(z)$ properties depend on the shape of the potential in the surface region near and outside the outermost atoms layer of the substrate crystal. A suitable description of this situation is obtained by dividing the potential into surface and bulk parts at z = 0, see Fig. 2-3. In the case of a metal crystal surface, the boundary plane can be chosen so that a good approximation, for the surface potential, has the image form $1/4z$ $(z<0)$, while the bulk potential is a periodic function of z. The required wave functions are solutions of the Schroedinger equation for the image potential that vanish for $z \longrightarrow \infty$ and join smoothly to the bulk wave functions at z = 0 (bulk wave functions vanish at z = 0). McRae (1979) concluded the following concerning the nature of the boundary conditions on the surface:

a) the overlap between wave functions with different indices n is small

b) wave functions with indices $n>1$ have relatively weak overlap with the bulk potential.

It follows, (at least for metals), that off-diagonal matrix elements $\langle ng \mid H \mid n'g' \rangle$ for which $n = n' = 1$, play the most important role in determining the boundary matrix. The energy matrix,(Equation 5), reduces approximately to:

$$\langle g|H|g' \rangle = \langle U_{g-g'} \rangle = \int_{-\infty}^{+\infty} \psi_1^* \, U_{g-g'} \psi_1 dz \ , \ g' \neq g$$

$$= e_1 + E_g^o(k_{||}) \ , \ (g' = g)$$

The quantity $\langle U_{g-g'} \rangle$ is the $(g-g')$th Fourier component of the "surface weighted potential", i.e. the potential weighted with respect to the electron density of the n=1 resonance.

The 2D nearly-free-electron description reduces to a 2D free-electron one if the off-diagonal elements are comparatively small, i.e. if the following inequality is satisfied,

$$| \langle U_{g-g'} \rangle | \ll E_g^\circ - E_{g'}^\circ \ , \ g \neq g'$$

$$e_1 \gg E_g^\circ(k_{||})$$

On the other hand, the lateral variation of the surface weighted potential causes comparatively large displacements of degenerate or nearly degenerate 2D free-electron levels such as occur for $\underline{k}_{||}$ values near the crossing of different branches of the free-electron band structure.

The interaction between 2D free-electron levels are generally accompanied by systemmatic variation of resonance intensities. These tendencies can be related to selection rules based on elementary symmetry properties. The only allowed resonances are those having the same symmetry as the incident wave field under the point-group operations of the surfaces, McRae (1979). For example, suppose that the reciprocal-lattice vectors $\underline{g}$ and $\underline{g}'$ are related as mirror images, with respect to the plane containing the incident beam and the surface normal. The interaction between 2D free-electron states $|1g\rangle$ and $|1g'\rangle$ results in resonances with wave functions and energies

$$|1g\rangle \pm |1g'\rangle \ , \ e_1 \pm \langle U_{g-g'} \rangle$$

In this case, the symmetric (+) combination is allowed and the antisymmetric (-) one forbidden by symmetry.

Example: Consider the band structure of Ni with lattice dimension $a_1 = 2.491$ Å along k_x axis at first Brillouin zone with lattice vector $g = 0$ and 1

$$E(k) = \frac{\hbar^2}{2m} \left| (k_x+G_x)^2 + (k_y+G_y)^2 + (k_z+G_z)^2 \right|$$

$\hbar = m = e = 1$ $\quad a_1 = 0.529a$ $\quad a = \frac{a_1}{0.529}$ $\quad 1Ry = 13.6$ eV

$k = 0$ $\quad k_x = \frac{0.4\pi}{a}$

Band	$G.a/2\pi$	E(000)eV	$E(k_x00)$eV
1	000	0	0.97
2,3	100,$\bar{1}$00	24.27	15.33
4,5,6,7	010,0$\bar{1}$0,001,00$\bar{1}$	24.27	34.95

The plotted graph in first Brillouin zone is shown in Fig. 1-11

Chapter 3

Apparatus and Experimental

3-1 Basis of Design

The formal requirement of secondary electron emission spectroscopy can be stated as follows:

i) An appropriate ultra high vacuum (UHV) environment ($\sim 10^{-10}$Torr) to eliminate or reduce surface contamination to an acceptable level for a sufficient period of time to conduct the experiment.

ii) The generation of an energetically well defined electron beam directed on to a solid target.

iii) The subsequent detection and energy analysis of the resultant emitted scattered electrons.

3-1.1 Vacuum

The vacuum requirements for SEE spectroscopy vary over several orders of magnitude, depending on the reactivity of the surface being examined. At a pressure of $\sim 10^{-9}$Torr, approximately one monolayer is adsorbed on the surface in $\sim 10^{3}$ seconds for a sticking coefficient of unity.

With the exception of clean metal surfaces, the sticking coefficient is normally much less than unity, and the vacuum requirements can be correspondingly less stringent. Similarly metal surfaces which have been exposed to the atmosphere are often covered by a thin oxide layer which is highly unreactive. In many cases, UHV is not required for surfaces of practical industrial interest. However, to study the chemical and

physical properties of a given surface for example a pure metal, a UHV environment is necessary which may be produced by one of several standard techniques, for example ion pumps and sorption pumps, or very carefully trapped diffusion pumps using special fluids such as polyphenyl ether; otherwise hydrocarbons pump oil are efficiently cracked by the incident electron beam and a carbon layer can accumulate over the area of spectroscopic examination.

3-1.2 Electron Beam

Electrons are particles reasonably easy to produce in sensible intensities for experimental work using standard electron guns and are easily focussed into beams and the energy can be varied by applying appropriate potentials. Electrons have an inelastic mean free path in a solid of only a few Å, depending on the energy and momentum of the electron and are therefore characteristic of interactions near, or on the surface.

The characteristics of the electron gun used in the present study to produce a focussed beam were described in detail by many authors, e.g. Marton (1967), it was a commercially manufactured electron gun (see Section 3-2.5) capable of producing a high intensity moderately well focussed beam about 50 μA into an area of about 1mm. For a better focussed beam, guns are available, but one was not required for this study since the surface was not being scanned.

3-1.3 Analyser

The gridded retarding-field-analyser (RFA) electron spectrometer is one of the most widely applied types of

spectrometer. It is used in planar, cylindrical, hemispherical and spherical geometries. The attractive features of the analyser seem to be its inherent simplicity, and particularly in spherical form, its high luminosity and, in the case of the present study, its inherent advantages at low energies of the order of a few electron volts. It is not, however, generally used in situations where resolutions greater than a few tenths of a percent are required, and the fact that integral spectra are generated has precluded its application under circumstances where the radiated spectrum has a low signal-to-noise ratio.

Application of the spherical-grid RFA spectrometer has been discussed by Weber and Peria (1967) and Palmberg (1968). Taylor (1969) has developed a detailed analysis of the various arrangements, and concluded that the resolving power of the analyser was limited by grid penetration effects. As Palmberg points out, these effects are particularly severe in the "three grid" optics as used by Weber and Peria, where the single retarding grid is surrounded by grids at relatively high positive potential. Palmberg's solution was to operate two retarding grids in parallel, so-called "four grid" optics, which resulted in a higher resolution.

The large angle of acceptance allows the grids to collect all secondary emission and obviates the need for an electron multiplier, a collector being used instead. Subsequently, this system can, if desired, be employed in conjunction with LEED measurements.

There are several alternatives to "gridded " RFA analysis,

some of which are:

(i) the cylindrical mirror analyser, Blauth (1957). A comprehensive description of this analyser is reported by Singh (1976) and Palmberg et al. (1969).

(ii) the spherical sector electrostatic analyser, Aston (1919). A more detailed account of such analysers can be found in Purcell (1938) and Kavei (1977).

(iii) spherical sector-uniform-magnetic analyser, Purcell (1938).

3-1.4 Detection Circuit

The detectors used in spectroscopy produce small electrical signals which must be amplified before they can actuate recording instruments. Electrical noise which originates in the detector, and in the first amplifier stage, is amplified along with the signal and this noise sets a limit to the usable gain of the amplifier; the usable gain, or what is equivalent, the signal-to-noise ratio, may often be increased by modulating the signal at some arbitrary frequency and then passing the resulting AC signal through a narrow-band amplifier tuned to the modulation frequency. The noise power, which is proportional to the amplifier bandwidth is thereby reduced at no cost, or at most, small cost. Noise sometimes may be reduced still further by choosing the modulation frequency in a range where the detector happens to have a low noise output.

A narrow-band amplifier followed by a lock-in detector (also called a synchronous detector, or phase-sensitive detector (PSD) constituted a lock-in amplifier (LIA). The lock-in detector is a circuit which responds selectively to that part of the incoming signal which is coherent with (i.e. has the same frequency and phase as) a reference signal derived from

the modulation oscillator.

An advanced version of the lock-in detector circuit, in addition to producing the simple mode spectroscopy, makes it possible to obtain the derivative of the analysis pulses, which permits high sensitivity and noise reduction.

3-2 Construction of the Apparatus

3-2.1 Introduction

The major constituent parts of the RFA type spectrometer such as UHV chambers, ion pumps, LIA, electron guns, power supplies and X-Y recorder were available at the beginning of the research. However, progress in research and equipment specification over the past few years motivated a number of system alterations. A series of improvements have been incorporated to obtain increased performance of the apparatus, and to give improved experimental results for the chosen surface.

The spectrographic methods used to obtain more information are based on AES, CEEL and SEE yield spectroscopy which can, in certain circumstances, lead to a consequent detection of the lateral structure of the crystal surface. For each individual investigation, the particular method employed will be described.

3-2.2 Fundamental Aspects of the Apparatus

Plate 1 gives an overall view of the complete experimental system. Regardless of electronic combination, Fig. 3-1 shows a block diagram of the SEE spectrometer, with the constituents of the system also noted. The particular parts which

Plate 1

The Experimental Apparatus Fig. 3-1

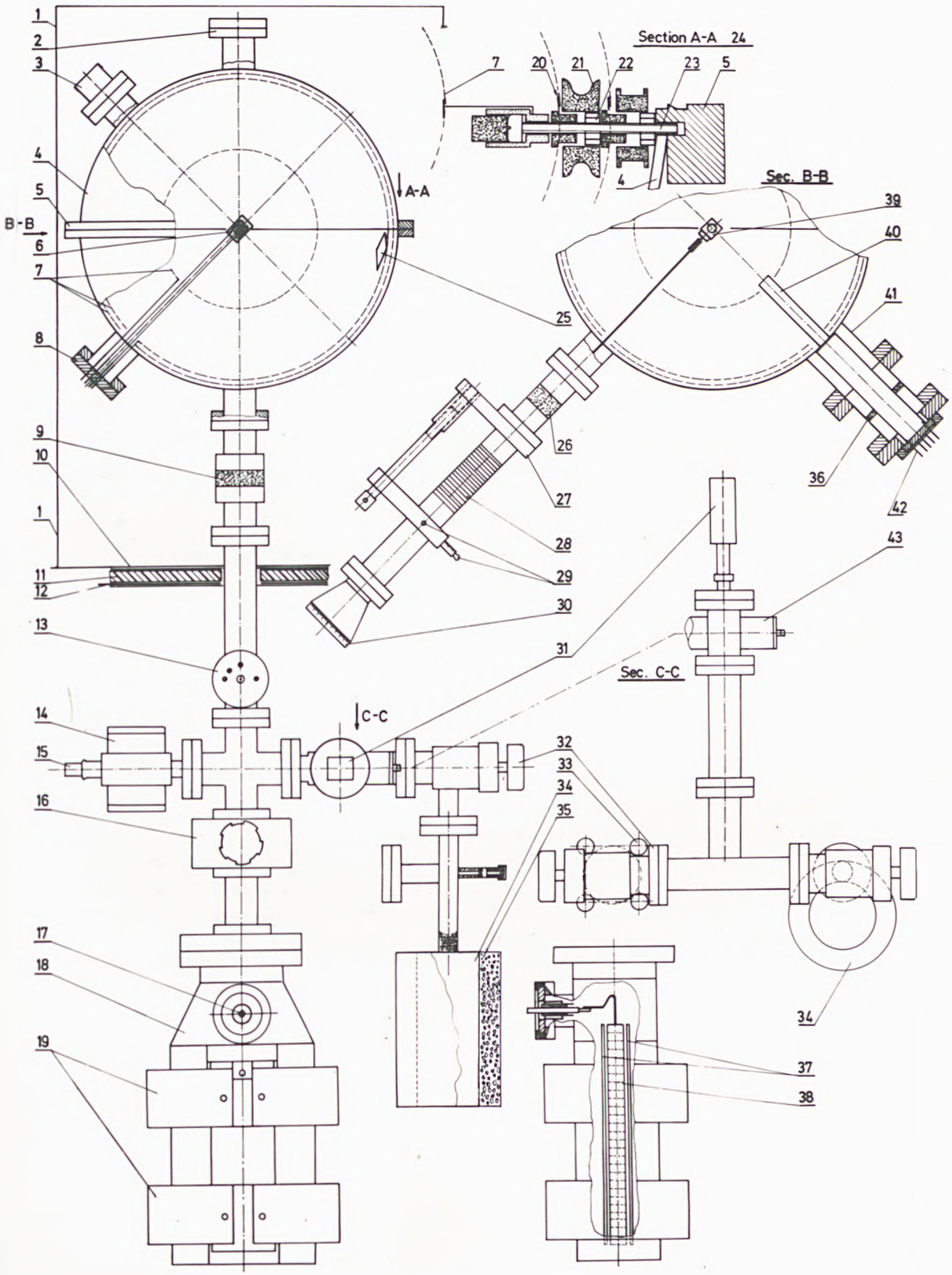

For label description see next page.

Scale ~ 1:3·6

Label description for Figure 3-1

1 - Aluminium cover for magnetic and radio frequency shielding
2 - Gas inlet port
3 - View port
4 - Chamber and Collector
5 - Flange
6 - 1000 W heater element
7 - Grids
8 - Grids and heater feed through flange
9 - Insulator
10 - Aluminium base plate
11 - Asbestor (base)
12 - Netic & Conetic magnetic shielding materials above and below the asbestor sheet
13 - Ionization guage head
14 - Ion pump magnet
15 - Ion pump (AEI P8)
16 - Isolation valve
17 - High voltage terminal for Ion pump
18 - Ion pump (FJD 50)
19 - Ion pump magnet
20 - Hemispherical Grid equatorial joint
21 - Sintox (Alumina, ceramic insulator)
22 - Nut to fix grids in position
23 - Grid mounting screw

Label description for Figure 3-1, continued

24 - Scale exaggerated
25 - Mirror
26 - Insulator
27 - Z direction displacer
28 - Bellows
29 - Vernier X,Y direction displacer
30 - Rotary motion drive

(27–30: manipulator)

31 - Pirani guage head
32 - Fore pump valve
33 - Sorption pump consisting of 16 off 230 x 20 mm tube filled with moleculatr Sieve
34 - Sorption pump with different construction
35 - Molecular Sieve
36 - Insulator
37 - Ion pump anodes
38 - Ion pump cathode
39 - Target holder
40 - Electron gun collimator
41 - Electron gun port
42 - Eight leads, and instrumentation feed through flange (for electron gun)
43 - Bakeable valve fore vacuum and chamber isolator

necessitate explanation are listed below; details of the construction of the main vacuum chamber can be found in Wright (1972).

3-2.3 Pumping System

Pumping of the system was carried out as follows: Rough pumping to 10^{-3}Torr, achieved by using a molecular Sieve sorption pump (the Sieve is a processed mixture of oxides of Al and Si, which has a very high surface area to weight and volume ratio). This ensures cleanliness from oil contamination which may come from mechanical fore-pumps.

Subsequently, UHV was obtained by use of combination of Getter Ion Pump FJD50 and AEI P8, and the usual baking procedures carred out on the main chamber. The pressure fell to $\sim 3 \times 10^{-10}$Torr.

Periodically it is recommended by the manufacturer that the Titanium plated (cathodes and anode) should be surface cleaned. In the present case, this surface cleaning was carried out by glass bead blasting the plates, and after that a good performance of the FJD50 ion pump was achieved. For cases of severe contamination, the manufacturer (Varian) has suggested a chemical cleaning procedure may be necessary, which can be seen in Appendix 1.

Some difficulties were experienced in starting the ion pumps and a bakeable valve was placed just above the FJD50 ion pump, isolating the pump from the whole system. This arrangement has two advantages:

1) Continuous operation of the ion pump which save starting

time and baking of the ion pump

2) The pre-vacuum necessary for ion pump operation, in an order of $\sim 10^{-2}$ Torr higher.

The apparatus was baked in an oven up to approximately 300°C. The oven used was constructed using a Dexion frame (72 x 60 x 60 cm) and was covered with a sandwich layer of wire mesh, Al foil and ceramic wool. Four 850 W heaters were distributed within the structure as evenly as possible.

3-2.4 Leak Detection

Leak detection was sometimes necessary, and accomplished by using a 20th Century mass spectrometer leak detector based on Helium. A number of leaks caused problems during the research. One particularly difficult leak, which involved much corrective work, was ultimately traced to a valve sealing fault in the bakeable valve, which had been used to separate the fore pumps from the system. To trace this problem the whole apparatus was dismantled.

3-2.5 Electron Gun

An electron beam, whose energy may be varied from a few hundred eV to some keV, was generated by an electron gun. A commercially made electron gun (Superior - 3K/5U) was used in the present experiment. This electron gun had an indirectly heated oxide coated cathode, Type KA809F, and the heater was type E7291 (Superior, U.S.A.), with a characteristic of 6.3 V, 0.6 A. The cathode was coated with barium and strontium oxide and if the cathode is exposed to the atmosphere, it is essential that the temperature (voltage) be raised steadily. In addition, the pressure should not exceed 5×10^{-9} Torr.

At a heater voltage of 6.3 V, the oxide matrix has no emission and requires some degree of chemical activation before it can become an emitter cathode, Jones (1963). This activation may be accomplished by the "flashing technique", i.e. by frequently raising the voltage to 7.2 V for 1.5 minutes, at 30 minute intervals.

The electron gun was shielded by a stainless steel tube "electron gun collimator", as shown in Fig. 3-1, for the purpose of preventing stray electrons reaching the detector. The electron gun element wires were spot welded onto an eight lead instrumentation feed through (TD/C8 12 Ferranti) flange. The filament supply (6.3 V, 0.6 A) was derived from a Farnell L30F power supply, floated up at the cathode supply voltage. The voltage for the other elements was obtained initially by means of the circuit shown in Fig. 3-2. Later, this set up was modified, and the commercially re-designed circuit was used. This device had a built-in filament supply, but because of the starting current of 0.1 A, it was not used before activation of the cathode.

The incident beam spot size was usually minimised by focussing to about 1 mm diameter on a convenient flouresecnt disc, see Section 3-2.7.

3-2.6 Retarding Grid Analyser

In AES and CEEL spectroscopy, the electrons emitted from the sample were analysed by the three grid system. The detector and grids G_1, G_2, and G_3 are spherical, with a common centre at the point where the incident electron beam strikes the sample surface.

Electron Gun Elements Voltage Supply Diagram

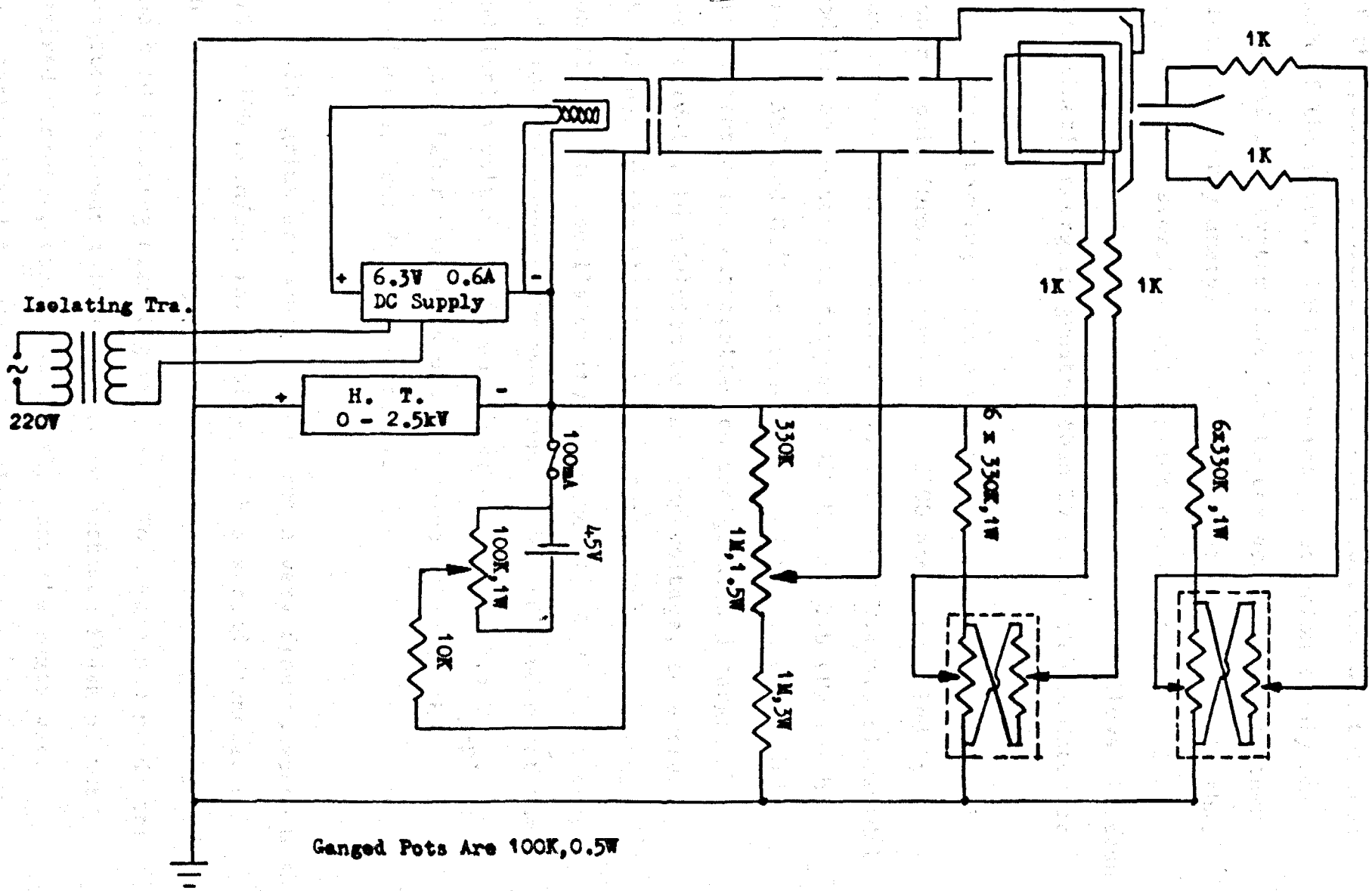

Fig. 3-2

The inner grid was at earth potential, so that the specimen was in a field free space. The retarding grids were strapped together to help reduce the effect of penetration of the positive voltage, on the collector, through the open mesh of the grids. This potential penetration simply makes the three grid system inferior to the arrangement of other electron energy analysers. The implication of this is that any hole or distortion on the grids can cause severe loss of resolution. A potential of -V on the grids allows electrons with kinetic energies greater than eV to reach the detector.

The retarding voltage was supplied by an operational power supply (OPS), (Kepco - OPS 2000 and controlled by a function generator FG 100). A small ($\sim$4V r.m.s.) sinusoidal modulation voltage of frequency 350 Hz and 2.6 kHz in the case of AES and CEEL spectroscopy, or 6 kHz in the yield measurement case, was applied to the grid, and target respectively, in addition to the ramp voltage, to extract the signal by the LIA (Brookdeal 9501). This voltage was supplied by an oscillator (type Brookdeal, 5012). The shape and width of Auger peaks was found to be independent of the modulation voltage up to an r.m.s. value of $\sim 2.5\ V_{p-p}$. Voltages higher than this optimum value affected the resolution, (see Results Section).

The grids are usually made from a very fine tungsten mesh (100 x 100 mesh/sq. In. density, with a strand diameter of 10^{-3} In). In cleaning one of the grids was damaged because of the bead blasting cleaning process. To make a new grid, the tungsten mesh was laid over a round-bottomed flask of the desired diameter, stretched tightly, and the edges were temporarily fixed to the flask surface. A 6 mm nickel strip

was formed into a ring, whose diameter was fractionally greater than that of the flask, and was placed exactly at the equator of the flask. The mesh was then spot-welded onto the ring, using a hand welder. This ring was then located on the flask by welding on wire retainers and the unwanted part of the mesh was removed. To preserve a spherical shape of the grid when removed from its former, it was necessay to lightly electroplate it. The overall transparency of a finished grid was about 80%.

3-2.7 Target Preparation

For an initial calibration of the system, the sample was a piece of Al (25 x 25 x 2mm) held at the end of a rod with the other end connected to a manipulator. The low energy section of Auger, taken for this purpose can be seen in Fig. 3-3. A commercially made rotary motion drive (Vacuum Generator, RD 1, see Figure in Appendix 2) was used to enable the sample to be rotated through 360^{o}. It was also possible to move the sample in all three planes (X, Y, Z) by means of a Keele workshop-built manipulator. This was not too essential for the experiment, because the sample was accurately lined up with the electron gun collimator. The beam could scan on the entire target by use of the electron gun deflectors.

In the experiments on antimony, because of the differing analytical requirements, the sample was mounted on a holder as shown in Fig. 3-4.

To ensure accurate beam alignment and focus on the target, a small disc shaped flourescent screen was placed on

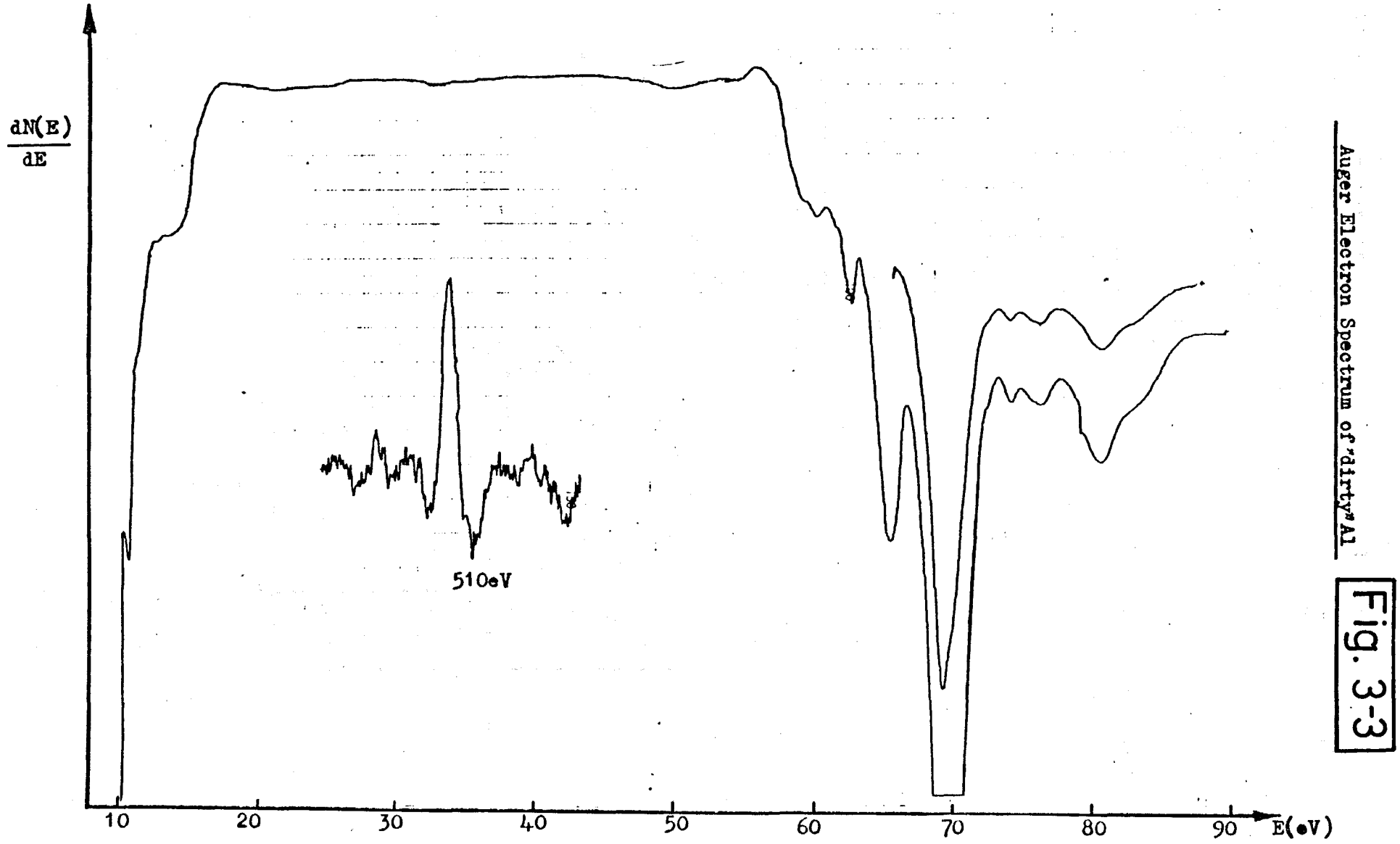

Auger Electron Spectrum of "dirty" Al

Fig. 3-3

Target Holder

Fig. 3-4

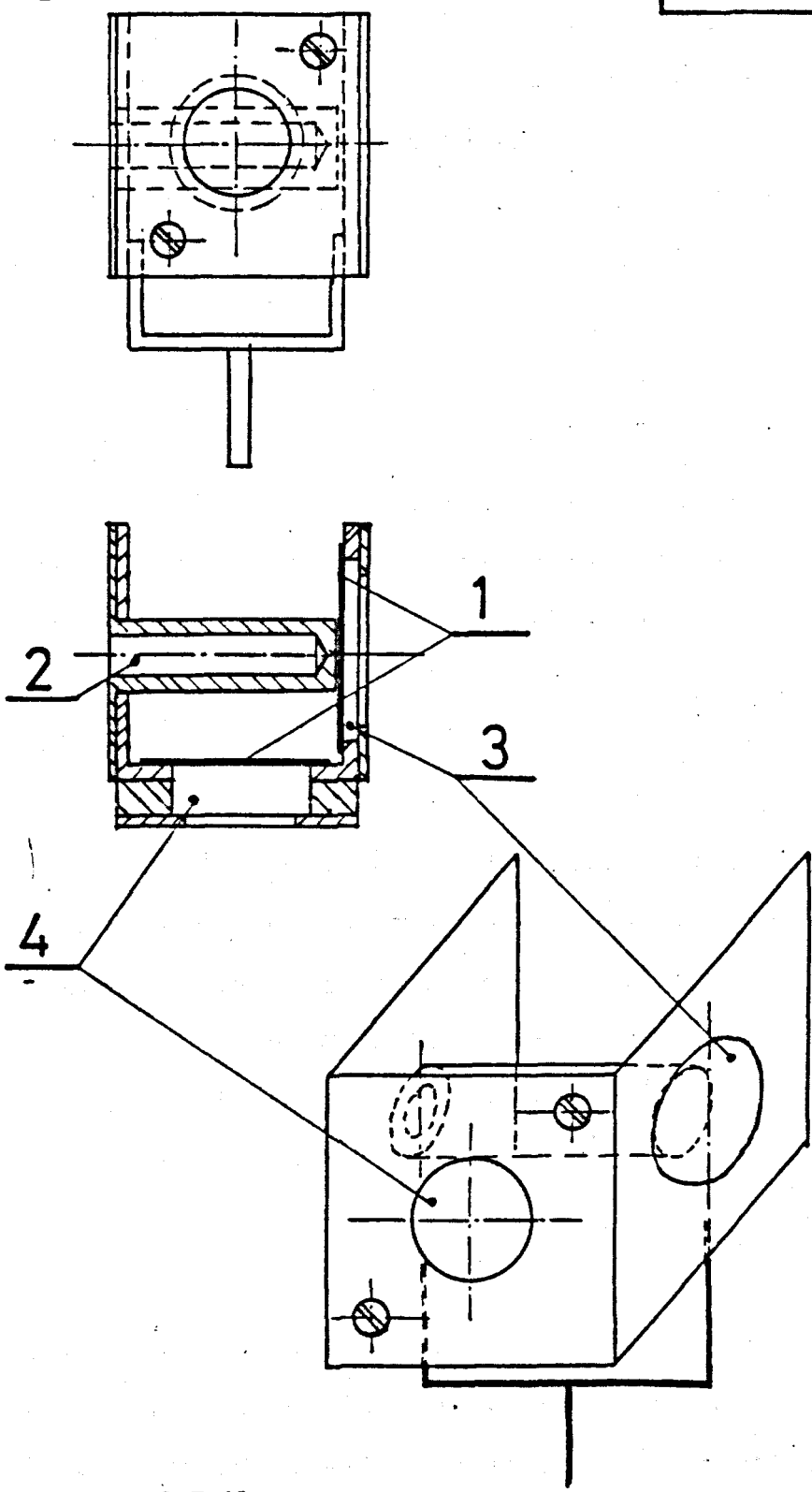

1 - Nickel Foil

2 - Faraday Cup

3 - Fluorescent Screen

4 - Sample

one side of the holder. When the flourescent screen was used to view the focussing, the beam width was adjusted to give a spot size of 1 to 1.2 mm. Such a spot size was necessary in order to obtain reasonably high resolution spectra. Spectra obtained with a diffused beam were found to have poor resolution. Due to the fact that direct viewing of this screen was impossible, (see Plate 1), a well polished stainless steel mirror was strategically placed to enable viewing of the screen through existing ports, see Fig. 3-1.

The flourescent screen consisted of a ceramic disc (12 x 1 mm) which had been immersed in a solution of a flourescent chemical (Zinc-ortho-Silicate Zn_2O_4Si activated with Mn) suspended in distilled water. A thin layer (0.1 to 0.2 mm) of Zinc-ortho-Silicate was deposited on the disc.

In addition, the holder also contained a Faraday cup. This Faraday cup is a stainless steel block and has a 3 mm diameter hole of 15 mm depth, (Henrich (1973)). The cup was coated with "Gold black" to minimise unwanted secondary electron emission. The beam strikes the sides of the hole at grazing incidence. The combination of grazing incidence, poor secondary emitting surface, and large depth-to-diameter ratio, make it an excellent absorber for electrons. If all the primary beam current (i_p) is absorbed by the Faraday cup $i_p = i_T$, $i_s = 0$, (where i_T is target current, and i_s is the secondary emission electron current) and the yield is zero ($\delta = \frac{i_s}{i_p} = 0$). When the retarding voltage applied to the Faraday cup was more negative than the electron gun cathode, however, none of the electrons can land on the target $i_t = 0$, and $\delta = 1$. By knowing these two points

(δ =0, and δ = 1), the scale of the yield spectra has been calibrated. A photograph of the recorded graph, which shows the scale of the yield, was produced and is shown in Fig. 3-5. Immediately after this, the yield spectrum was taken and is illustrated in Fig. 4-15. In case there was any change in the experimental conditions, (e.g. angle of incident beam, modulation voltages, frequency of modulating signal), the scale was monitored.

3-2.7a Gold Black Coating Using Speed Vac 6E4 Coating Unit

The unit was allowed to pump down at stand-by according to the manufacturer's recommendation. While it was running, the Faraday cup was mounted some 5 cm above the Tungsten wire basket containing the gold wire. The chamber was then pumped down to 10^{-5} Torr. Argon was bled into the chamber using the needle valve controlled gas inlet, until the chamber had been flushed. The pressure, at this stage was $\sim$0.5 Torr. Evaporation of the gold under this pressure of argon produced a gold black coat covering the Faraday cup. Several attempts were made in order to obtain the optimum pressure of argon in the chamber, to produce a satisfactory result, Thomas and Pattinson (1969).

3-2.7b Specimen Preparation

The sample was a 10 x 1.5 mm disc of antimony (100) crystal supplied by Metal Research Ltd., (Cambridge, England). A surface of the disc was ground on wet 15 μA abrasive paper and polished with grade A diamond paste to within the desired crystal plane. Then it was ultrasonically cleaned in distilled water. Later the disc was electrochemically cleaned in a recommended solution of 30% hydrochloric acid in distilled

Yield Scale Calibration Curve

Fig. 3-5

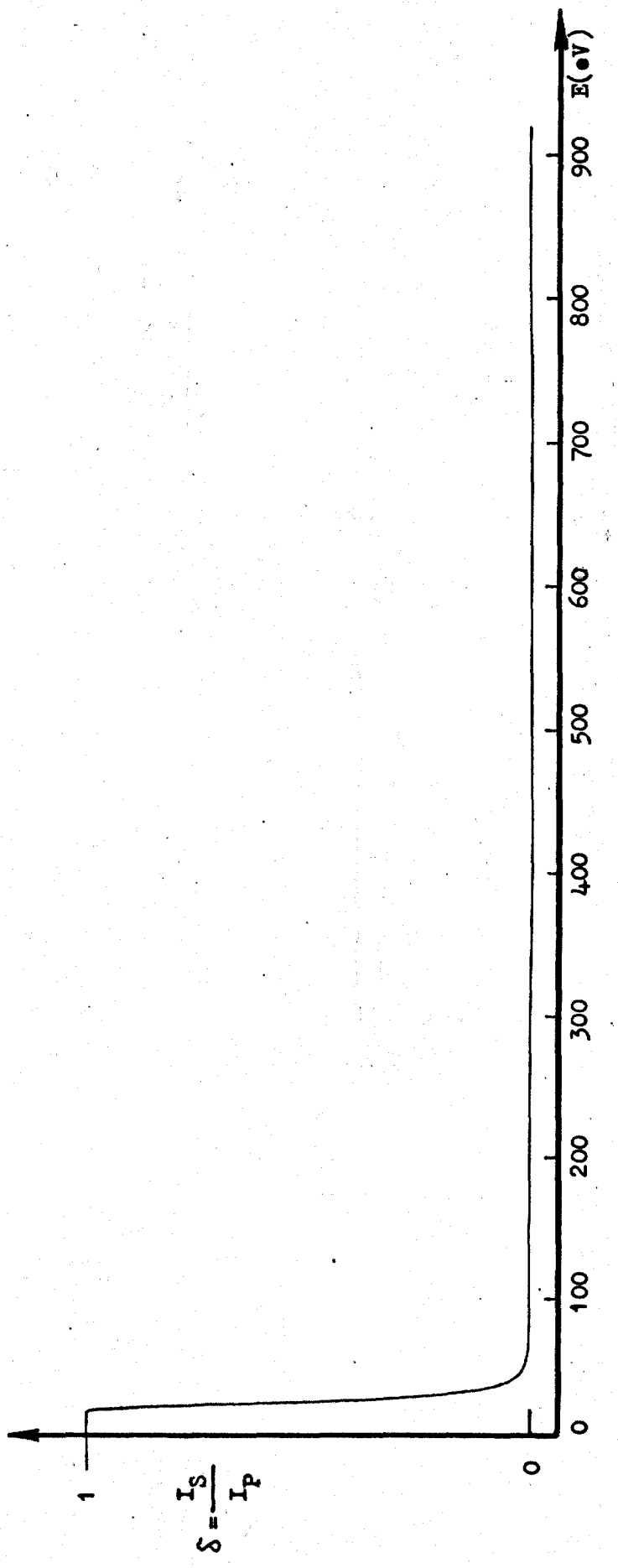

water with 5% hydrogen peroxide for 5 minutes, Smithells (1955). Finally the disc was washed in distilled water immediately before mounting in the vacuum chamber. The electro-chemical operation removes most of the damage introduced by mechanical polishing and leaves a relatively thin layer of oxide on the surface, (see below). The residual oxide and other contaminations were then removed by electron bombardment. This electron bombardment was carried out by a projection lamp filament of 1000 W used as an electron emitter, and with a high positive voltage on the disc. The high voltage caused the emitted electrons to hit the sample at high speed and causing local heating thus removing several surface layers of atoms.

Due to the proximity of the projection lamp filament to the sample, extended operation (in excess of 2 to 3 hours) evaporated the copper and aluminium targets that were intended for calibration use. Consequently, the Sintox (alumina insulator) ceramic which held the grids in position were covered with a thin layer of both metals, and became conducting. These then had to be disassembled and cleaned with nitric and hydrochloric acids respectively, but still proved unsatisfactory. New ceramics were fitted and an aluminium sample (25 x 25 x 2) was mounted for calibration purposes.

When the antimony disc was placed in the chamber, electron bombardment was necessarily carried out with the projection lamp operating at (~27 V, 2 A , AC) and also a high voltage 3.1 kV applied to the antimony disc. Unfortunately, after one hour, because the evaporating point of antimony is almost the same as that for Al, the Sb crystal disc was evaporated completely, and thus was lost. However, in case of any

possibility of conduction (however slight) the Sintox supports were modified as in Fig. 3-1.

The new antimony crystal took the form of a (10 x 4 mm) disc, which was supplied by the aforementioned company. The sample was mechanically polished as described previously, and then ultrasonically cleaned in distilled water. Subsequently, it was chemically etched for two minutes in a solution of 5 parts concentrated H NO_3 (% 69 minimum), 1 part HF, 6 parts of H_2O at room temperature and finally washed in distilled water. This procedure was recommended by Jona (1967) and was much more effective than the first, this being clear from the surface appearance. Plate 2a shows the specimen surface before polishing with magnification of 320, and Plate 2b is the specimen surface after polishing, with magnification of 650. The appropriate time for electron bombardment was 10 minutes at (27 V, 2 A, AC) across the filament, 3.1 kV applied on the disc with the current on the target being 0.6 A. In the experiments, electron bombardment as described above was found to be the only cleaning process necessary.

3-2.7c Surface of Metal after Mechanical and Electrochemical Polishing

Many investigators stress a single characteristic, and either ignore or underestimate the importance of other parameters. This may lead to incorrect conclusions concerning the properties of metallic surfaces. For instance, the work function of a surface in any medium is markedly affected by the method of surface preparation. The mechanical, electrical, magnetic, optical, catalytic, and other properties of a metallic surface also depend to a great extent on the state

Plate 2

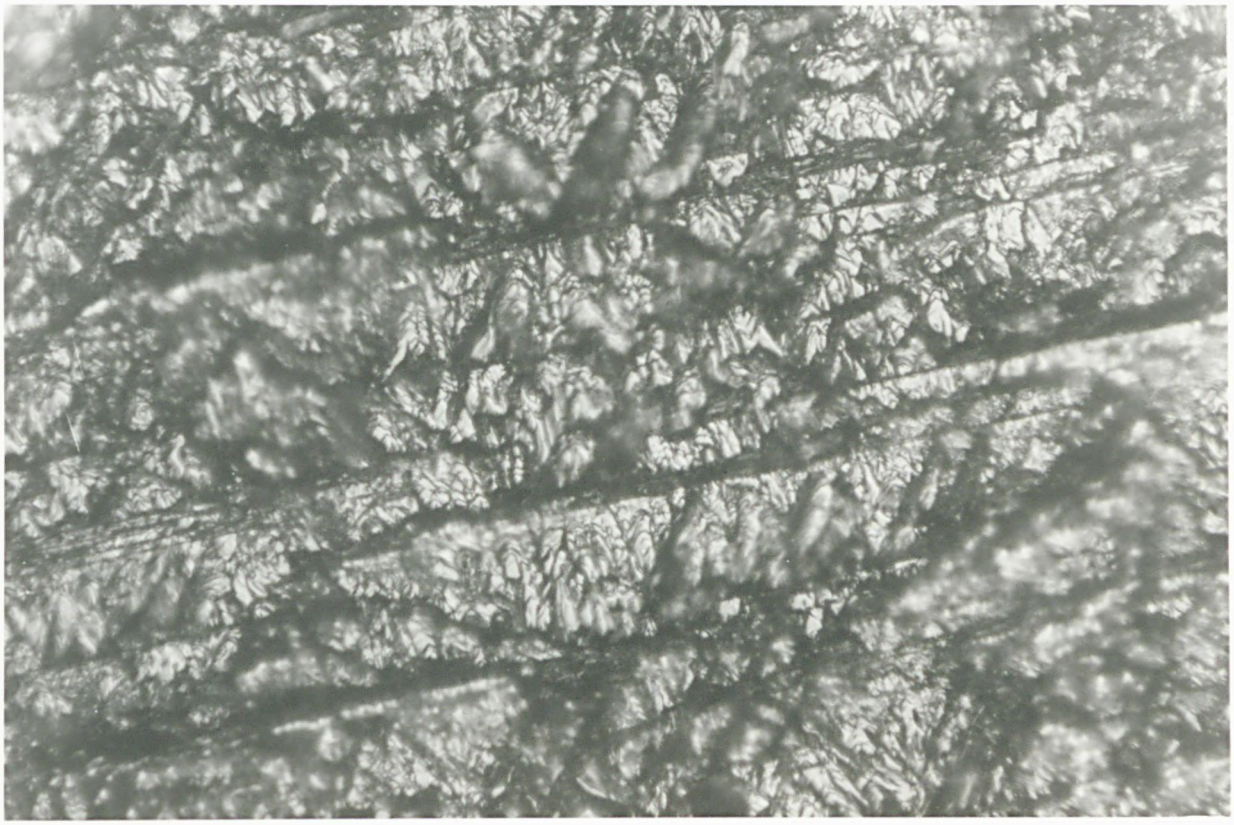

a) Specimen surface before polishing with magnification of 320

b) Specimen surface after polishing with magnification of 650

of the surface.

Beilby (1921) has shown that the outer surface of mechanically polished metal differs markedly in its structure and properties from the underlying layers. This is attributed to the fact that, as a result of the mechanical forces acting during the polishing, the upper layers of the crystalline lattice are destroyed or deformed, and moreover, the surface of the metal is contaminated with abrading particles. In addition, the friction has some thermal effects which accelerate the oxidation of the metal (by oxygen from the air) and which in some cases lead to surface re-crystallisation, and a consequent change in the surface structure. Thus, mechanical polishing produces non-uniform (from the stand-point of their physical and electrochemical properties) surface layers.

The thickness of the deformed "amorphous" layer, known as the Beilby layer, on mechanically polished metals may reach tens of microns, depending on the method of polishing. Indeed, the outer surface layer of mechanically polished metals consists of very fine crystals (sub-micro crystals).

Mechanically polished samples have surface layers of heterogeneous (and complex) chemical composition. The exact composition depends on the surface micro-geometry and structural characteristics on the nature of the metal and on the polishing technique used.

Electron diffraction studies of mechanically polished metal surfaces have confirmed that in all cases in which the polishing was carried out in the presence of air or moisture

is left an oxidised surface, Kranert and Raether (1943).

Electro-polishing removes the outer deformed layer and reveals the true structure of the metal. However, electron diffraction studies have shown that oxide films are also present on electro-polished surfaces. Nevertheless, in certain baths, and under carefully controlled conditions, surfaces are left oxide free, Kranert et al. (1944).

In many cases, electro-polishing improves the mechanical properties, since it removes surface peaks or cracks, as well as surface stresses and strains.

3-2.8 Detection System

The electrical signal from a detector can often be small, as to be comparable with the electronic noise from the first section of the amplifier. This is especially important for low energy particles in the eV - keV region. Consequently, a discussion of detectors is incomplete without a discussion of an appropriate amplifier and electronic detection unit.

3-2.8a Detection Mode

Spectroscopic methods of material analysis are based on the emission of particles (in this case, electrons) with characteristic energies from the excited material. Electronic differentiation by synchronous detection methods enhances the sensitivity of the detection and reveals the spectral features which are not readily observed by more direct measurements. Since the background is relatively uniform, it will not contribute to the $\frac{dN(E)}{dE}$ and therefore the signal is small, except at regions where Auger peaks appear. In fact the

presence of a large background of inelastically scattered electrons contributes to peak broadening, and can mask weak peaks. The Auger and characteristic energy loss emission of antimony were detected in the first derivative mode, whilst those of the yield were taken in the normal mode.

3-2.9 Auger and Characteristic Energy Loss Detection

The electronic equipment necessary to monitor and differentiate the energy distribution is shown in Fig. 3-6.

In operation, the retarding grid potential was swept at a slow rate between zero and E_p , where E_p is the primary electron energy. A small retarding signal at a frequency f was superimposed upon the sweep voltage by means of an isolating transformer with a ratio of 1:1 (700 turns of a 0.5 mm diameter varnished copper wire sandwiched between the two Mullard (Vinkors) pot-core formers from the 45 mm range). The construction of the transformer was such as to withstand the necessary high voltages ~2 kV. Consequently, the collector current contains both a component of this frequency, whose amplitude is a function of the gradient of the transfer characteristic, and a component at a frequency 2f, (of lesser amplitude), proportional to the rate of change of gradient, i.e. the first derivative of the transfer characteristic, Palmberg and Rhodin (1968). These components may be examined by using a frequency selective amplifier (i.e. LIA). However, a large signal at a frequency f will be present, due to capacitive coupling between the retarding grids and the collector and must be eliminated. This can be done, to some extent, by a fundamental frequency rejector (tuned load). The tuned load is a circuit which resonates at 2f and rejects most of

AES & CEEL Circuit Diagram

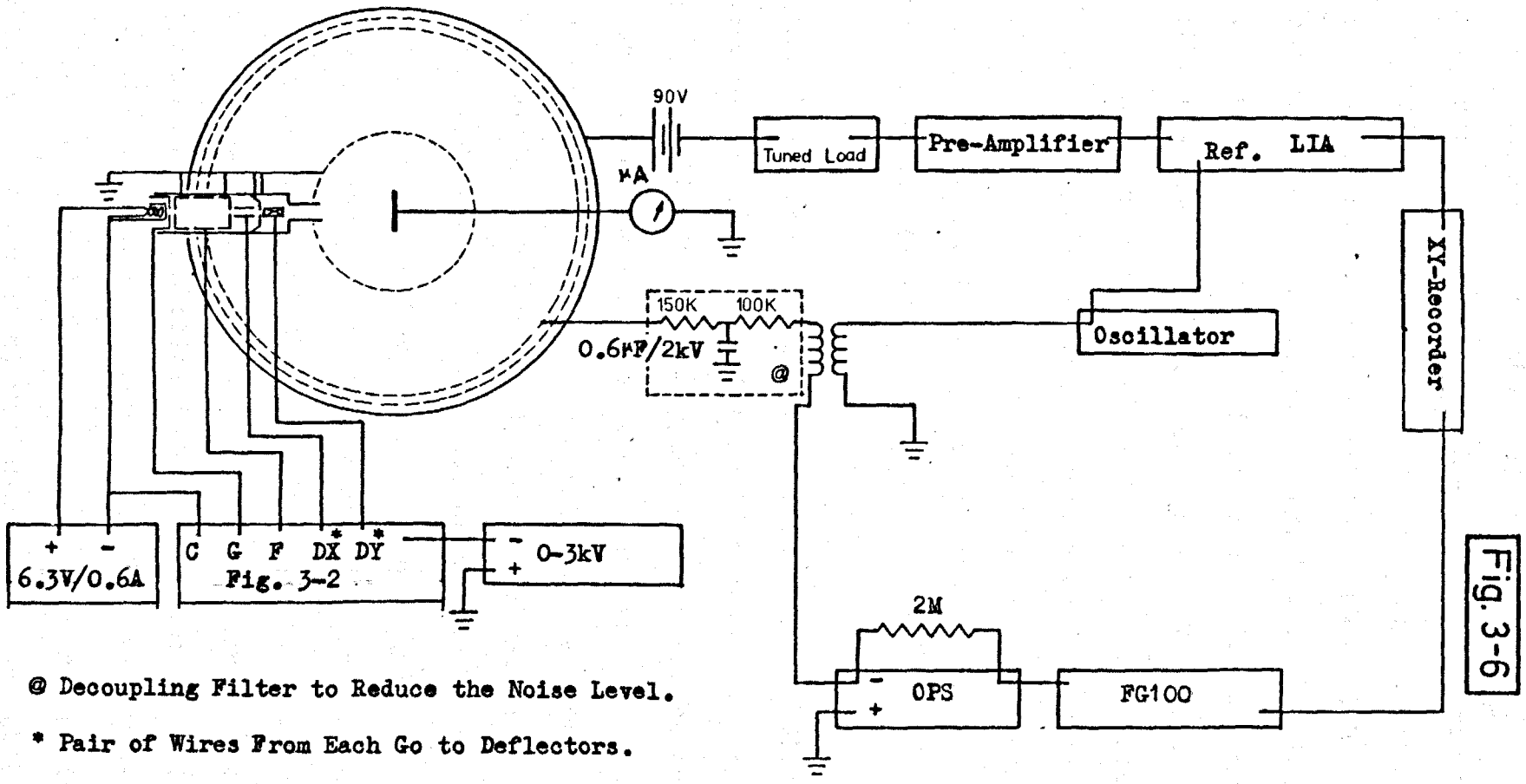

Fig. 3-6

@ Decoupling Filter to Reduce the Noise Level.

* Pair of Wires From Each Go to Deflectors.

the f as shown in Fig. 3-7. To examine the frequency effect on the signal, two tuned loads were used, one at f = 2.227 kHz with a rejection ratio of 160, and the other at f = 350 Hz with a rejection ratio of 120. These resonant frequencies were obtained when the tuned loads were coupled with the collector, which has a capacitance to earth of 500 μF. (This capacitance is not shown in Fig. 3-7). The low frequency tuned load give a greater sensitivity but with a higher noise level than the high frequency tuned load. The current sampling impedence was then purely resistive ($\sim 10^8$ ohms) which gave a good signal to noise ratio, since the recovered signal was proportional to the load resistance, whereas the noise voltage is proportional to the square root of the load resistance, Harris (1972).

The signal from the oscillator (Brookdeal 5012) was a sine wave of ~ 2.5 V_{p-p} amplitude (see results) with good frequency stability (0.1%/C° typical). The reference signal output wave form was a square wave. This ensures that there were no even harmonics in the modulating wave form which, for the Brookdeal 5012, the total distortion of which was 0.05, and for the 2nd harmonic was 0.005; this was clearly an important requirement. The signal on the collector was processed by a band pass amplifier and the detector used to measure the amplitude of the various components of this current. The band pass amplification was carried out in two stages; first a pre-amplifier (Brookdeal 5001) amplifies the signal from the tuned load, and second, the Brookdeal Lock In Amplifier (LIA) amplifies. The LIA is a combination of an amplifier and a frequency detector (frequency shift detector). In addition to amplification, the signal was

Tuned Load

Fig. 3-7

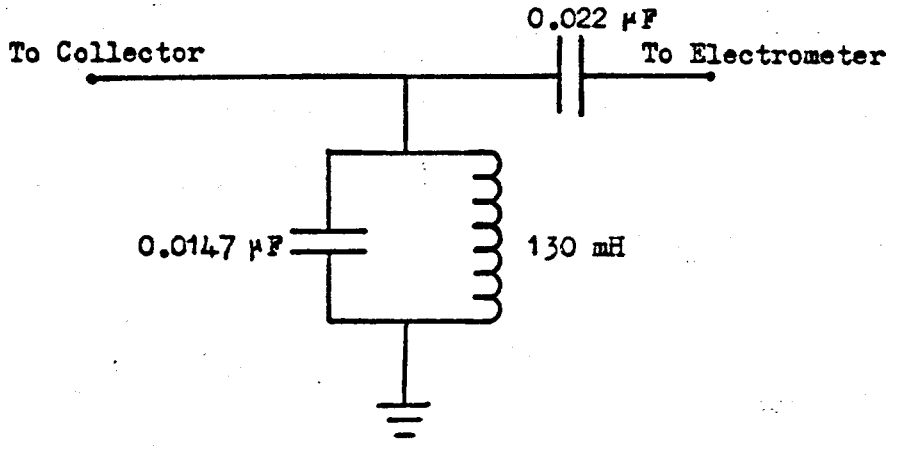

f = 2.227 kHz

$$\text{Rejection Ratio} = \frac{\text{Modulation Voltage Amplitude at f}}{\text{Modulation Voltage Amplitude at 2f}} = 160$$

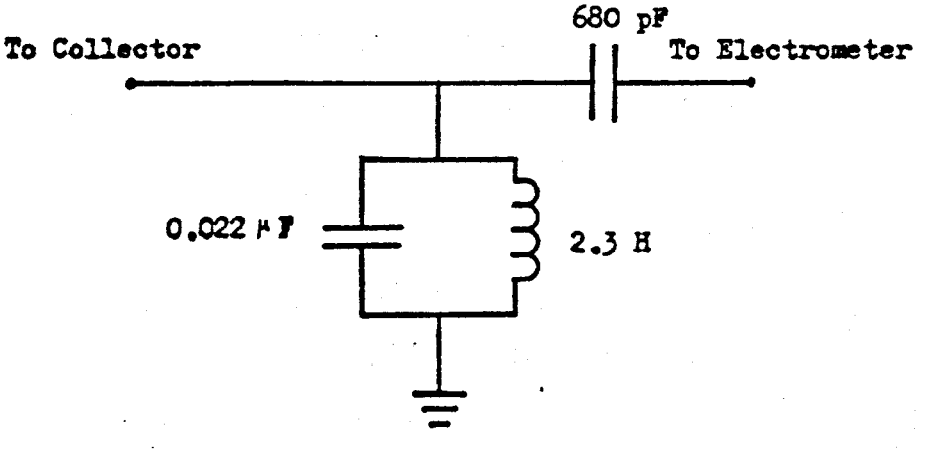

f = 350 Hz

Rejection Ratio = 120

filtered (by Brookdeal 5011 filter) to suppress the fundamental f. Hereafter, the filtered signal (largely 2f) was then amplified and detected by the LIA, allowing good signal resolution.

The output of the LIA was connected to the Y channel of the X-Y recorder to record the spectrum. The signal monitor of the LIA was connected to an oscilloscope to monitor the signals which were being detected by the PSD component.

3-2.10 Noise

The signal is a product of the combination of the true signal with spurious signals from extraneous sources. The effect of this combination is to limit the sensitivity of a detector, a fact encountered by many experimentalists, e.g. Thorne (1974), Jones (1959), Potter and Eisenman (1962) and Marton (1967).

In this work, noise was considered to have come from several different origins.

a) Fluctuations in the background radiation; the statistical fluctuations of grid current; a current decrease as the grid potential becomes more negative, or electron emission by the grid which can produce a reverse grid current. Use of the LIA in a differential mode considerably reduces these background effects.

b) The electron source itself (Flicker noise); Johnson (1925) has shown that noise is caused by the random variation in time of the emissivity of localized spots in an oxide-coated cathode, with further contributions from instabilities in the filament power supply and mains frequency pick up in the electron gun voltage supply circuit (see Fig. 3-2).

The latter was reduced by the use of the built-in-filament power supply.

c) Electrical and thermal variations in the detector; the large surface area of the detector increased the effect of thermal fluctuations, and the nature of construction and shape made the collector prone to stray field pick up. The detector takes the form of a hollow metal sphere, which, due to its external surface exposure, required elaborate external electro-static and magnetic shielding. For the above reason, the ion pump was also shielded with further shielding between the pump and the collector (chamber) effected by insertion of magnetic shields under the aluminium plates of the base table, see Fig. 3-1. The chamber electrostatic shield was an aluminium box (650 x 700 x 750 mm) with all other shields formed from high flux (Netric and Contic) magnetic shield. However, despite these precautions, there was still severe noise pick up, which limited the absolute sensitivity. There was, in addition, some earthing problems; the external (or main's) earth was sometimes inadequate for low noise work.

d) Fluctuations in the amplifying circuit, such disruptions were kept to a minimum by using the advanced Brookdeal LIA. Other electronic equipment was felt to be satisfactory in this respect. To suppress random spikes (40 mV at the OPS output), a modification at the output of the OPS was made by the use of a decoupling filter (see Fig. 3-6). At the start of the work, an ordinary low noise oscillator (Advanced Instrument SG68A) was used and to minimise second harmonic distortion, a filter was employed as shown in Fig. 3-8.

Variable Rejection Circuit f= 4·2 to 4·5 kHz Q=1

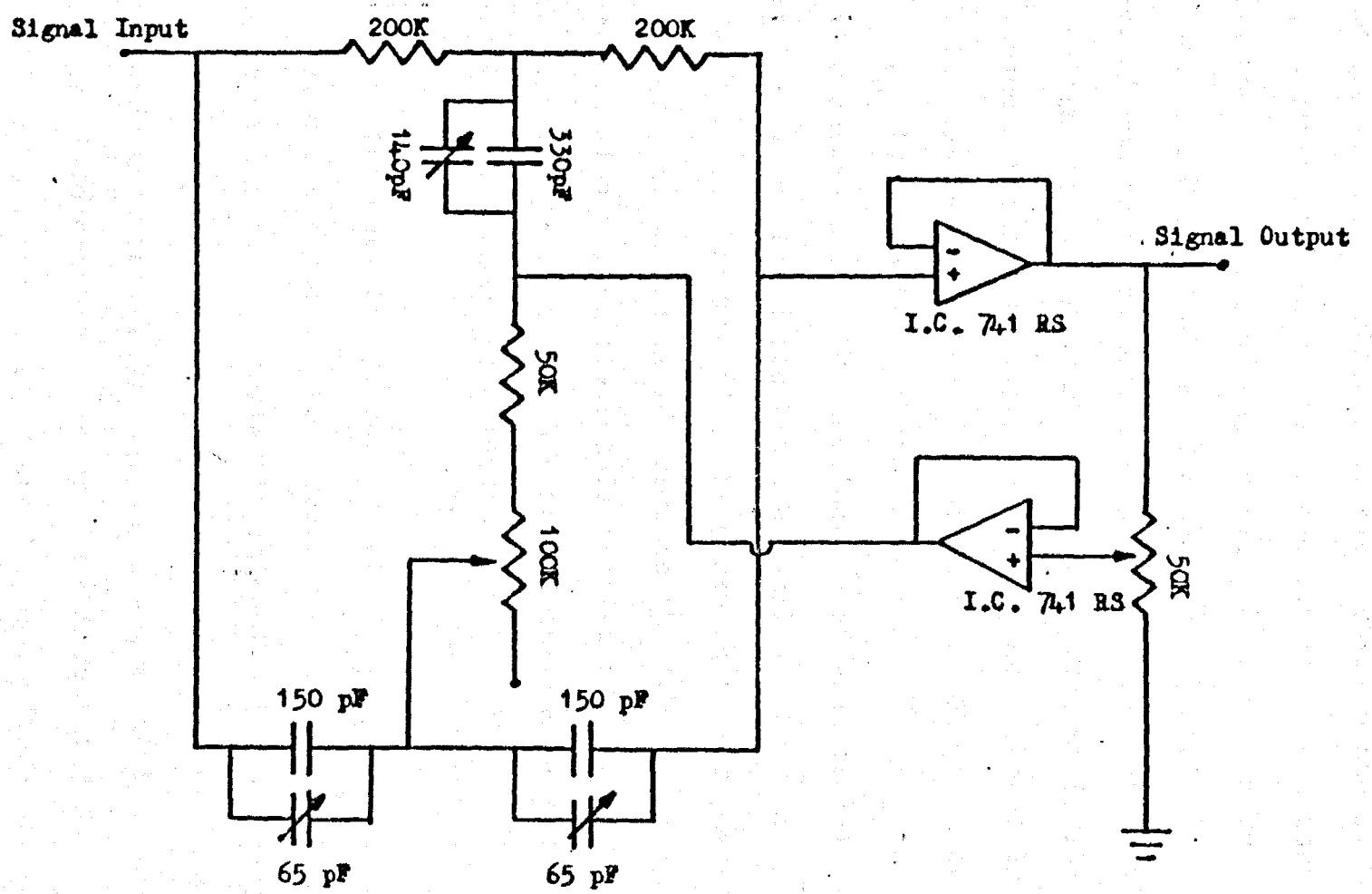

Fig. 3-8

3-2.11 Yield Measurement

Secondary electron emission spectroscopy can provide information concerning the distribution of those states in a solid that are located above the vacuum level, i.e. the unbound states. Information concerning these unbound states can be obtained from knowledge of the detected structure through the ratio, δ , of the average SEE per primary electron, termed the yield measurement as a function of primary energy. A number of methods have been used to measure yields, e.g. Bruining (1954), Henrich (1973,1975), Wright (1974) and Suleman and Pattinson (1980). In experiments, the yield, $\delta = \frac{i_s}{i_p}$ is measured as a function of incident electron energy, E_p . i_p is the primary electron current and i_s the secondary current, i.e. the combination of elastically and inelastically scattered electrons as well as the true secondaries. Some of the fine structure that is superimposed on the generally smooth yield curve in the low energy region is due predominantly to elastically reflected or diffracted electrons. The present work has been mainly devoted to studies of this special category of electrons.

Since the emission properties of a surface can change with time, due for example to surface contamination or radiation damage of the sample, it is desirable to make yield measurements rapdily. An improved circuit over that used by Suleman and Pattinson (1980) was employed, with high sensitivity for yield measurement over the entire incident energy range (0 - 1000 V) or at any desired range. The apparatus was used in junction with AES by simply operating the external detection system in the yield mode.

The schematic instrument for yield spectroscopy is shown in Fig. 3-9. Low energy electrons, i_s , are obtained by applying a negative retarding potential with a small modulating voltage ($\sim 3\ V_{p-p}$ see result) to the sample while maintaining a fixed accelerating potential on the electron gun. In this way, the retarding field serves as an additional focussing control for the primary beam, it reduces distortion of the beam due to stray electro-magnetic fields, and the primary beam current was constant for all incident energies. In the case of yield measurements by Wright (1974), these advantages have been neglected due to the electron gun being connected to the ramping voltage.

The yield was obtained from the current flowing into (elastic and inelastic reflection) or out of (elastic and inelastic emission) the target, McRae (1979). Therefore, the target current must be measured in the presence of high voltage (the current cannot be measured with respect to earth). The target current has frequency components extending all the way down to DC, so transformer insulation cannot be used. The current was too small to measure directly with a DC probe, and so a load resistor R_L was used to generate a voltage proportional to the target current, which was then amplified by a circuit as shown in Fig. 3-10. The value of R_L was optimised at 33 kΩ so that the integrated circuit amplifier was not overloaded at the maximum target current of 20 μA. Since the entire amplifier circuit floats at the retarding voltage, it was most convenient if battery powered (see Fig. 3-10) and screened cable was used throughout to minimise stray capacitance to ground. This unwanted capacitance was further reduced by adding a capacitance to the opposite

Simplified Schematic of a Yield Spectrometer

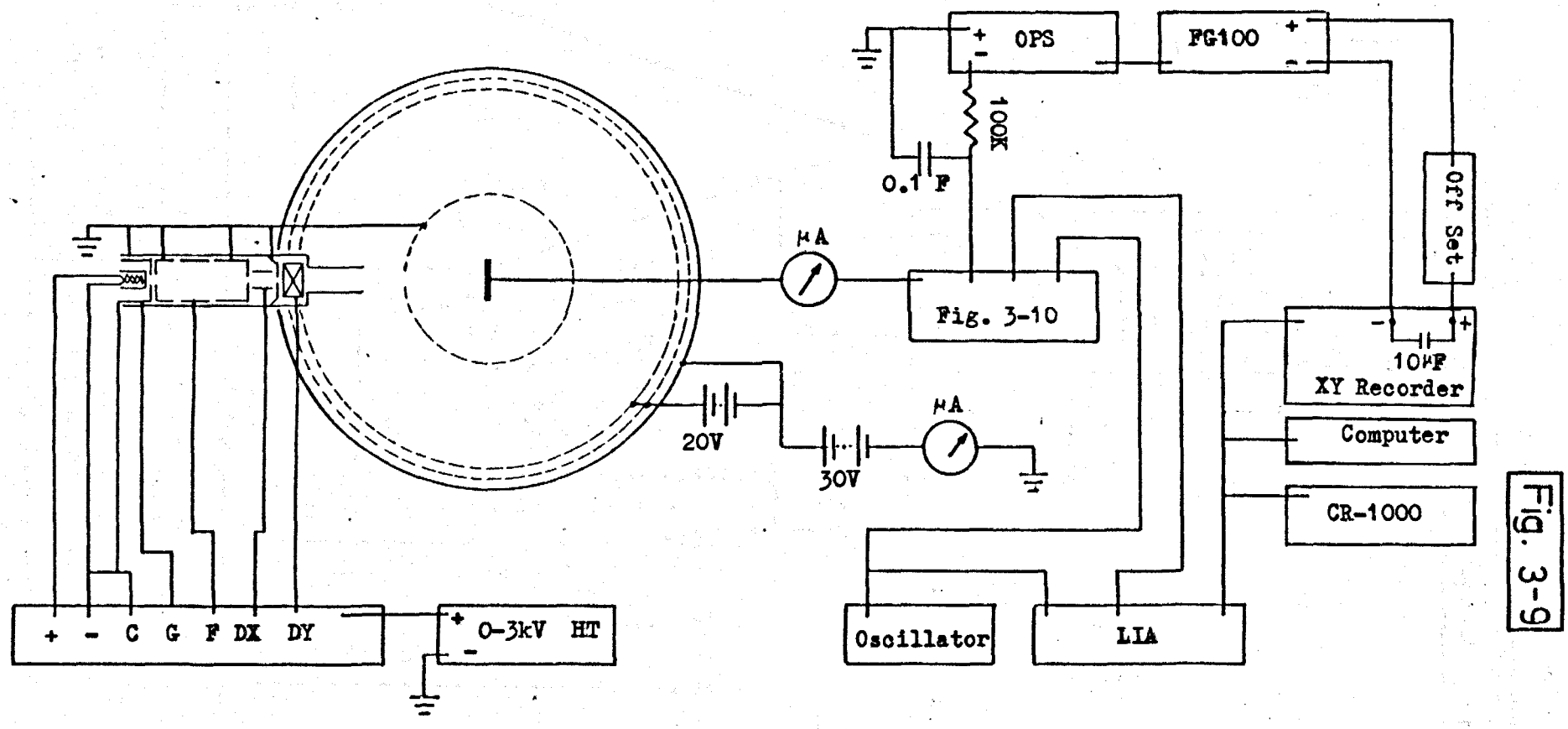

Fig. 3-9

Yield Circuit Diagram

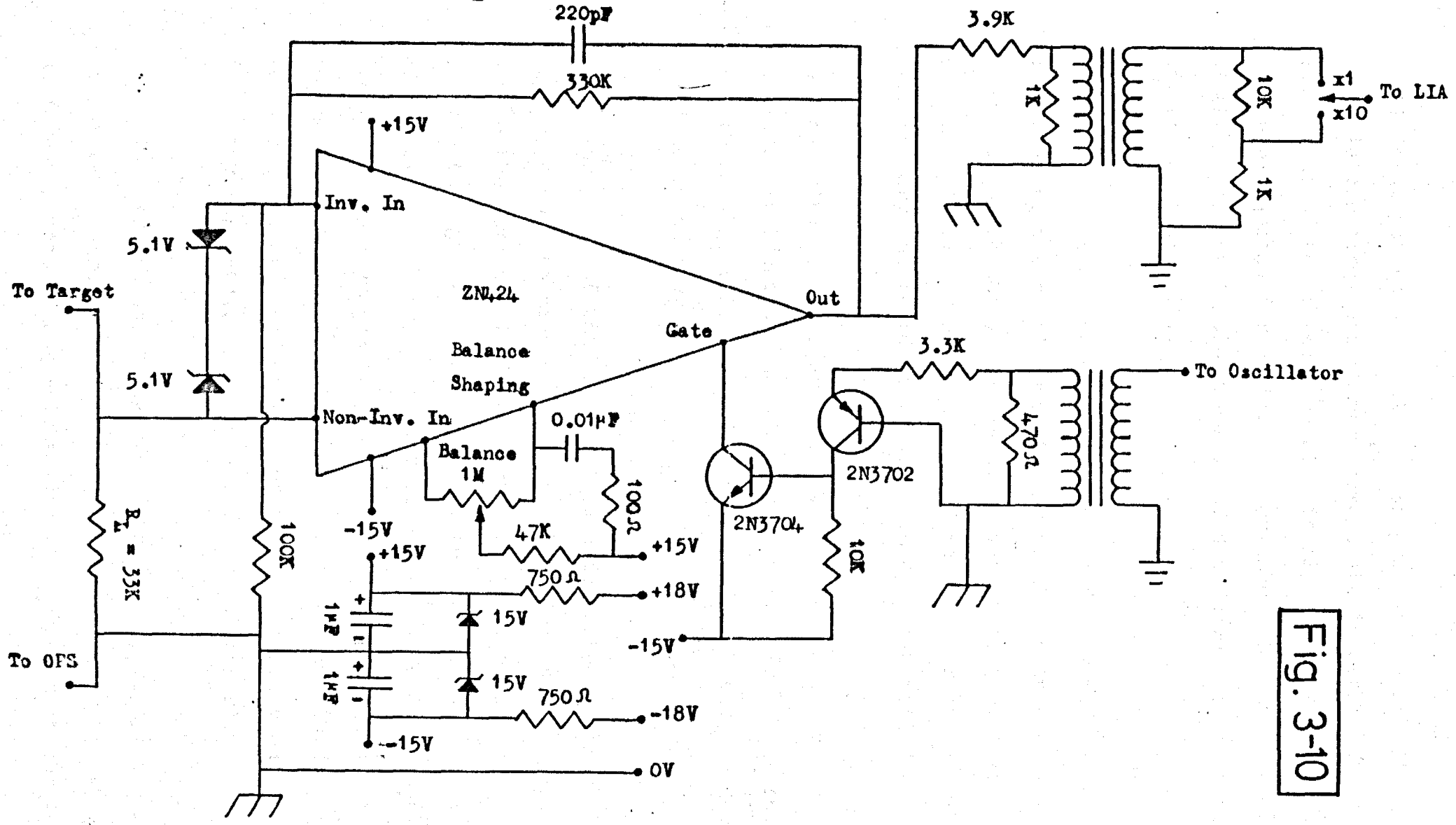

Fig. 3-10

amplifier input (cancellation). In practice, a 220 PF variable capacitor was shunted across the inverting input and output of the integrated circuit amplifier (2N424), which was then adjusted for optimum performance. Too high a value of the capacitor (>350 PF) was found to have a detrimental effect on sensitivity.

The electron gun was run in the ordinary mode at an accelerating potential equal to, or greater than the maximum energy at which the yield was to be measured, generally (V_{gun} = 1 kV). Consequently, the retarding ramping voltage used to vary the incident electron energy was applied to the sample at about 10 V more negative than the electron gun cathode voltage, i.e. (0) - (-1010) V. The energy of the electrons incident on the sample thus varies from V_{gun} to less than zero, i.e. so that the beam is reflected and does not land on the target.

The grids of the three grid RFA described on Page 69 were used only to provide a spherical equipotential space around the sample. The inner grid and final electrode of the electron gun were both earthed, to ensure that the energy of electrons impinging on the target was equal to the projection energy (cathode voltage). Small positive voltages were applied to the grids G_3 and G_2 (18 V) and the collector (60 V). The actual values used were found to be relatively unimportant (~ + 10V for grids, and, ~ + 60V for collector).

The circuit was tested for linearity by applying a known linear ramp current (0-20 μA) derived from the OPS 2000 at (0-50 V ramp). A straight line was achieved at the output

This test circuit is shown in Fig. 3-11.

In Fig. 3-9 (the yield measurement circuit), the output signals were amplified and detected by a LIA. The output signals were of sufficient amplitude as to require no pre-amplification. When the yield spectrum was taken over a 0 - 1000 V range the Y axis of the X-Y recorder was driven from the output of the LIA, and the X axis was connected to a function generator, (FG 100). Since the yield spectrum was expanded (1000 - 930 V) to study the band structure of the surface, an offset voltage was necessary to suitably bias the X axis.

3-2.11a Calibration of the Yield Circuit

As is noted in the results section (Section 4-3), the yield detection circuit was calibrated by means of the Faraday cup. To determine the accuracy of performance of the yield detection circuit, its output was compared with a manually constructed yield curve. The production of this latter yield curve is based on the following considerations. When a beam of electrons hits a target, secondary electrons are produced at different voltages, and can be monitored simply by a micro-ammeter. However, the SEE yield of a material is given by $\delta = \frac{i_s}{i_p}$ where i_s is the secondary electron current, and i_p is the primary current. Since $i_s = i_p - i_T$, where i_T is the target current, substitution for i_s in the above gives, $\delta = 1 - \frac{i_T}{i_p}$. Therefore, if i_p is kept constant the yield is directly proportional to i_T as a function of the primary energy. Thus, a yield vs. energy can be produced.

Using a Faraday cup, prepared to be as good an absorber

Yield Circuit Checking Diagram

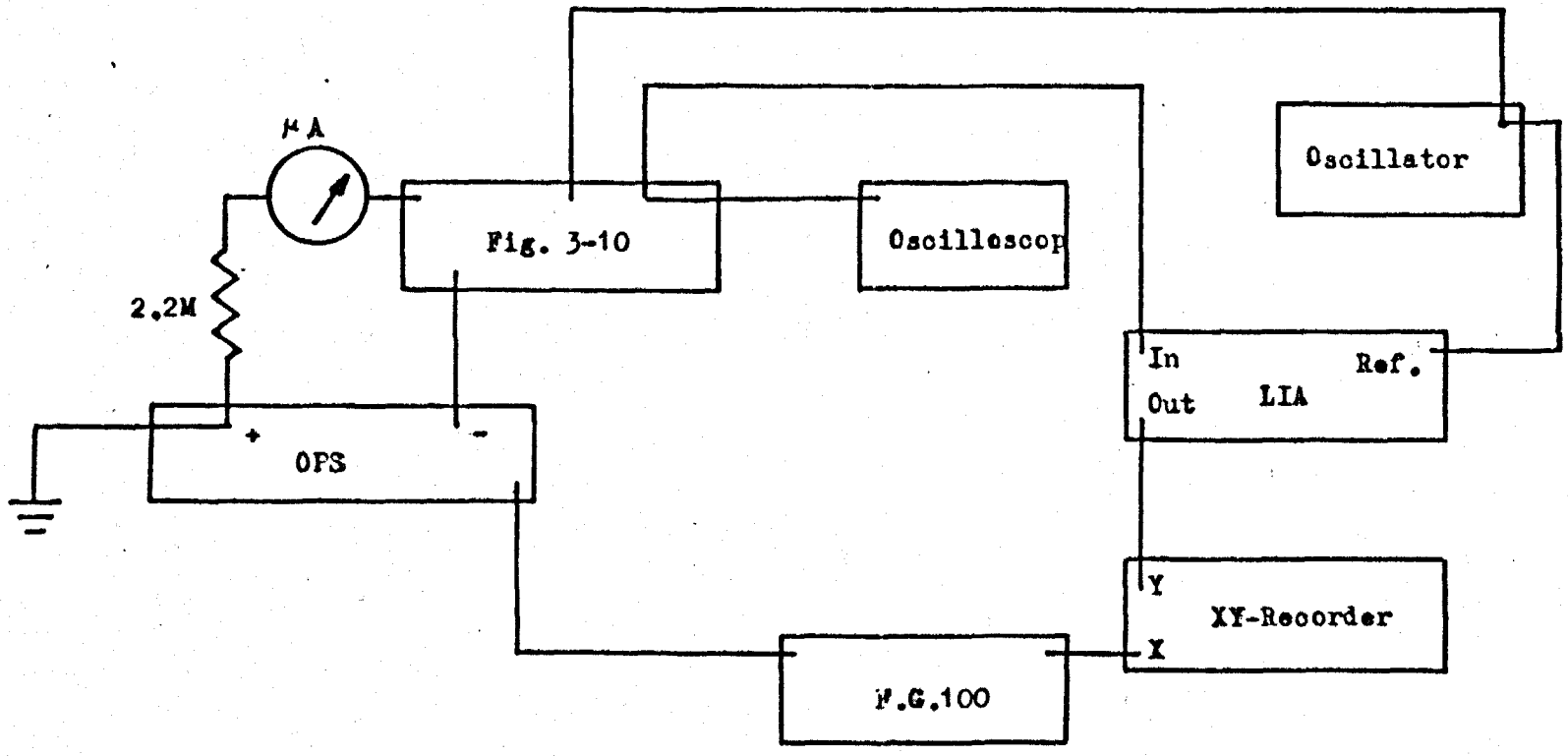

Fig. 3-11

of electrons as possible, (see Section 3-2.7), i_p was measured. When all of the primary beam current is absorbed by the target ($i_s = 0$), then $i_T = i_p$ and the yield is zero ($|V_T| > |V_p|$). With the beam projecting onto the Faraday cup, i_p is measured, and when the electron beam impinges on the antimony sample both were accurately aligned to the incident beam direction. The sample is perpendicular to the Faraday cup. At different voltages, the target (antimony sample) current was measured, and δ is calculated. A plot of δ vs. primary energy was traced, shown as Fig. 3-12. Fig. 4-15 shows the result using the automatic yield detection circuit over the same range. Comparison of Figs. 3-12 and 4-15 shows that the automatic yield circuit result compares well with that obtained by direct observation and thus proves the yield circuit suitable.

The circuit diagram for manually producing the yield curve is illustrated in Fig. 3-13.

Manually obtained yield curve

Fig. 3-12

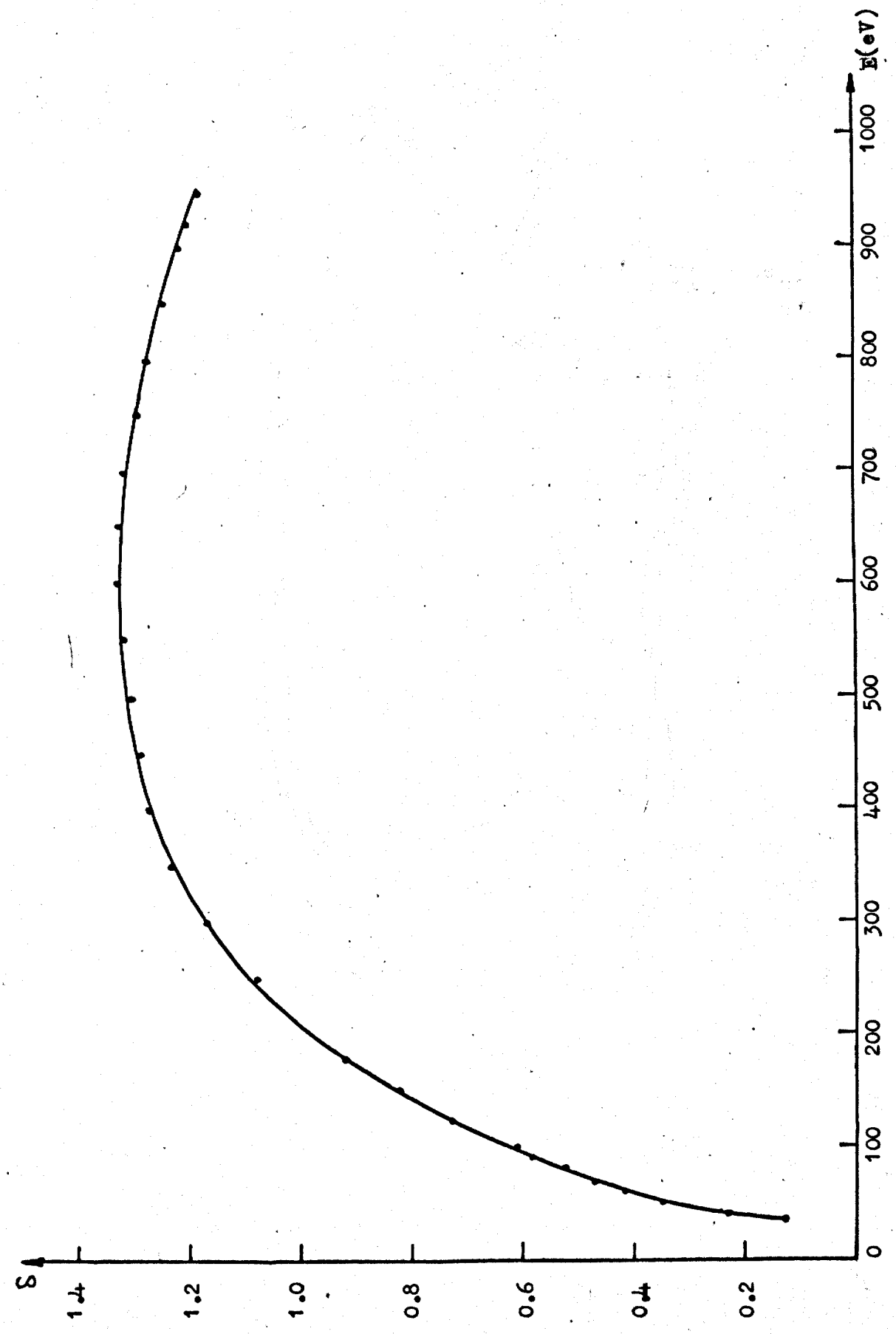

Manually Controled Yield Measuing Device

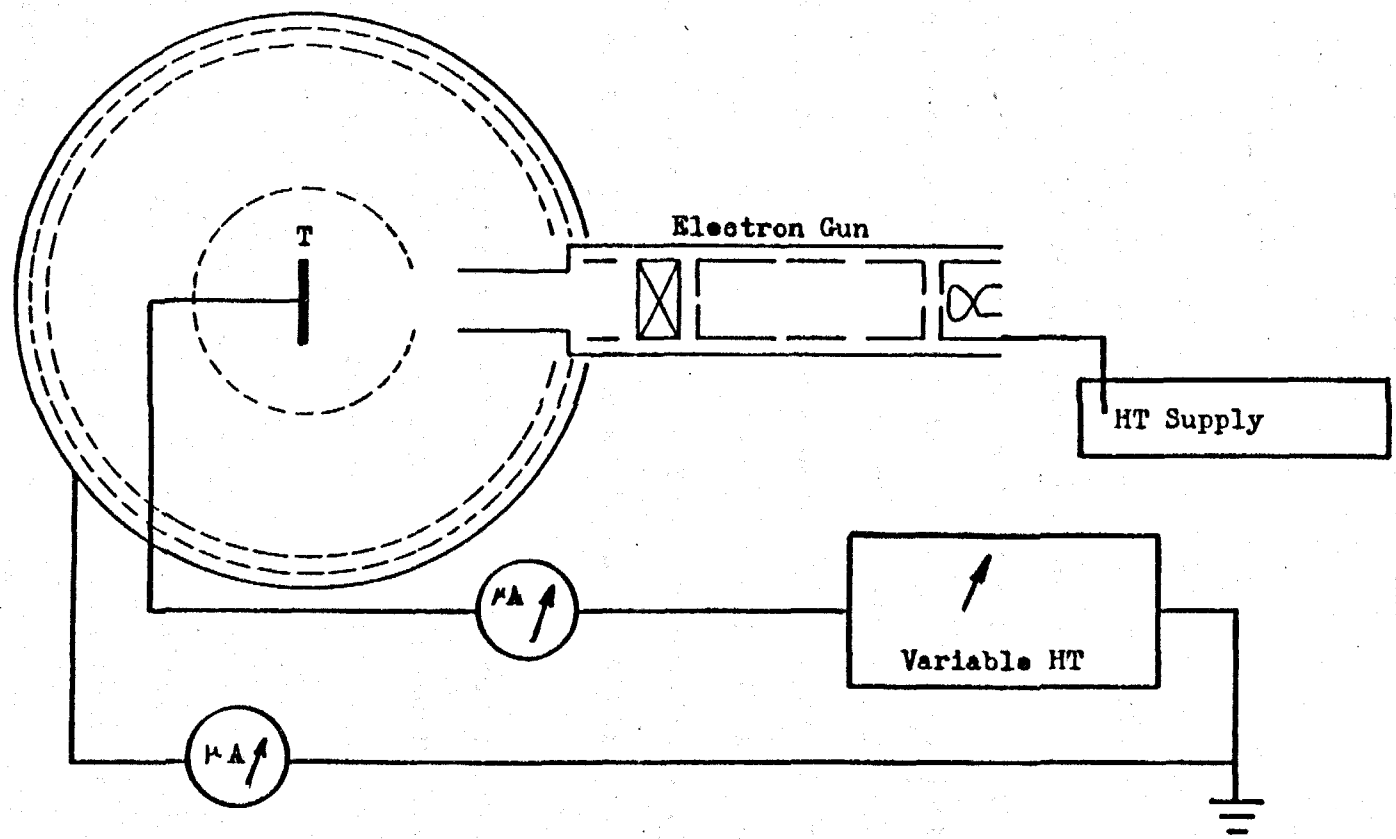

Fig. 3-13

Chapter 4

Results and Discussion

4-1 Auger Spectra

Auger and CEEL spectra were obtained from the antimony sample after baking out of the chamber, but before any specific cleaning procedure (see Chapter 3) was attempted. In this case, the spectra were of fairly low intensity and it was therefore necessary to heat the sample to just below evaporation ($>550^{o}$ C at 3×10^{-10}, Diels and Jackel (1966)) to obtain usable spectra. This heating removes all surface contamination to below a detectable level. This ensures that only the characteristics of the clean metal were observed and that all evidence of impurities were removed.

The Auger electron spectra obtained from a polished antimony crystal surface with the present spectrometer are presented in Figs. 4-1 to 4-4.

These spectra were taken at different incident energies and incident beam angles (as measured with respect to the target normal). The reasons for the variations in spectral characteristic are discussed below.

Auger electron spectra were obtained in the derivative mode for reasons of increased sensitivity. In the ordinary mode, the energy distribution function N(E) and the Auger peaks are superimposed on a smoothly varying background.

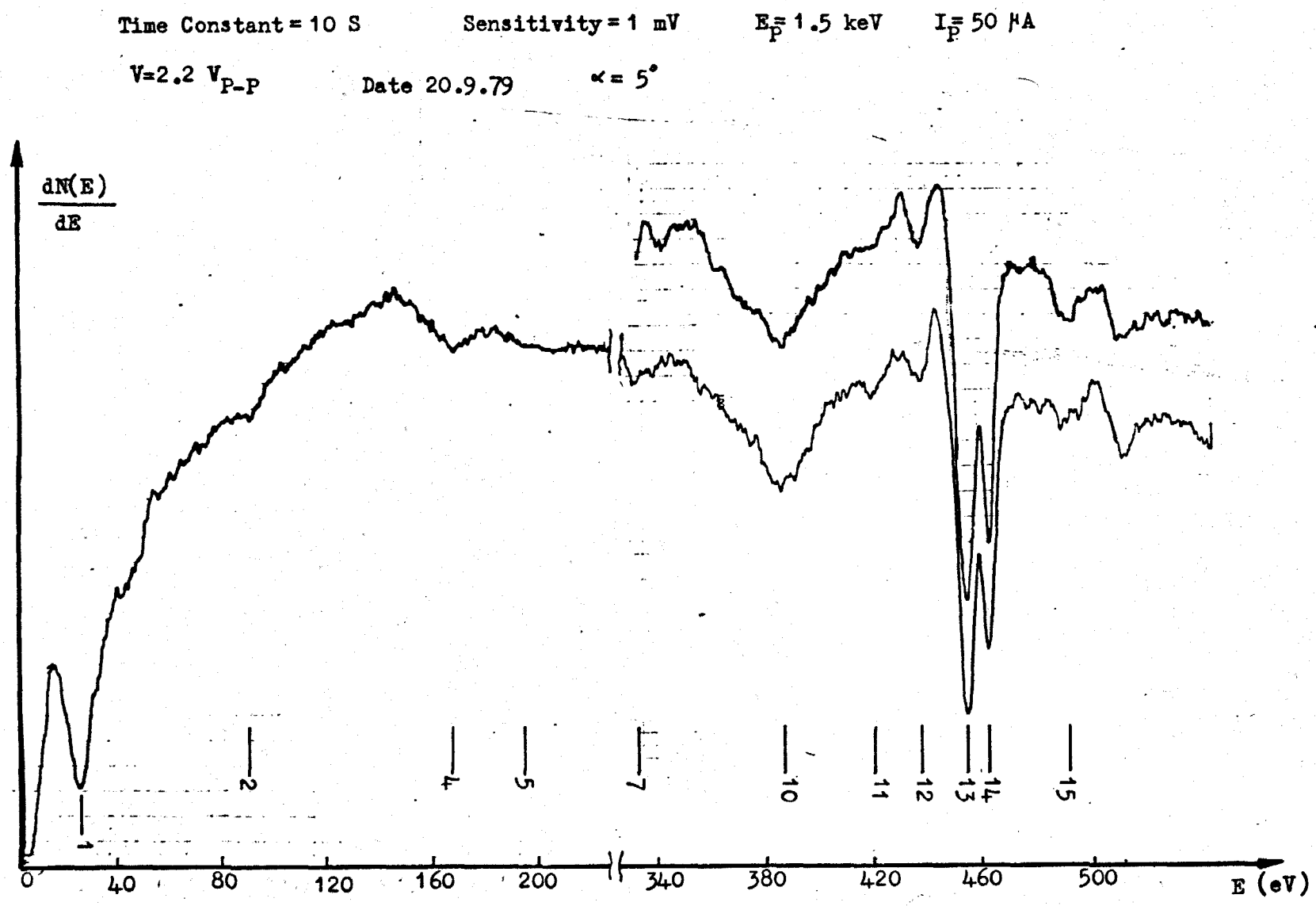

Auger Electron Spectrum of Sb

Fig. 4-1

Auger Spectrum of Sb

Fig. 4-2

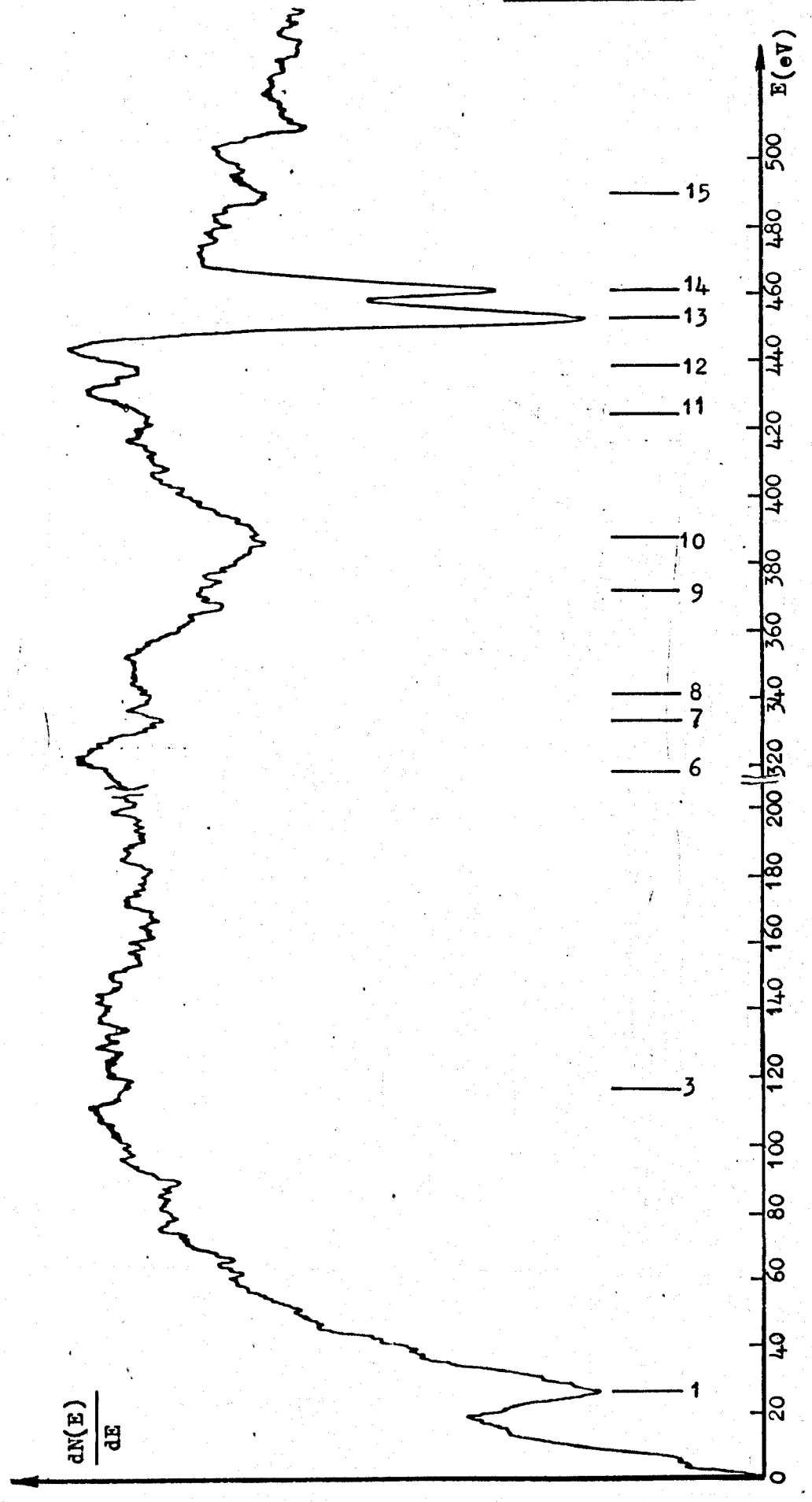

Auger Electron Spectra of Sb

Fig.4-3

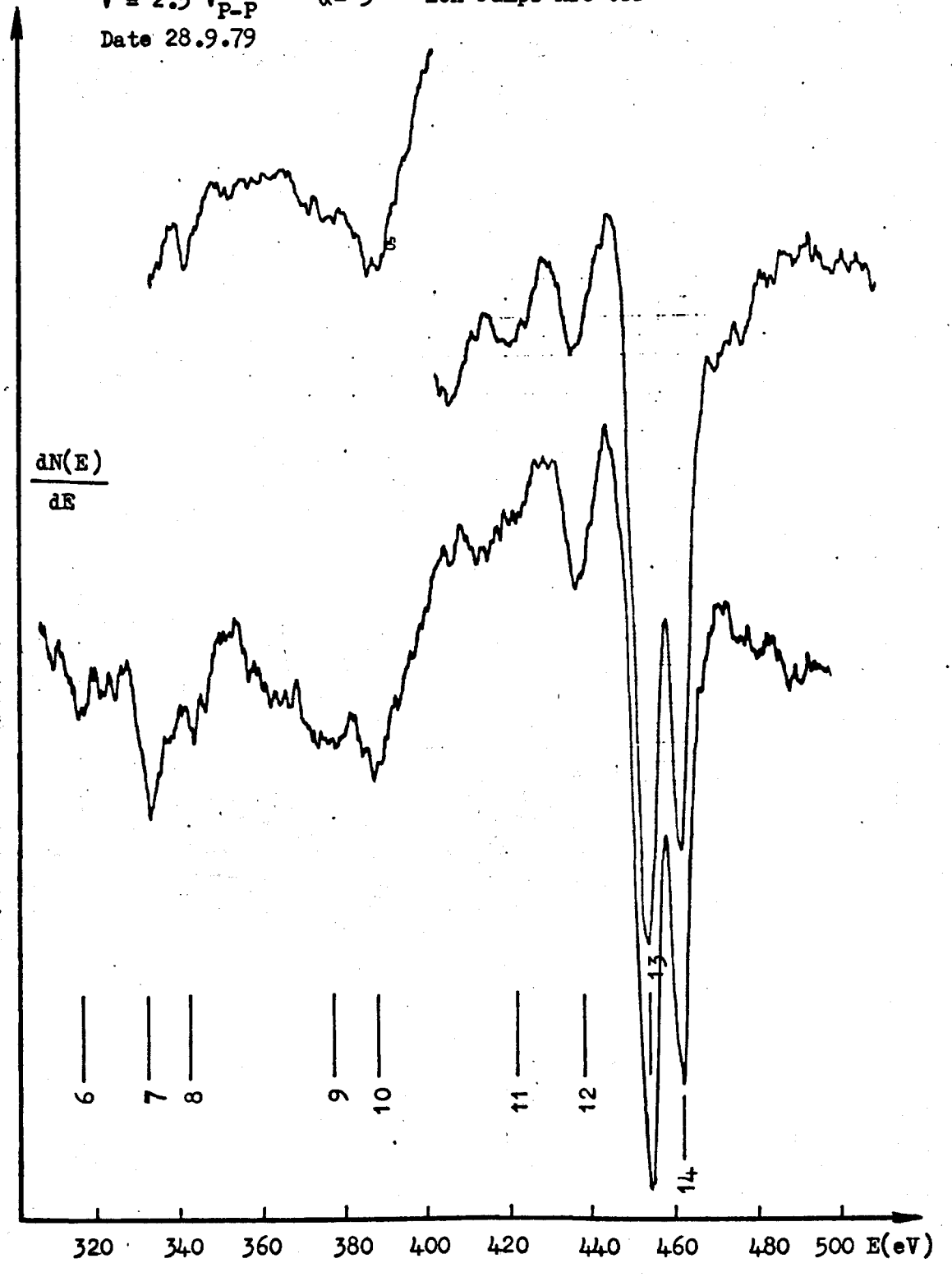

Auger Electron Spectra of Sb at different angles.

Fig.4-4

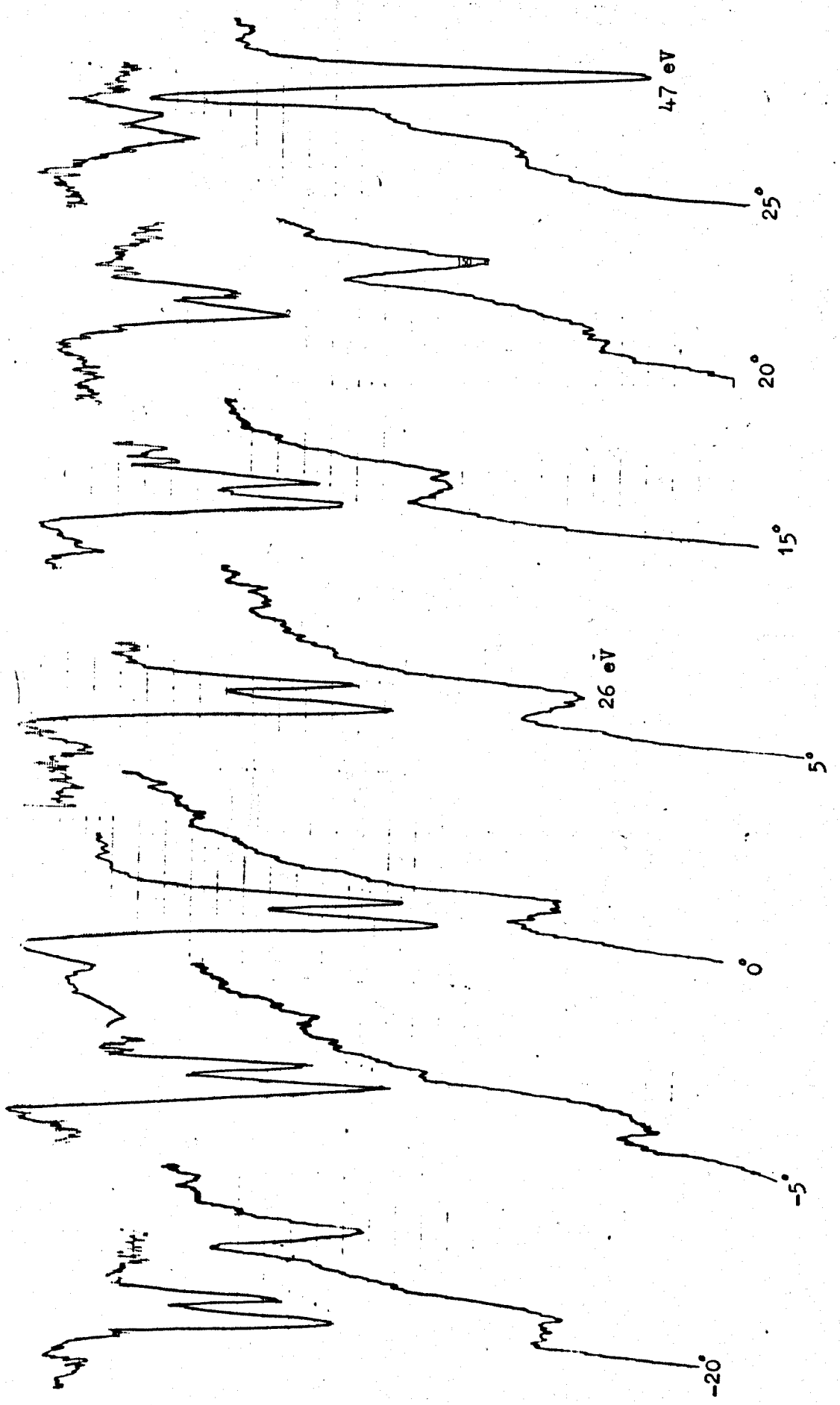

In the range of the slow secondary electrons (0-60 eV), the slope of the distribution function decreases rapidly with decreasing energy (see Fig. 4-1). It is necessary, therefore, to decrease the sensitivity of measurement in the low energy range. The energy range of 0-1 keV was scanned but no transition was found above 500 eV. The energy of 0-500 eV is therefore shown in the figures which are photographs of the actual spectra. Also, there was no evidence of structure in the 220-340 eV energy range, and therefore is omitted in Figs. 4-1 and 4-2. High energy transitions are generally excited at high incident energies, (3 or 4 times the transition energy), Haas et al. (1970) observed such transitions with lower incident beam energies (about twice transition energy). Antimony is a semi-metal and has weak Auger transitions, which coupled with the strong harmonics of the plasmons, tends to obscure the weak Auger signal at such voltages. The high-energy transitions can be excited by incident electron energies of not less than 1.7 keV. There is no critical dependence on sensitivity on the beam energy, as long as it is sufficiently large to effectively ionize the inner shell electrons, giving rise to Auger electron transitions.

The optimum incident electron energy is 1500 eV, as illustrated in Fig. 4-5. This figure is the energy distribution of the doublet, 454 and 462 eV over the range 900-2000 eV incident energy. The effect of variation in the background noise level and other experimental conditions during the relatively long period required for obtaining these data were minimised by taking an alternating sequence of spectra of these two lines involving a total of two separate spectra

Incident Energy Distribution for 454 and 462 eV Auger peaks of Sb.

Fig. 4-5

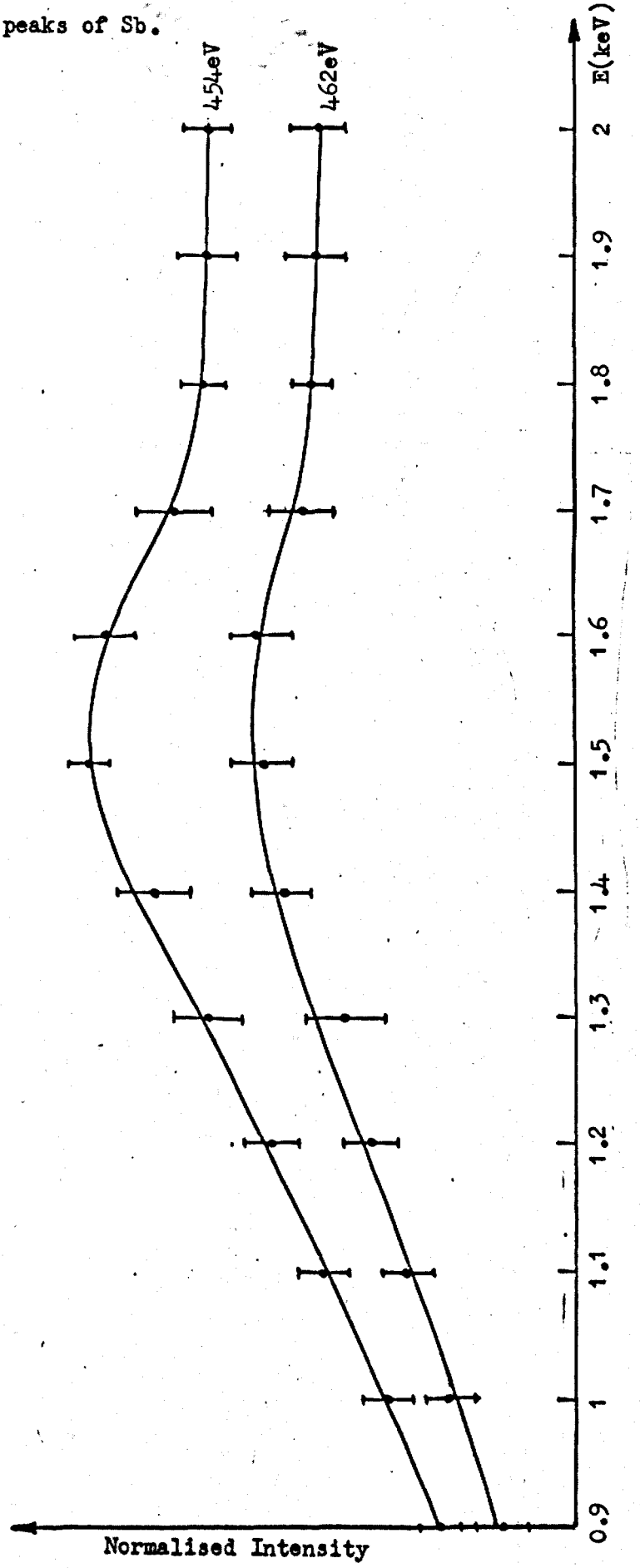

for each beam energy. The line intensities used to plot Fig. 4-5 have been normalised to 454 eV line at 1100 eV. The energy distribution has been checked for apparent variation of spot size with energy. Error bars presented ± 1 standard deviation are based on the two sets of data.

The spectra presented are for a single crystalline antimony surface. Singh (1976) recorded the spectra from single crystalline and poly crystalline samples. The latter were prepared by depositing antimony vapour on the substrate. He observed no difference between these two spectra. This result is expected, since Auger transitions primarily involve individual atoms and are only weakly dependent on structural environment.

The observed energies of the characteristic Auger electrons of antimony are tabulated in Table 1. This table shows those transitions which have been consistently observed in spectra taken at 1.4 and 1.5 keV at 5° incident electron angle with respect to the surface normal. Features in the spectra which are not distinguishable from the background noise have been omitted and suspicious lines are identified in the table. The spectra lie on a background which, principally arises from direct (non-resonant) ionization.

The presented spectra confirm no significant surface contamination on the antimony crystal surface. This was predicted, because antimony is a relatively non-reactive metal, and if the surface is cleaned in accordance with the processes reported by Singh (1976), or Jona (1967) no contamination should be expected.

Table 1

Observed Auger electron transitions on Antimony

Line No.	Fig. 4-1	Fig. 4-2	Fig. 4-3	Average
1	26	26	-	26
2	91*	NR	-	91
3	NR	115*	-	115
4	166	NR	-	166
5	195	NR	-	195
6	NR	320	317	318.5
7	332	333	NR	332.5
8	NR	342	342	342
9	NR	375	378	376.5
10	388	388	388	388
11	421	425	422	422.7
12	438	438	438	438
13	454	454	454	454
14	462	462	462	462
15	492	492	NR	492

* Suspicious line

NR Unresolved line

- Not included line

The line numbers correspond to the numbering in Figs. 4-1 to 4-3. This data was taken at particular references as stated, on the spectra graphs. The instrumental resolution was estimated by measuring full width half maximum (FWHM) of the observed spectral lines, and were approximately 4 eV (corresponding to 454 eV line) and therefore set an upper limit to the resolution.

The energy scale was normalized to the work of Palmberg et al. (1972), using the transitions at excited-state energies 26, 388, 454 and 462 eV. This is necessary, due to unknown instrumentation voltage differences existing in the system including contact potential difference between grids and collector, and to identify the weak transitions. Comparisons were made between the present data with those of Palmberg et al. (1972), Singh (1976), Harris (1972) and Wright (1974), and the theoretical work of Coghlan and Clausing (1971). Assignments for the transitions of the observed peaks, and normalised multiplicities are taken from Coghlan and Clausing (1971), and these are summarised in Table 2. The normalised multiplicity is the product of the number of electrons (electron population in each subshell, see Appendix 3 for Sb) in the three levels involved in the transitions for antimony, normalised to a maximum of 100 for the largest value. This number was calculated because it certainly enters into the intensity calculation and may be a crude measure of relative intensity. The underlying assumption in this case is that all transition probabilities are equal which, of course, is not true in general. Bearden and Burr (1967) reported the adjusted values for the various energy levels, together with the respective probable errors for eighty-one elements. This

Table 2

Comparison of the present study of Auger electron transitions of Sb, and assignments

Line No.	Present work	Palmberg 1972	Singh 1976	Wright 1974	Harris 1972	Coghlan & Clausing (1971)		
						Calculated value	Normalisation Multiplicity	Assignment
1	26	26	25			27	100	$N_{23}N_{45}N_{45}$
2	91					92.5	2	$M_2M_4N_1$
3	115		113			111.5 115.5	24 13	$M_3M_5N_{23}$ $M_1M_3N_{45}$
4	166		166			170.5	26	$M_3M_4N_{45}$
5	195		195			197	5	$M_3M_4O_1$
6	318.5		319			319	36	$M_5N_{23}N_{23}$
7	332.5	334	333.5	335	332	328 332	24 20	$M_4N_{23}N_{23}$ $M_5N_1N_{45}$
8	342	342	341.7			341	13	$M_4N_1N_{45}$
9	376.5		378	367	370	375 375	4 2	$M_4N_1O_{23}$ $M_1M_4O_1$
10	388	388	388	386	388	387.5	60	$M_5N_{23}N_{45}$
11	422.7		421.4			421.5	18	$M_5N_{23}O_{23}$
12	438	440	438.7	438	436	430.5	12	$M_4N_{23}O_{23}$ or plasmon loss of $M_5N_{45}N_{45}$
13	454	454	455.1	453	452.2	456	100	$M_5N_{45}N_{45}$
14	462	462	463.2	462	459.5	465	66	$M_4N_{45}N_{45}$
15	492	492	490.8	488	490	490 491.5	30 13	$M_5N_{45}O_{23}$ $M_4N_{45}O_1$

list proved most valuable for calculation of the Auger transitions of these elements, including antimony, simply from Equation 2-1 (see Section 2-2). the energy level values for antimony are listed in Appendix 3.

Fig. 4-4 illustrates the incident beam angle variation effect. In this figure, the variation of the doublet formed by the 454 and 462 eV lines and the 26 eV transition are shown at specified incident angles. At large incident angles, a line at 47 eV appears on the spectrum, the amplitude of this line increases as the incident angle gets larger. The 47 eV line is related to Fe (from the target holder). This indicates that with angle variations the beam hits different points on the target. Of course, this result was obtained when the target was adjusted to the optimum position. Nevertheless, after taking a long period of time to adjust the target position, by rotating the target ($\sim 20^{o}$) the beam never hit the target at a spot. If it had, then in the spectrum the 47 eV peak would have disappeared. The conclusion was,

a) the spot size was actually bigger than seen on the mirror, due to distortion caused by the mirror angle (see Plate 1 and Fig. 3-1). Reducing the spot size was found to marginally reduce the 47 eV amplitude.

b) the target was not located exactly at the collector centre. Although the location was monitored by the electron gun collimator (see Section 3-2.7), and furthermore the electron beam position on the target was optimised as in Fig. 4-4, altering the target location by means of the manipulator, (see Section 3-2.7), gave the same result as the electron beam position change. Finally, it was

discovered that there was eccentricity on the target holder, which was minimized to ± 0.3 mm for a $\pm 10^{\circ}$ change of angle, acceptable enough for studying the band structure of the Sb surface. The eccentricity was due to the long length and small diameter of the holder, and alteration of the holder mechanism was not feasible in the short term.

The modulation voltage amplitude has a severe effect on the received signal. At low modulation amplitude, the spectrum was too weak to record ($V = 1.6\ V_{p-p}$) and at large amplitude ($V > 4\ V_{p-p}$) the spectrum was distorted. This confirms the Grant et al. (1974) study of this effect. The peak broadening resulting from large oscillation amplitudes also produces marked changes in the relative peak-to-peak height of the various Auger features. Detailed studies of this parameter were not presented in the present investigation.

It should be noted that the sharp Auger maxima are obscured if any one of the above factors is not optimised. In addition to these three major parameters (energy, angle and modulation amplitude) there are many other phenomena that affect the spectrum, e.g. stray electro-magnetic fields, incident electron current, and stray radio frequencies. During the recording of the spectra, suppression of noise from the ion pumps due to the discharge was desirable, so the ion pump power supplies were switched off.

Every precaution was taken to obtain high resolution, but the figures of Auger electron spectra indicate that the Auger results do not compete with those of Singh (1976) due to his advanced apparatus. Compared with Wright's results,

which were taken on the same apparatus, the improvement is encouraging. However, it must be remembered that the main motive for the present studies lies in the low energy transitions which are related to the band structure and it is in this region that present apparatus has significant advantages.

The primary electron energy was such that only the M, N and O levels were ionized. However, no transitions could be identified related to other levels, such as the L shell.

The 438 eV line is probably due to the M_5N_{45} N_{45} electron (454 eV) exciting a plasmon as it exits from the solid. The energy difference agrees well with the observed plasmon energy value (16.7 eV) of antimony and,additionally, no strong Auger transition could be identified with this energy. The large width of the parent peak would make resolution of the surface plasmon loss very difficult. The losses from the M_4N_{45} N_{45} transition at 462 eV is, of course, masked by the 454 eV line loss. The 447.4 eV line which was supposed to be the plasmon loss from M_4N_{45} N_{45} electron reported by Singh (1976), was not observed in the present study, again possibly due to transition masking by the 438 eV. It is rather difficult to locate the positions of the lower energy peaks precisely, because of the poor signal-to-noise ratio and the large background slope, 91 and 115 eV lines , and the many unresolved lines in this region, shown in Table 1, supports this.

In conclusion, all the observed peaks are assigned to

Auger transitions between core levels. The number of valence electrons (2 in O, and 3 in O_{23} subshells) is small in comparison with the number of electrons in the N_{45} level (10 electrons), so that transitions involving the N_{45} level would be expected to be stronger. This is in fact found to be so, as the strongest observed peak at 454 and 462 eV are assigned the M_5N_{45} N_{45} and $M_4N_{45}N_{45}$ transitions respectively. For this pair of peaks, the difference in energy is 8 eV, compared with the 9 eV difference in binding energy of the M_4 and M_5 electrons, as given by Breaden and Burr (1967).

The Auger spectra of antimony is influenced by Coster-Kronig transitions as the M_3N_{45} N_{45} transition at 694 eV (expected to be of the same intensity as the M_4N_{45} N_{45}, and M_5N_{45} N_{45} transitions on the basis of the number of electrons involved (normalised multiplicity)) was not observed. It is possible that vacancies created in the M_3 sub-shell are filled by Coster-Kronig transition of the type M_3M_4- and M_3M_5- . Indeed, peaks due to such transitions are observed at low energies, as seen in Table 2. The vacancy distribution in the M_4 and M_5 sub-shells is thus enhanced by increasing their relative intensity.

The transition observed at 26 eV is associated with the inner-shell super Coster-Kronig excited state, with the configuration $N_{23}N_{45}$ N_{45}. The vacancy of the N_{23} hole decayed with the creation of two other N shell holes.

Aksela (1971) investigated the MNN Auger transitions in several metals. His measurements reveal that the spectrum is made up of the main lines (M_4N_{45} N_4 and M_5N_{45} N_{45}) of which

the one at lower energy (M_5N_{45} N_{45}) is always much broader and is split more or less clearly into two peaks. In the present study and also in that of the other authors, no such split was observed. The reason for this splitting not appearing in the present work is most probably due to the relatively poor resolution of the analyser.

4-2 Characteristic Energy Loss Measurement

The explanation of the energy distribution of a fast electron beam losing energy to the conduction electrons in a crystal surface is based on the assumption that the conduction electrons constitute a Fermi-Dirac gas and that the fast electron undergoes only fractional energy and momentum changes. This distribution exhibits both collective interaction characteristics of the surface and individual interaction characteristics of the surface.

Figs. 4-6 and 4-7 illustrate two typical derivatives of energy distribution curves, i.e. operating in the derivative mode, $\frac{dN(E)}{dE}$. They are taken from an antimony sample excited by an incident electron beam with different energies, angles and beam current. Starting at the high energy end of these curves, a number of significant features are noted. The final sharp peak (elastic peak) is due to reflected primaries, as reported by Powell et al. (1958) and Whetten (1966). This elastic peak provides a sharp reference point, useful for calibration of the energy scale, but was not otherwise used in this study.

There are a number of peaks evenly spaced below this elastic peak. These discrete loss peaks are usually due to

Characteristic Electron Energy Loss Spectrum of Sb

Fig. 4-6

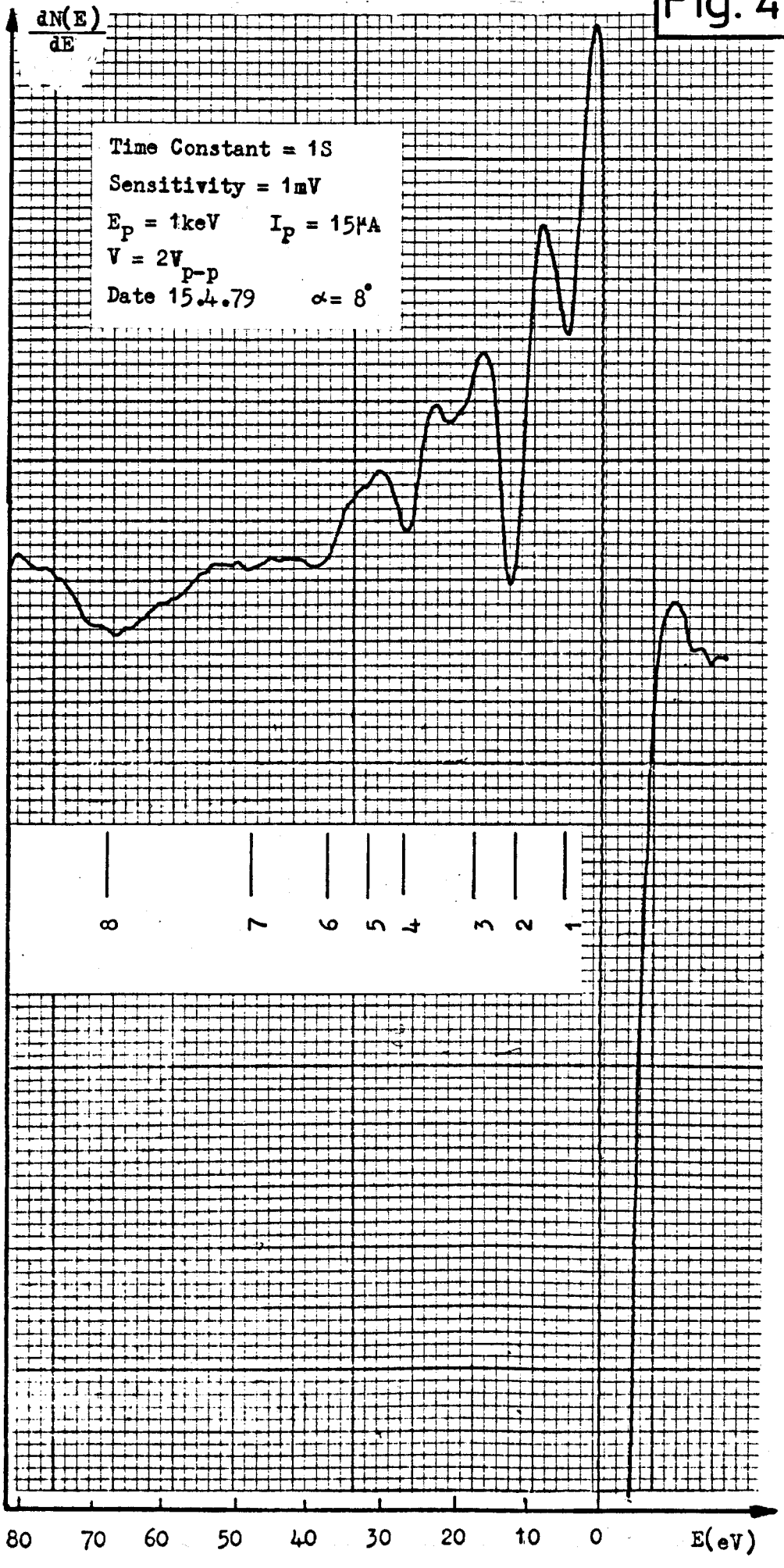

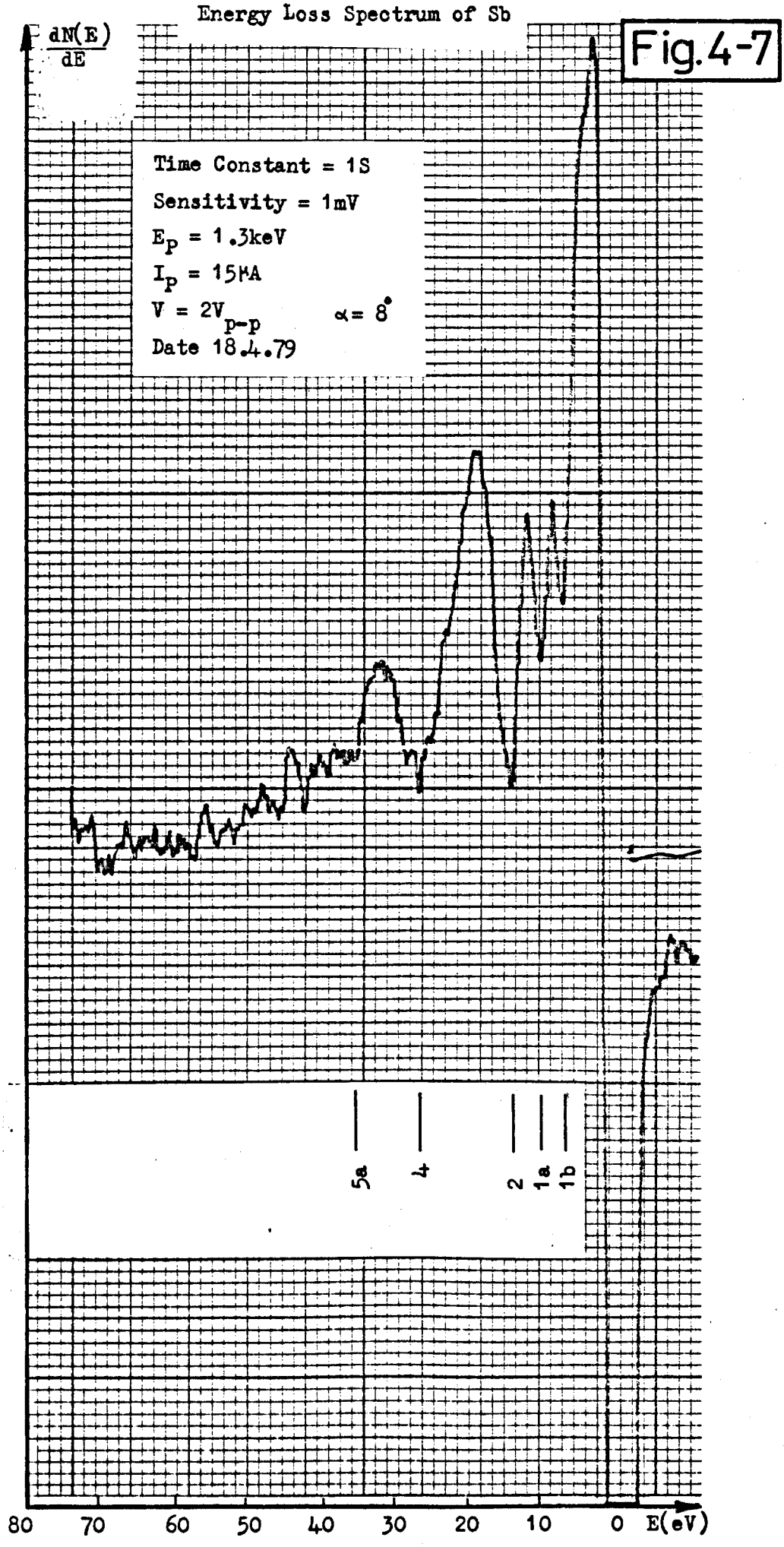
Energy Loss Spectrum of Sb
Fig.4-7
dN(E)/dE
Time Constant = 1S
Sensitivity = 1mV
E_p = 1.3keV
I_p = 15μA
V = $2V_{p-p}$
α = 8°
Date 18.4.79
5a
4
2
1a
1b
80
70
60
50
40
30
20
10
0
E(eV)

plasma oscillations (plasmons) of the valence electrons in the solid. The losses may, therefore, be due to either surface or bulk plasmons. Plasmon losses are readily observable with the experimental arrangement employed, and are useful in interpreting other parts of the electron spectra.

Some small peaks also occur at a fixed interval below the elastic peak. They are due to electrons which have been reflected after losing only that energy necessary to excite them from the valence band up to the Fermi level of antimony (ionization loss). While the energy loss is characteristic of the material, the peaks are usually very small and difficult to detect. However, in the present work, because of the wide range of investigation, some losses are well observed, e.g. see Figs. 4-6 and 4-7.

The energy loss spectra were observed with primary excitation energies ranging from 1.1 to 1.7 keV, and incident beam angle of + 12° to - 20°, with respect to the surface normal. Spectra were also recorded with,

a) different beam currents (ranging from 9 to 15 μA) by varying the electron gun grid voltages;
b) at different modulation voltages (in the range of 1.2 to 2.6 V_{p-p}).

These spectra are discussed later in this Chapter. Because the CEEL spectroscopy is part of the total electron spectra, which includes the AES, the effect of these variables was only studied in CEEL spectroscopy. All these spectra were recorded after characterising the Auger spectra to that of Sb. The Auger spectra recorded before and after obtaining

energy loss spectra were identical, thus indicating no change in the surface properties.

Fig. 4-6 illustrates the CEEL spectrum scanned between 0 to 80 eV range. Due to unknown instrumental potential differences in the spectrometer, it was not possible to fix the energy scale absolutely, and so a normalisation procedure was adopted, whereby two strong lines in the electron emission data of Singh (1976), corresponding to two prominent peaks in spectra, were used as calibration points. These were CEEL lines at 11.3 and 26.7 eV. The line numbers in the figures correspond to those given in tables. The corresponding energy loss values for an Sb crystal surface were obtained from the mean of the measured values. A summary of characteristic losses observed under different conditions, detailed above, is tabulated in Table 3.

The losses for the antimony crystal are compared with those from previous works carried out by Powell (1960), Harris (1972), Wright (1974) and Singh (1976). These are presented in Table 4. In general, agreement is good, particularly with the values obtained by Singh (1976). As Singh (1976) has stated, Harris (1972) and Wright (1974) observed some features which Singh did not see, and the lack of these features in the present work tends to support the argument that they were due to other elements (perhaps oxygen or carbon) on the surface. Uneven deposition of antimony onto the substrate could also be a possible explanation for these features.

The energy loss spectrum of antimony has already been

Table 3

The measured value of the characteristic energy loss transitions of Sb at different variables

No. Peaks	1	2	3	4	5	6	7	8	9	Variables			
Figures	Energy (eV)									E_p eV	I_p μA	α	V_{p-p} V
4-6	6.1	11.3	16.7	26.7	31.8	37.1	48.4	66.6		1000	15 μA	8°	2
4-13	6.5	11.3	16.9	26.7	31.6	37.1	48.2	66.05		1000	X	12°	2
4-11	6.1	11.3	17	26.7	31.8	37.1	48.3	@		1000	14 μA	X	2
4-10	6.2	11.26	16.7	N.R.	N.R.	N.R.	N.R.	N.R.		1000	14 μA	X	2
4-12	6.2	11.34	16.4	26.7	N.R.	N.R.	N.R.	N.R.		1000	14 μA	X	2
4-14	6.42	11.3	17	26.7	31.8	37.7	@	@		1000	15 μA	12°	X
4-7	*	*	*	*	*	*	*	*		1300	15 μA	8°	2
4-8	*	*	*	*	*	*	*	*		X	14 μA	8°	2
4-9	*	*	*	*	*	*	*	*		X	15 μA	8°	2
Mean Values †	6.25 ±0.15	11.3	16.78 ±0.21	26.7	31.75 ±0.09	37.25 ±0.25	48.3 ±0.081	66.325 ±0.275					

* Not included
X Variable parameter
@ Not measured
N.R. Not resolved

† The quoted errors in the measurements are the probable errors of the mean values. (Standard deviation)

Table 4

Characteristic Energy Losses of Sb and assignments found in present work and by other Authors

Line No.	Present work	Singh 1976	Wright 1974	Harris 1972	Powell 1960	Calculated energy	Assignment
1	6.25	6.6	7	6			O_1 → Fermi Level
2	11.3	11.3	11	11.5	11.3 ± 0.2	10.9	SP
3	16.78	15.8	15	16		15.4	BP
4	26.7	26.7	28	28	26.5 ± 0.5	26.3	SP + BP
5	31.75		32		32.3 ± 0.3	30.8 32.7	N_{45} → Fermi Level
		34.1		34			2BP + 3SP
6	37.25						
				43			
7	48.3	49	47	49	47.9±0.3	46.2	3BP
			52			53.6	
			59			61.6	N_{23} → N_{45}
8	66.33	66	68	63		67	4BP
		80	80	81		77	5BP
			91			92.4	6BP

extensively discussed by Singh (1976). There are several earlier studies in this area for example, Leder (1956) and Gauthe (1959), which are not included in Table 4.

Figs. 4-8 and 4-9, show the effect of primary electron energy variation on the observed spectra. The figures indicate that as primary electron energy is reduced, the surface plasmon loss becomes stronger than the bulk loss. This result was expected, because it has been shown on various occasions, Prutton (1975), that the low energy incident electrons can penetrate only a few layers of the surface.

The line 1, corresponding to the ionised antimony loss at 6.25 eV was split as a doublet (4.5, 7.9 eV) at the beam energies 1.1, 1.2, 1.3, and 1.4 keV.By observing the spectrum at different incident-beam energy it is possible to identify two-electron transitions. There was no evidence of these lines on any other spectrum, and many attempts to reproduce these lines failed. Indeed, the line 1 position is the average of these two line values, and the other transitions are unchanged, apart from 11.3 eV. The calibration of Figures 4-7, 4-8 and 4-9 was carried out by superpositioning the spectra on Fig. 4-6 before photographing/drawing. Due to unreproductability of these spectra, no explanation is given for the line 1 splitting in this thesis, and they are omitted in Table 3.

It can be seen in Figs. 4-6, 4-11, 4-10 and 4-12 that, at a large angle of incidence, the surface plasmon losses become predominant, and surface losses down to the 3rd order are visible. The energy loss at 6.25 eV becomes weak at 12^{o}. Above 17^{o}, the beam impinges on surfaces other than the sample

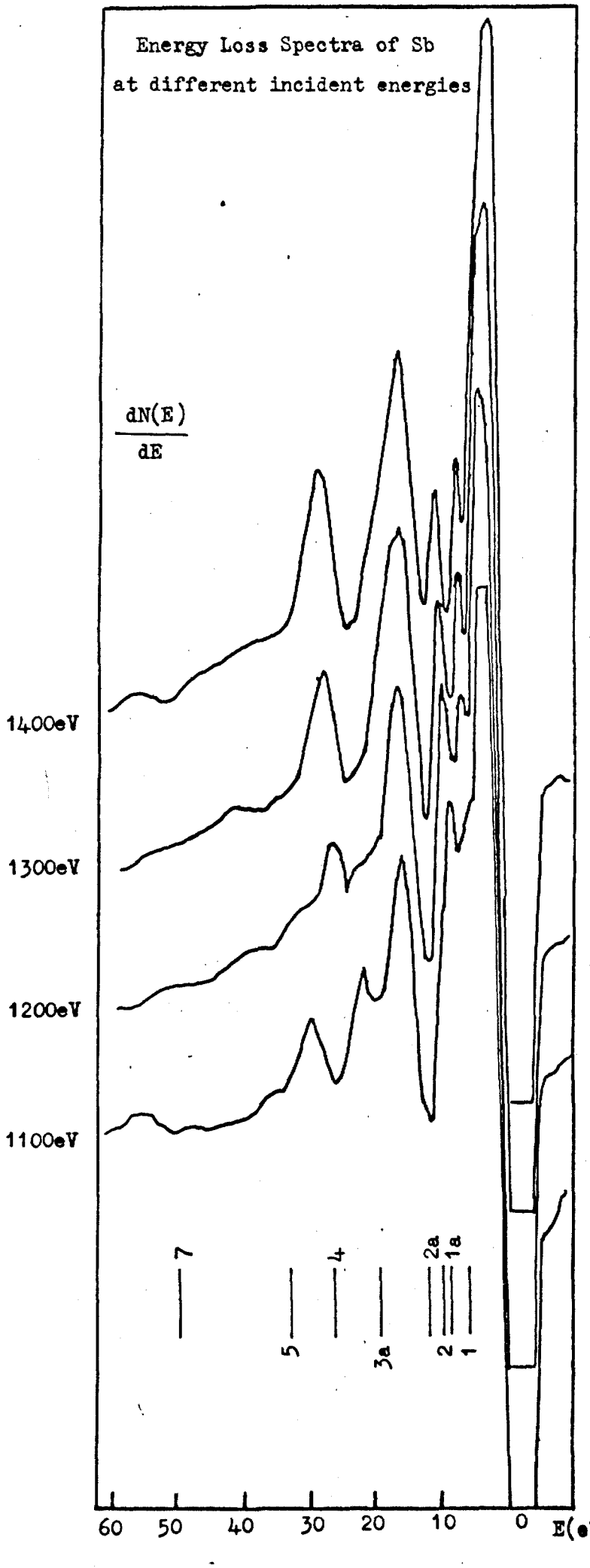
Energy Loss Spectra of Sb
at different incident energies
dN(E)
dE
1400eV
1300eV
1200eV
1100eV
7
5
4
3a
2a
1a
2
1
60
50
40
30
20
10
0
E(eV)

Fig.4-8

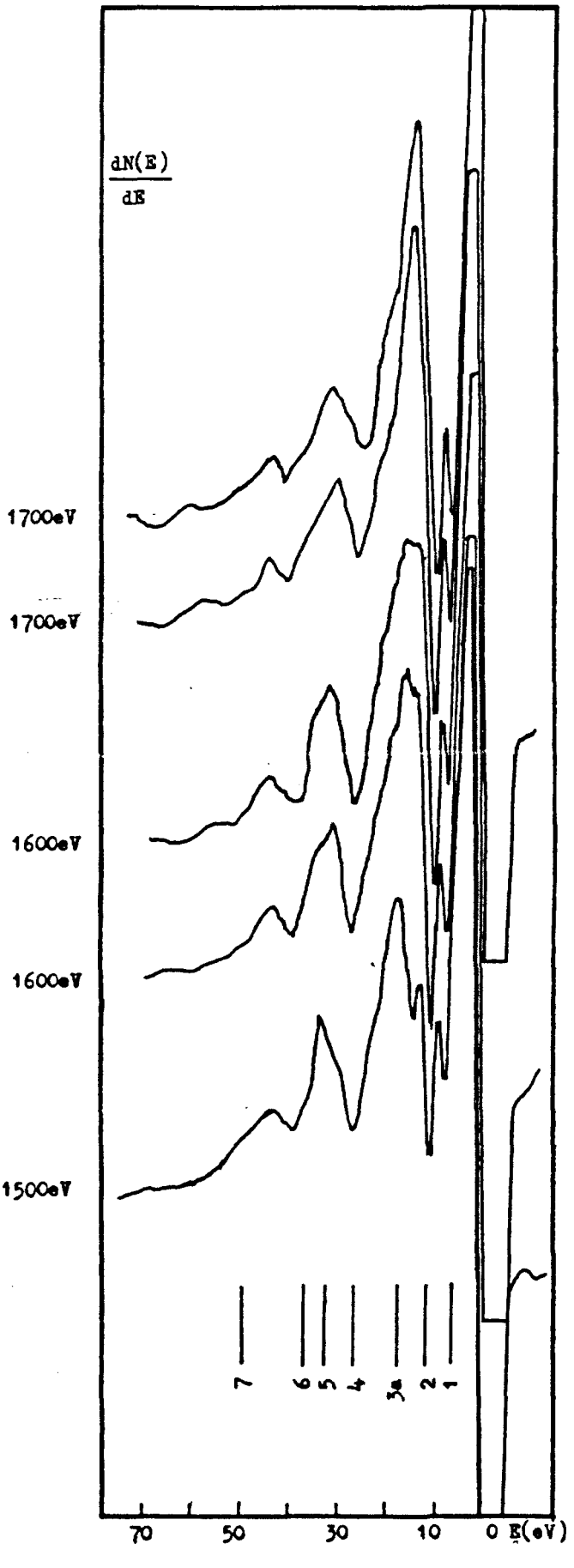

Fig.4-9

Figure 4-8 Continued

Energy Loss of Sb at different incident angles

Fig. 4-10

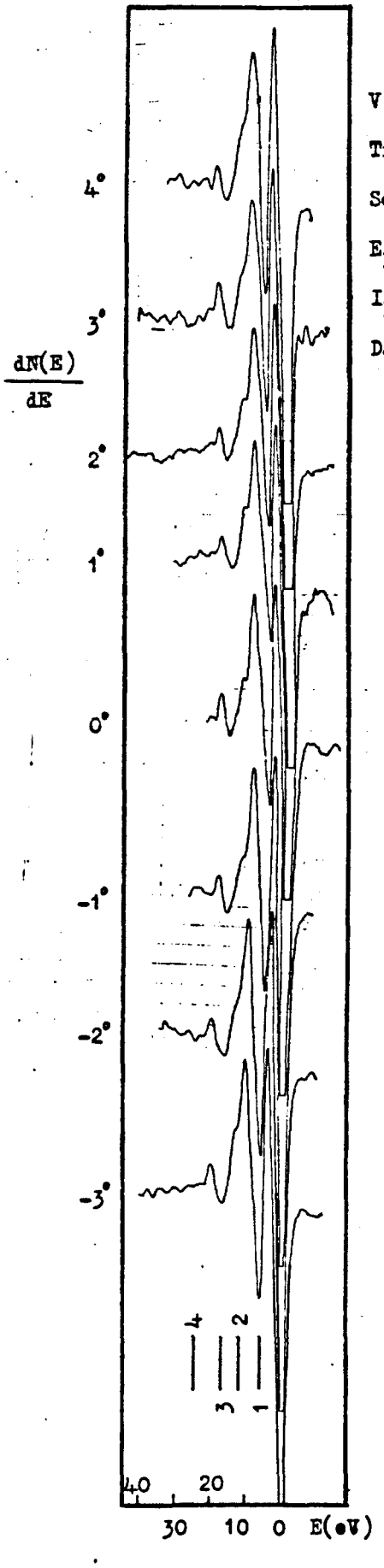

Fig. 4-11

Figure 4-10 Continued

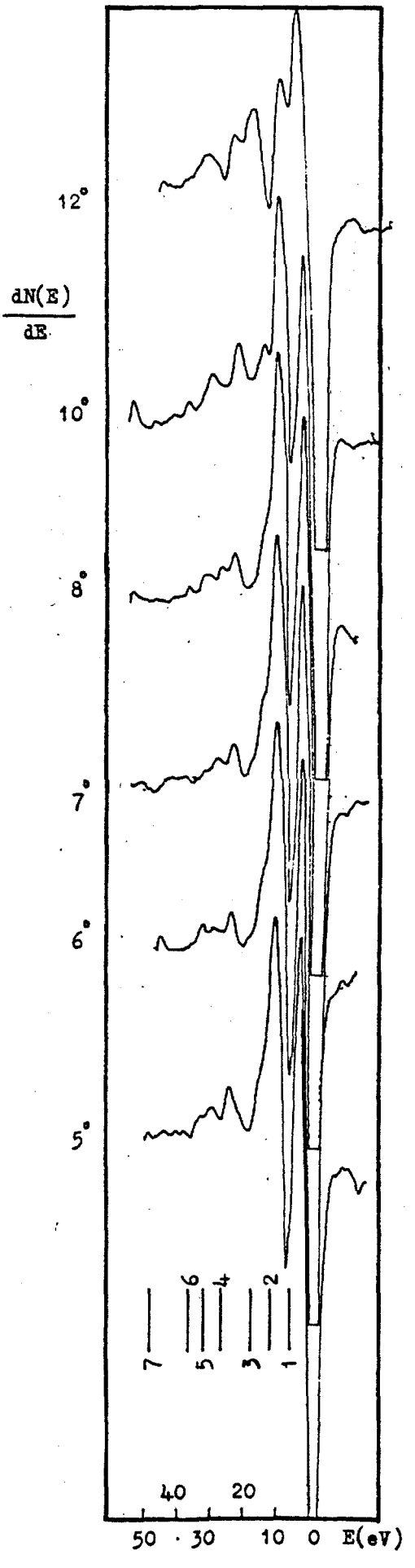

Fig. 4-12

Fig. 4-10 Continued

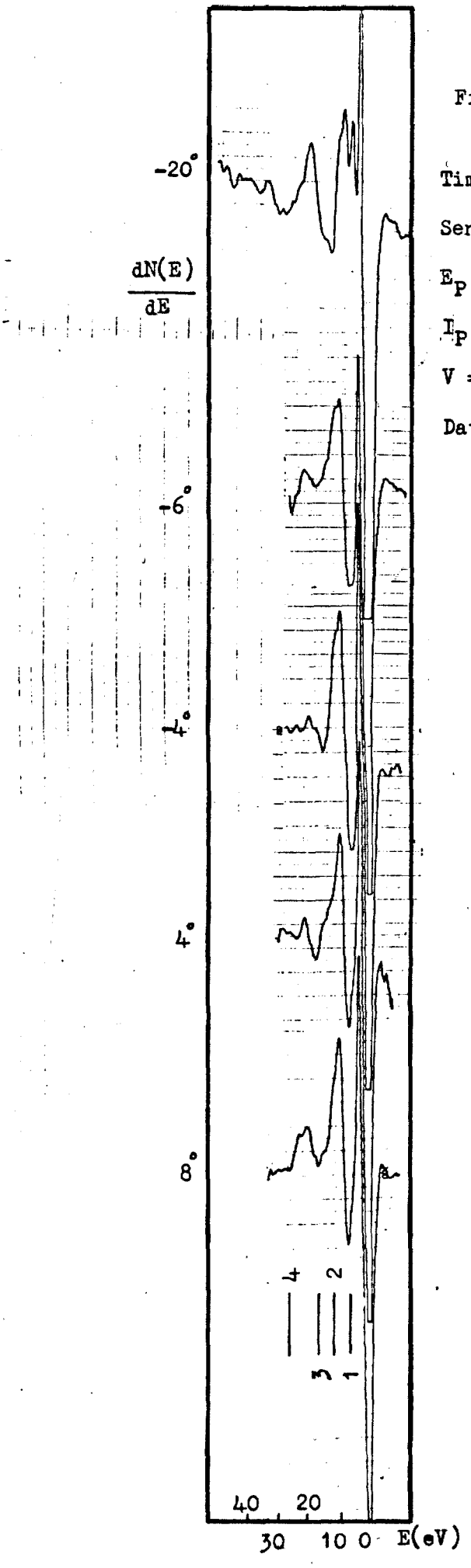

Time Constant = 1S

Sensitivity = 1mV

E_p = 1000eV

I_p = 14 μA

V = $2V_{p-p}$

Date 10.4.79

and structure of the losses is then completely different than obtained normally. This is illustrated at -20^{o} in Fig. 4-12.

Variation of the beam current gives no alteration other than intensity of the spectral features, but as the current decreases the transition becomes weaker, until at 6 μA the spectrum is unidentifiable. Fig. 4-13 is a combination of some spectra taken at different currents.

Investigations were carried out at different modulation voltages. The effect of modulation amplitude on electron-excited Auger data is reported by Grant et al. (1974). They pointed out that the background is essentially eliminated in the derivative data. The reported Auger spectrum indicates that the magnitude and shape of these spectra are better behaved as a function of the modulation amplitude. The strength of the features vary almost linearly with low amplitudes, and are almost unchanged at intermediate amplitudes. The effect of distortion is simply to broaden the features at large amplitudes. The peak broadening resulting from large oscillation amplitudes also produces marked changes in the relative peak-to-peak height of the various Auger features.

The present study shows, at low amplitudes the second order losses to be vanishing, as shown in Fig. 4-14. At large amplitudes (4 V_{p-p}), the spectrum is quite distorted, and is not included in the figure. At intermediate amplitudes, the spectra are unchanged.

It is clear that the loss spectra,with several exceptions,

Characteristic Electron Energy Loss of Sb with different incident current.

Fig.4-13

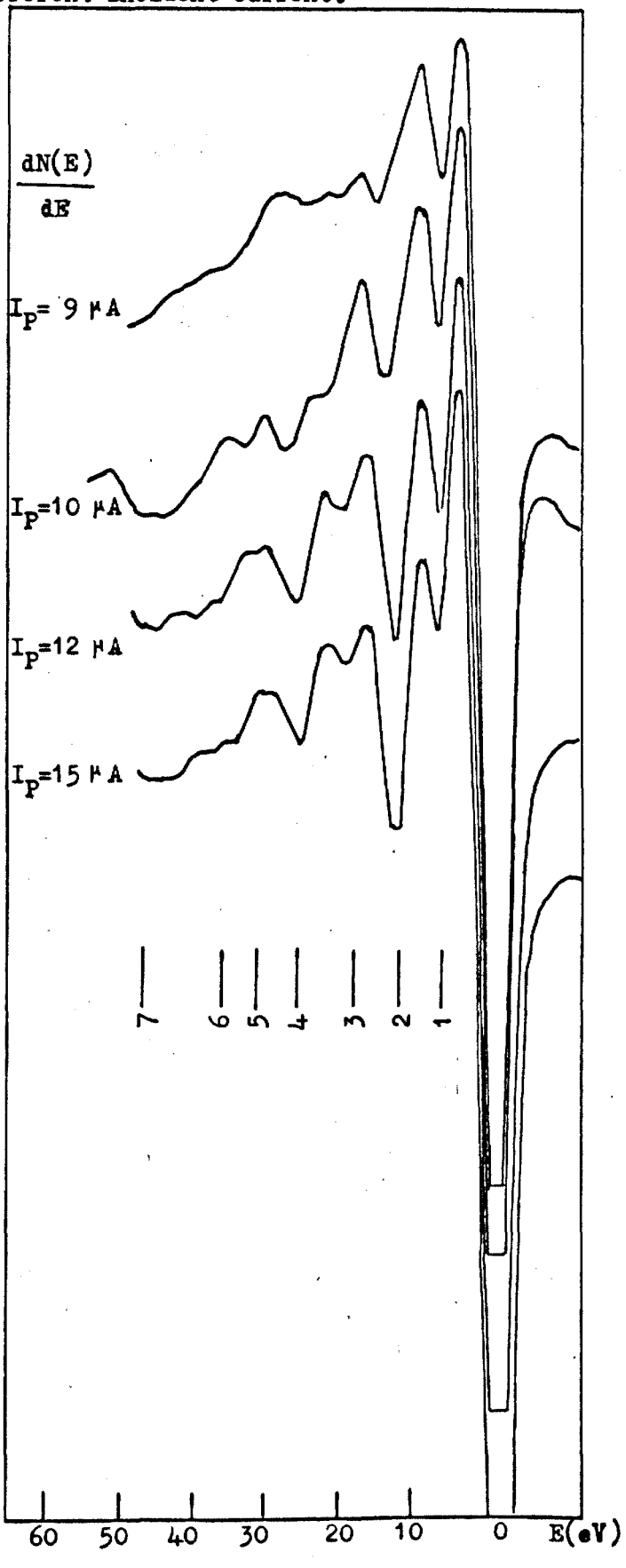

Fig.4-14

Energy Loss Spectra of Sb
at different modulation Voltages

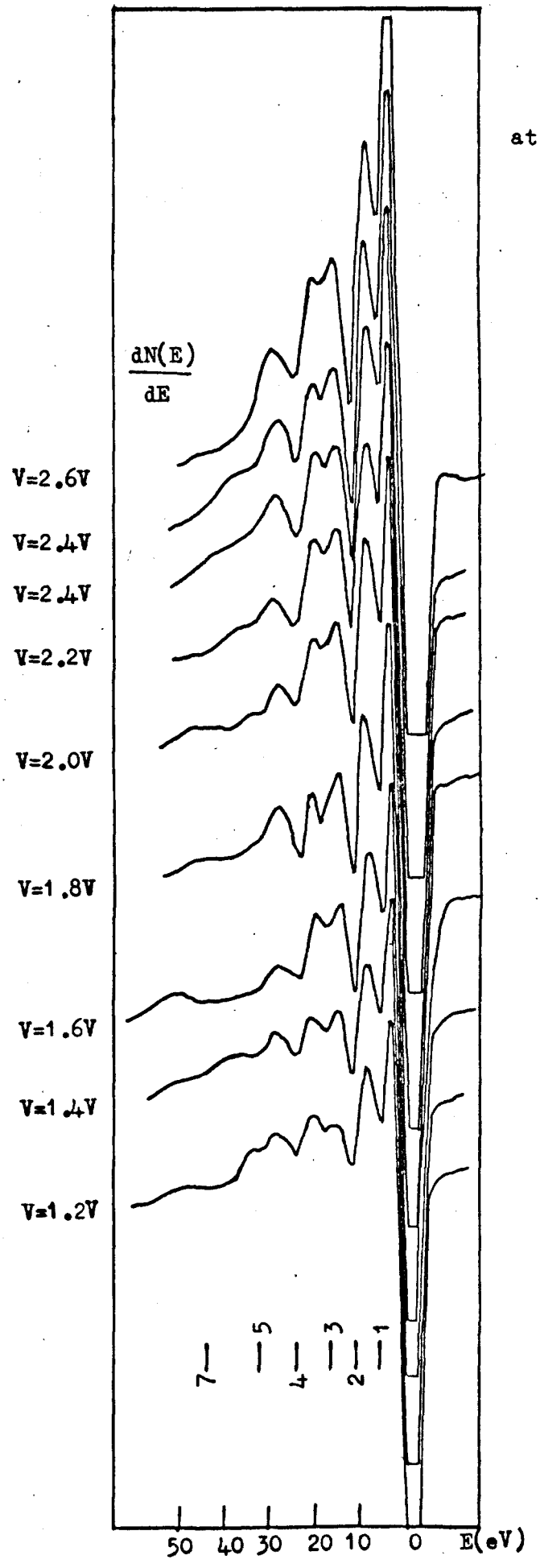

can be described almost entirely by combination of 16.78 and 11.3 eV losses. The former is identified as the bulk plasmon loss, and the 11.3 eV loss tentatively as the surface plasmon loss, which was first proposed by Ritchie (1957). The ratio of these energy losses is then 1.48, slightly greater than the ratio of 1.41 predicted by Ritchie.

Lemonier et al. (1973), in an optical measurement in the range of 0-16 eV, reported a maximum loss peak in the vicinity of 15.8 eV for the bulk plasmon, and 11 eV for the surface plasmon. The calculation of bulk plasmon loss energy, by considering five valence electrons ($5s^2 5p^3$) of each antimony atom behaving as free-electrons, gives a bulk plasmon energy of 15.1 eV, compared with the experimentally obtained value of 16.78 eV. The discrepancy can be partly explained by the influence of inter-band transitions.

The theoretical bulk loss to surface loss ratio is $\frac{1}{\sqrt{2}}$ (or 0.707), Pines (1956), and Lemonier et al. (1973)'s result is in agreement with this. In the present study, this ratio was found to be slightly lower at 0.67 .

The 6.25 eV loss is possibly due to the ionization of the O_1 electrons to a state near the Fermi level. The binding energy of these electrons is 6.7 eV, Servier (1972), and comparison with the observed value of 6.25 eV, gives some indication of the loss mechanism.

The observed peak at 31.75 eV is associated with ionization of the N_{45} electrons, to states just above the Fermi level of the solid. This energy value of 31.75 eV

compares well with the 32 eV reported by Servier (1972).

The remainder of the transitions are multiples of the surface and bulk plasmons. The appropriate configurations are summarised in Table 4, as well as the possibility of $N_{23} \longrightarrow N_{45}$ electron excitation contributing to 66.33 eV peak.

The losses of antimony consist of strong plasmon features as depicted in the loss figures. It has been pointed out by Wright (1974), that the losses of semi-metallic antimony are anomalous because they resemble the losses of a metal such as Al, which has a free-electron-like character. Powell (1960), has mentioned the free electron gas like behaviour of antimony and other elements in group V of the Periodic Table, and the other poor conductivity solids such as Si, in the region of plasma resonance. One explanation is based on a region of high electron density being produced, in poor conductivity materials, by the primary beam. Free electron-like plasma oscillations then occur in this confined plasma. This suggestion was criticised by Singh (1976) because it does not explain why the plasmon energy (calculated by regarding the valence electrons as undergoing free-electron gas like oscillations) agrees so well with the observed plasmon energy for a large number of solids.

The result shows that the plasmons in antimony and other semi-metals, such as silicon, are excited in the valence band electrons. These valence band electrons appear to behave in a free electron like manner for high frequency plasmon oscillations, although they may not display a free-

electrons gas like character for other properties, such as conduction.

From the full width half maximum (FWHM) of a plasmon loss peak, the life time of an oscillation can be estimated, by using the Uncertainty Principle $\Delta E = \frac{\hbar}{\Delta t}$. The loss spectra recorded with 1000 eV primary electrons in Fig. 4-6 was used to estimate the FWHM of the first plasmon loss peak, which was found to be about 3 eV. To determine the true FWHM of the plasmon peak, the instrumental contribution value which is the FWHM of the elastic peak ($\sim$3 eV), should be subtracted from the practical value of plasmon peak of slightly greater than 3 eV. The life time of an electron-excited plasmon oscillation is then calculated to be 10^{-14} seconds.

Singh (1976) reported a value of 2×10^{-15} seconds for a plasmon oscillation, and the discrepancy is most probably due to the more sensitive CMA (apparatus) he used. Lemonier et al. (1973) obtained the plasmon oscillation life time value of 2×10^{-16} seconds from optical measurements. From this figure, they indicated that the plasmon decay phenomenon is due to electron-electron collisions.

4-3 SEE Yield Measurement

The measurements were made on the antimony crystal surface which was prepared as stated earlier (see Section 3-2.7b). The surface was characterised by an Auger analysis taken after the internal cleaning operation was completed, and then the yield spectra were recorded.

A typical spectrum for a 1.1 kV electron beam at normal incidence with respect to the target is presented in Fig. 4-15. The spectrum shows a largely flat curve, and it is difficult to determine the exact location of the maximum. Some structure is discernable in the low energy section of the yield curve. In order to observe the variation of yield characteristics the spectra were taken under different circumstances, e.g. energy, but no essential differences were found apart from slight differences with different angles of incidence, as seen from Figs. 4-15 and 4-16. Goto and Ishikawa (1972) in a method for detecting fine structure in the SEE yield spectra, observed the fine structure of Si for the whole energy ranges, (20-2000 eV). Therefore it may well be possible to see similar fine structure in antimony SEE yeild spectra, which may change in different situations.

In general, the SEE yield spectrum for clean Sb has a maximum at 660 eV, with δ = 1.32 and a first cross over at 266 eV (see below). These values have been obtained from an average of some 20 spectra. The result is in agreement with the experiments on Sb by other workers, as may be seen in Table 5. The spectra at different incident energies show, at low incident energy the maximum point slightly shifted towards the lower energy side. This may be related to the defocussing of the beam at low primary energies. With no retarding voltage, a 1.1 keV beam exhibits a spot size of about 0.75 mm, with a faint cone shape corona. The beam intensity and spot size is directly dependent on the electron beam energy, a lower electron beam energy giving a large diameter corona with high intensity, (diffused beam). Because

Secondary Electron Emission Yield of Sb

Fig. 4-15

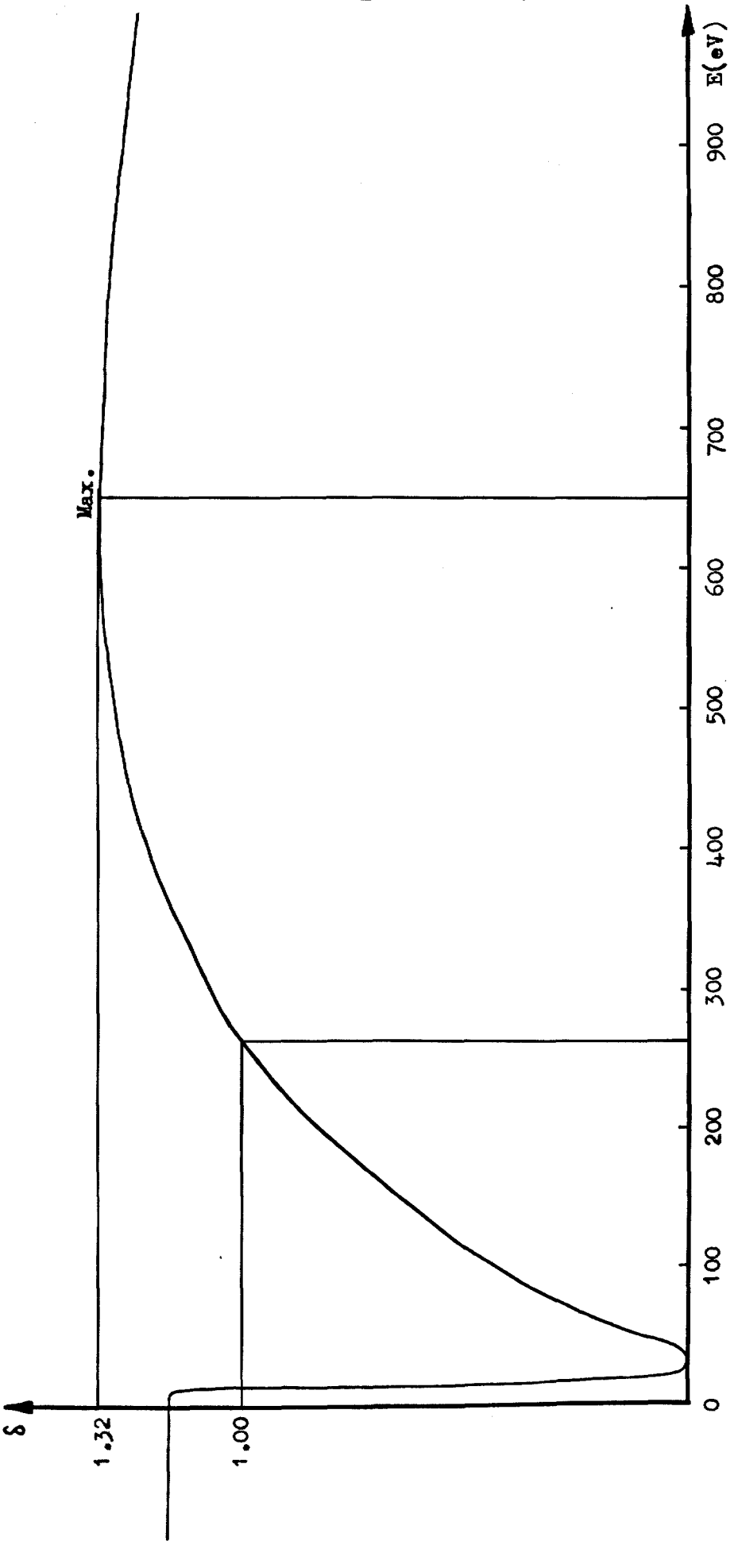

Fig. 4-16

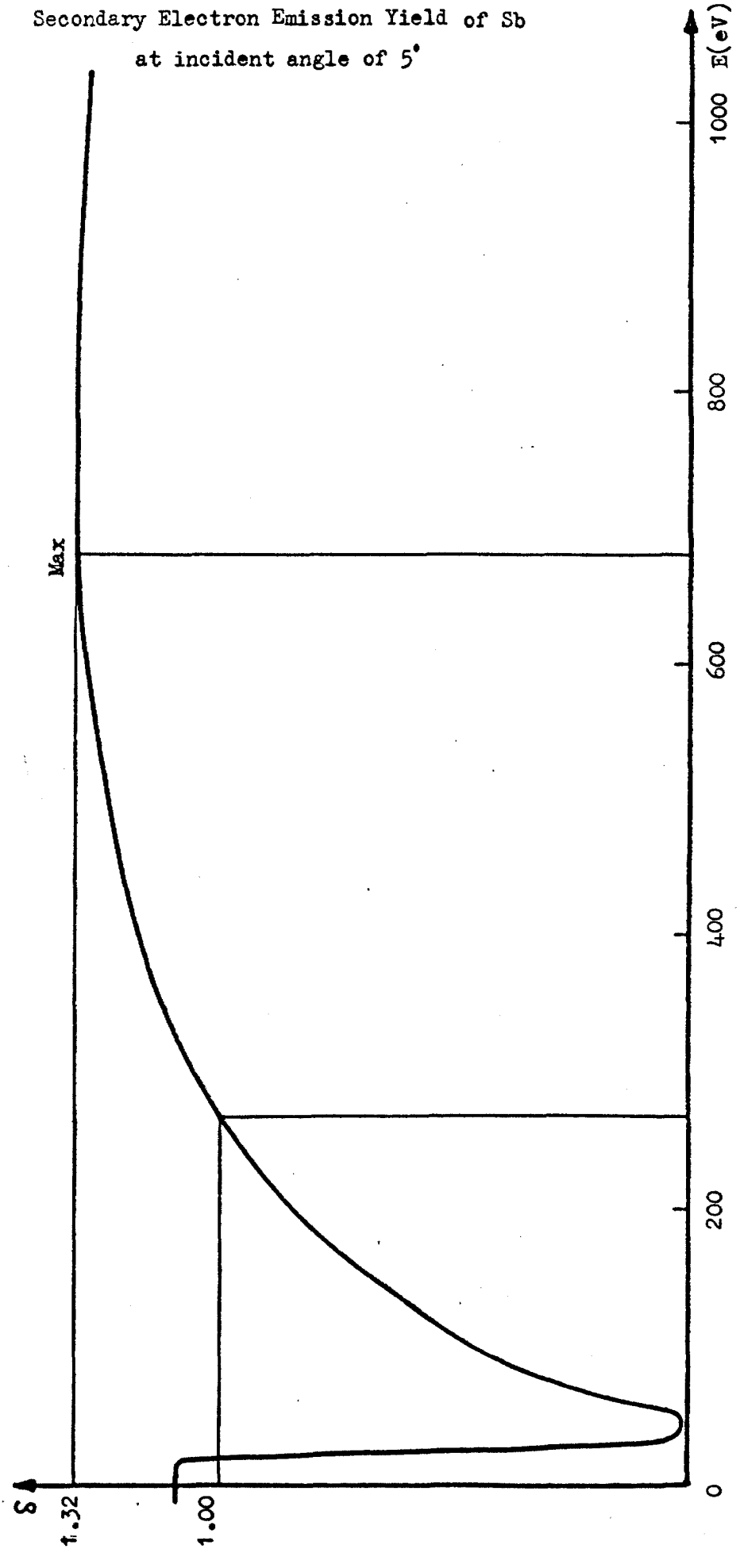
Secondary Electron Emission Yield of Sb
at incident angle of 5°
E(eV)
1000
800
600
400
200
0
Max
δ
1.32
1.00

Table 5

SEE yield data for Sb

		δ	E_I	E_{max}	E_{II}
Present Work		1.32	266	660	-
Kollath (1956)		1.3	250	600	2000
Appett & Hachenberg (1960)		1.17	320	700	2400
Kaneff (1960)		1.3	300	650	3500
Ono & Kanaya (1979)	Theory	1.34	-	680	-
	Experiment	1.2-1.3	-	600	-

of the small antimony crystal disc size (8mm diameter, see Fig. 3-4), at some angles electrons tended to hit the stainless steel surface surrounding the crystal (although it is covered by antimony vapour, see Section 3-2.7), producing secondary electrons. As a consequence of this, a slight shift was observed at a beam energy of 700 eV, whereas for beam energies greater than 800 eV, no shift was detectable.

Secondary electrons are emitted by all materials; due to the mechanism of the excitation of electrons in the solid by the incident electrons, the diffusion of electrons to the surface, and finally the escape of excited electrons through the surface barrier. The secondary electron emission yield, $\delta = \frac{i_s}{i_p}$, for a given material varies by a function of primary energy, δ increasing with this energy up to a maximum, before decreasing again. As the energy is raised beyond the maximum, electrons are excited from an increasing depth within the material, so that many of them are unable to diffuse to the surface and surmount the potential barrier to escape.

The two energies at which the yield is unity are denoted the first and second cross overs (see Fig. 4-15). As shown in Table 5, the present study did not allow the second cross over point to be recorded, due to limitations of the equipment in not being able to go over 2000 eV for the energy.

The SEE yield depends also on the angle of incidence of the primary electron beam with respect to the surface

normal, Müller (1937), see Section 1-3. Müller's results show that variation of ± 10° about the surface normal has no marked effect on the magnitude of the yield. Fig. 4-16 is the photograph of the yield spectrum at 5° incident angle.

A small calibration of the full yield spectra of about 10 eV arising from the instrumentation was usually necessary. This value was deduced from the calibration of Auger and energy loss spectroscopy, (see Section 4-1).

The secondary electron emission yield of a material is interesting for various applications. The present particular interest of the study is in the low energy range (0-50 eV). To prevent possible errors in this low energy region, the complete spectrum (0-1.1 keV) was recorded and checked for accuracy. Then the part required for analysis was recorded with increased amplification.

4-4 Surface Resonances and Crystal Surface Structure

The reflection coefficient intensities have been recorded in order to study the internal structure of the Sb (100) surface . An attempt was made to study these structures in the manner similar to that described by McRae and Caldwell (1978) in their work on clean low index metal surfaces (in particular Ni). In electron reflection spectroscopy, the total secondary-electron yield (δ) is measured as a function of incident electron energy E_p. It was shown by Goto and Ishikawa (1972,1973) that the fine structure that is superimposed on the generally smooth yield is predominantly due to the elastically reflected or diffracted

electrons, particularly for low voltages between target and incident electron $V \leqslant 50$ eV.

The mode of operation of the spectrometer was to use a constant electron beam energy. This gives a constant beam current, (see Section 3-2.11), spectra were then obtained by scanning a retarding voltage applied to the target. A small modulation voltage (~ 3.4 eV) was applied to the sample to feed the signal to the LIA. The electronic scan system was very sensitive to the amplitude of modulation voltages, small increases ($\sim 0.5\ V_{p-p}$) overloading the LIA. This was also sensitive to the modulation frequency. The frequency and amplitude however, affect the yield and surface band structure spectrum which necessitated adjusting the circuit by taking the yield spectrum in the full range (0-1000 eV).

The resonance peaks are extremely sensitive to the nature of the sample. In order to identify these peaks, sets of reflectivity curves for antimony were recorded. Within each set, the successive curves correspond to 1° increment in the angle of incidence. The surface resonances are also very sensitive to lattice geometry, and ideally would be best adjusted by means of a LEED facility which was not available on the present apparatus.

Typical results of the net current electron reflection measurement on Sb are shown in Figs. 4-17 to 4-20. A series of very small peaks are observed on each set of curves. Figs. 4-17 to 4-20 are two sets of spectra taken at different incident beam currents. Large currents either cut off the Bragg peak at high sensitivity, or at low sensitivity the

Fig. 4-17

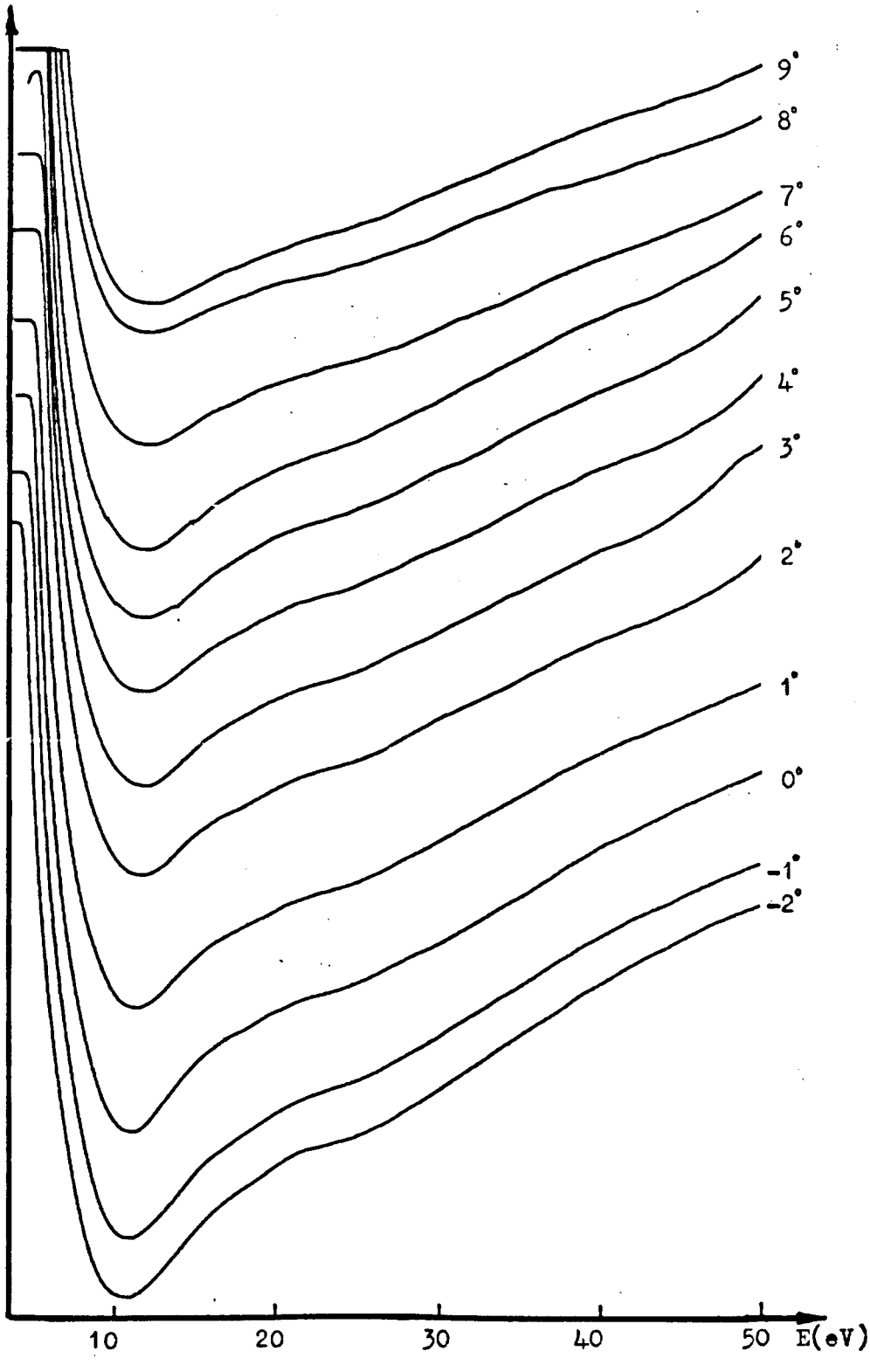

Raw electron-reflection data for Sb(100). The numbers against the curves denote incidence angles (deg.), relative to normal incidence. Data corresponding to both senses of rotation away from normal incidence are shown, for incident current of 20μA.

Figure 4 - 17 Continued

Fig. 4-18

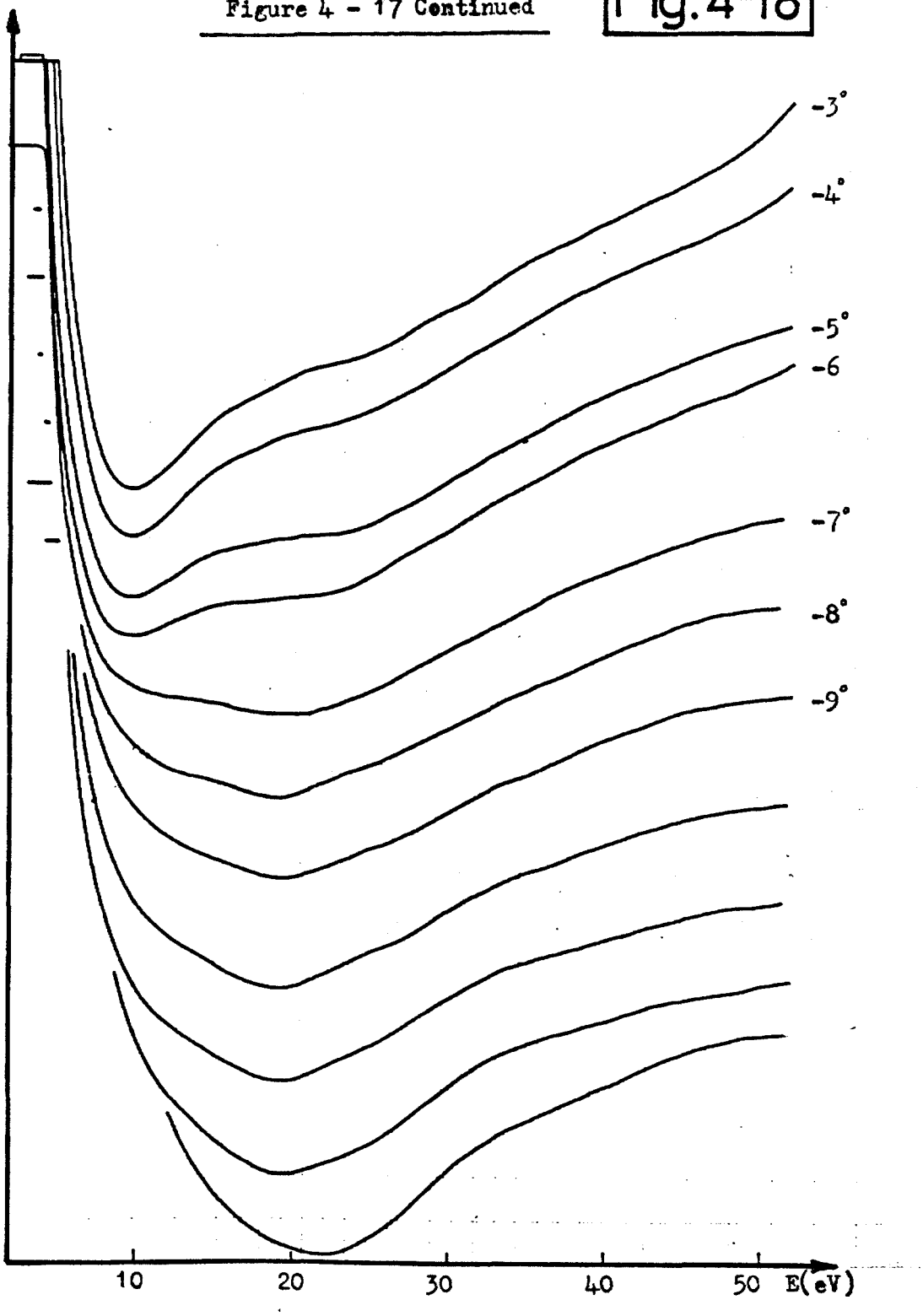

Fig. 4-19

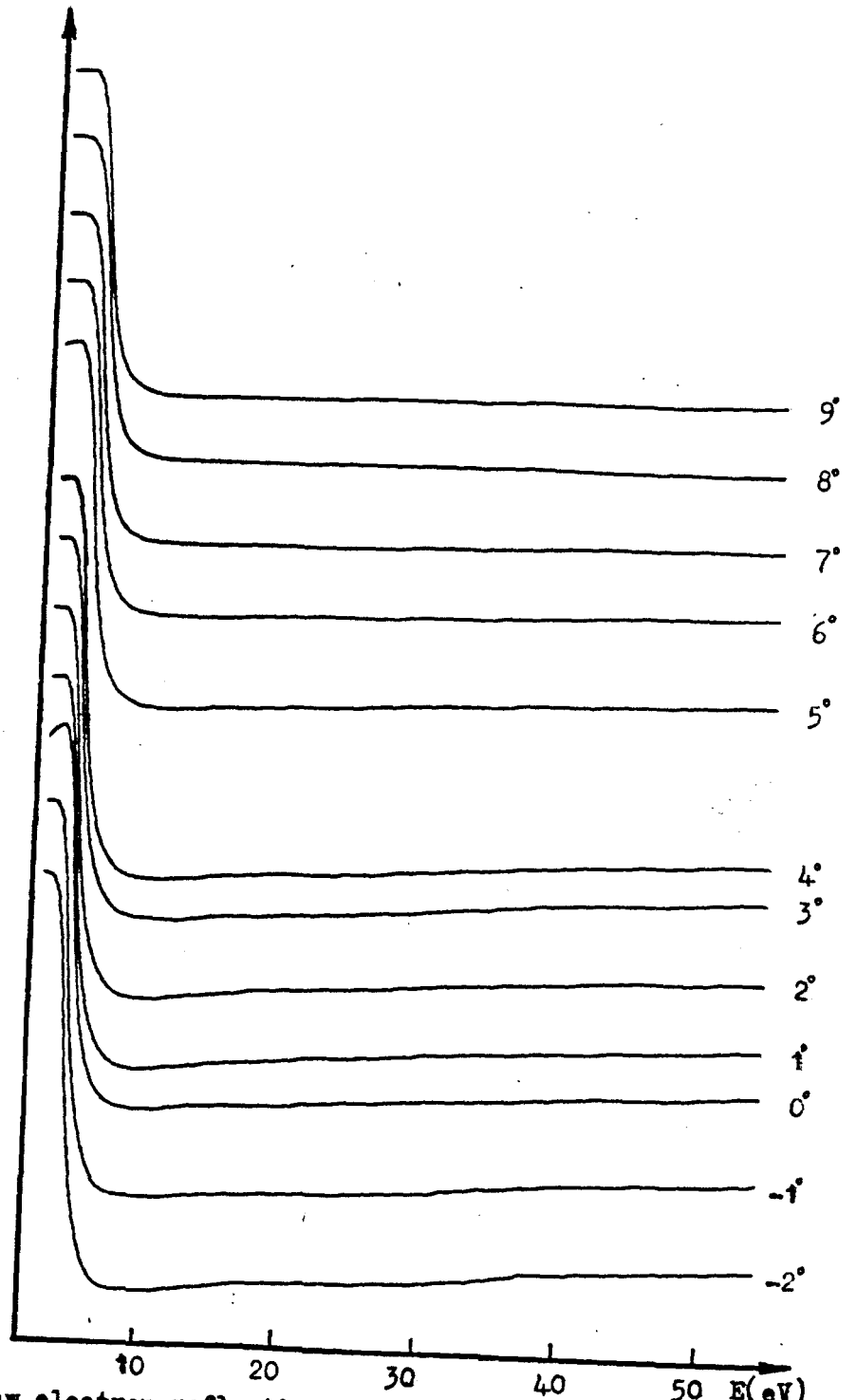

Raw electron-reflection data for Sb(100), at low incident electron current (I_p = 5μA).

Figure 4 -19 Continued

Fig.4-20

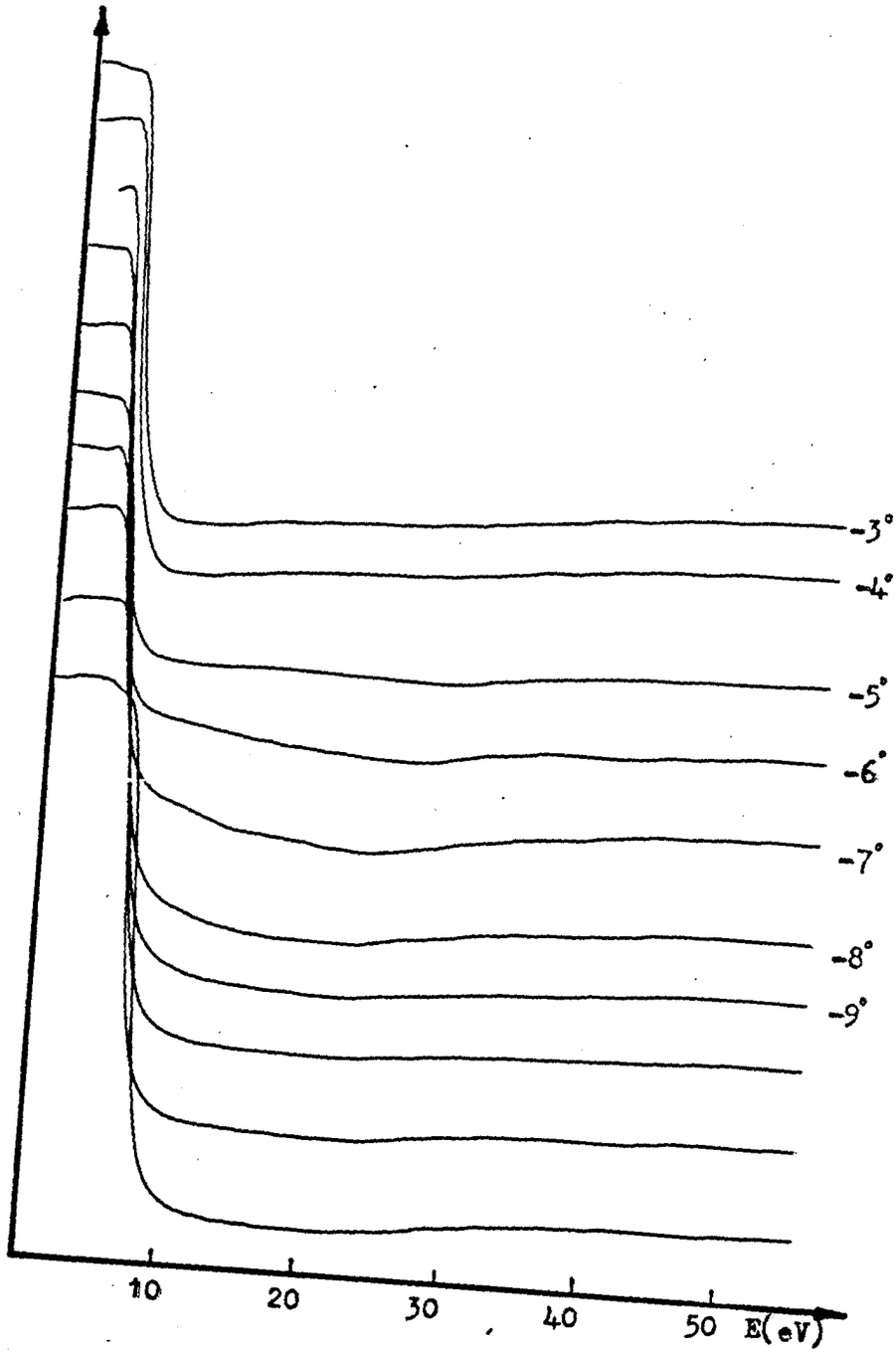

resonance band structures are not discernable. Therefore, for unambiguity, two sets of spectra are included. The consistency of the results from set to set may be further seen in the eight sets of spectra in Appendix 5. The peaks that make up these series are not observed throughout the entire range of the applied angle of incidence, but were seen in certain ranges of the angle of incidence to be submerged in more prominent intensity peaks. The figures are direct photographs of the spectra in the range of 0-50 eV electron energies at different angles for incident energies of 1 keV. At different energies, if the incident current was normalised, little difference was found between the spectra. At different current, only the intensity of the peaks are changed. As the angle alters, the resonance peaks are shifted. Since they follow the E vs $k_{||}$ band structure, which is part of the parabola, altering the angle alters $k_{||}$. In the case of McRae and Caldwell (1978), the precision of measurement was greatly enhanced by the use of digital methods of data handling, including a digital filter to remove the background due to inelastic and non-resonance elastic scattering. At the time of the present studies, the data handling facilities involving an Analog-Digital converter and a microprocessor linked to a computer, which are currently being developed in the Department, were not available (as was originally intended) to emphasise the surface resonances. Nonetheless, an attempt at interprettion has been made and the surface resonance band structure is explained by a two-dimensional nearly-free-electron scheme.

Experimentally obtained data by angle-resolved electron emission spectroscopy, which is simple and does not present

very difficult or costly problems, is necessary for the determination and interpretation of the surface band structure. The experiment consists of measuring the dispersion of electronic surface resonances at energies of the order of 10 eV above the vacuum level. This gives rise to structure appearing in the inelastic part of the spectrum, which reflects the electronic energy band structure of the unbound states at the surface.

The features identified as resonances comprise very weak and narrow structures. These structures are displayed against, or submerged in, a background, and it is very hard to accurately position the peaks. The position of the structure have been obtained by comparison of the position of the peaks from ten different sets of spectra, which were taken on different occasions and at different energies. The calibration of the spectra was obtained from related yield spectrum, which was presented in the previous section.

The figures represent the negative of the net-current against the incident-electron energy. The numbers against the curves denote the incident angles (degree), relative to normal incidence. Data corresponding to both direction of rotation away from normal incidence are shown in Fig. 4-21. These data are not symmetric as expected, (curves for Ni were symmetric, (McRae and Caldwell (1978)). This is perhaps an antimony crystal physical property, (the reproductability of the spectra indicating this) or possibly because of the eccentricity of the manipulator rod (see Section 4-1). This was quite satisfactory for Auger spectroscopy, but may not be sufficiently accurate enough for these measurements.

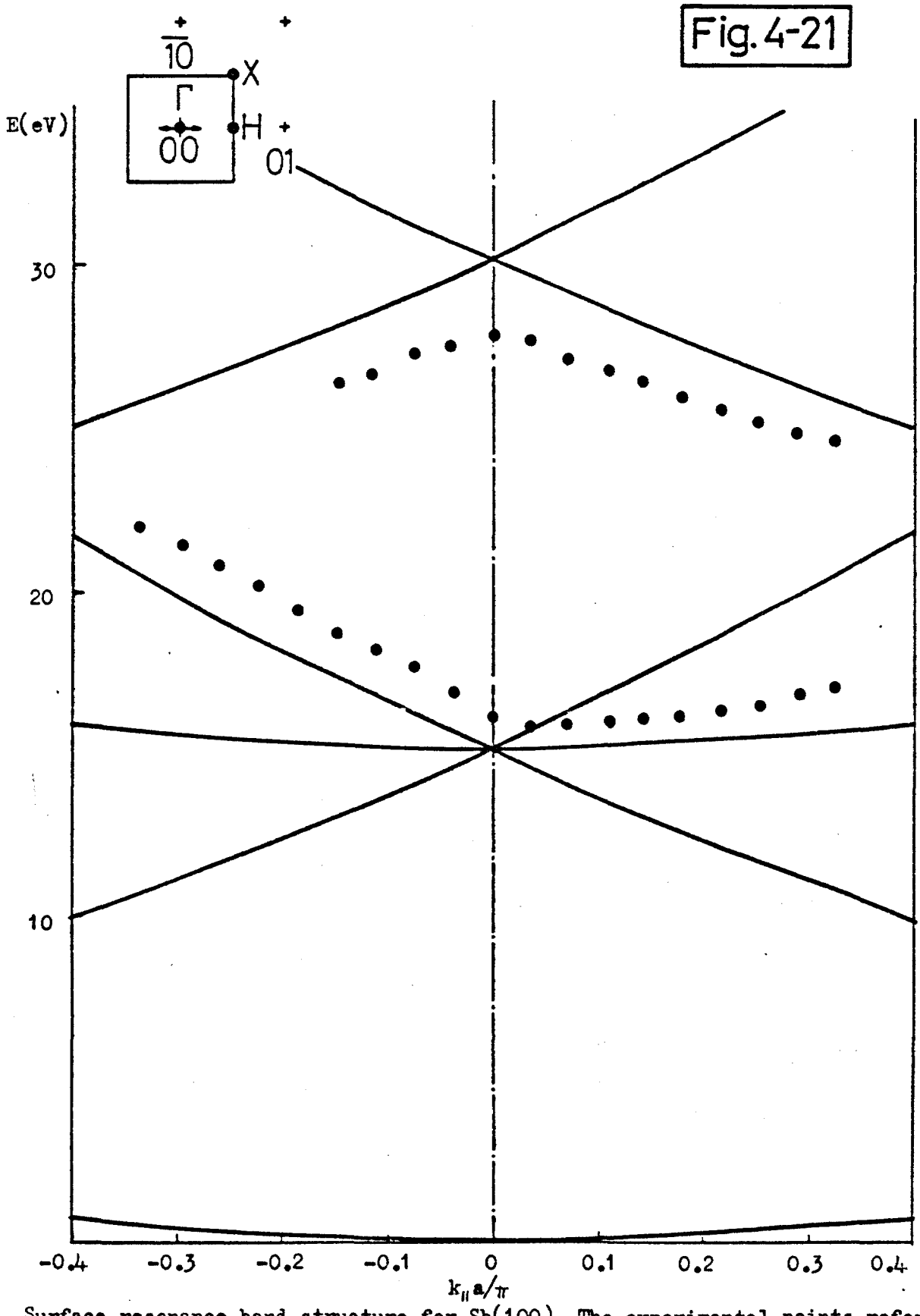

Surface resonance band structure for Sb(100). The experimental points refer to minima taken from averaged data of unfiltered spectra,(see text). E denotes electron energy, $k_{\parallel}$ denotes reduced parallel momentum, and a denotes the unit mesh side for Sb(100),(a=3.13 A).The full lines are free-electron resonance energies,(see Sec. 2-3). The inset at upper left shows the first two-dimensional Brillouin zone (square), reciprocal-net points (crosses) and symmetry points (filled circles) for Sb(100) surface. The arrows indicate approximately the range of $k_{\parallel}$, relative to the Brillouin zone, represented by the with of the figure.

Consideration of McRae's work, (see Section 1-4), and application of these principles to the present study, (see Section 4-4.1), demonstrates that:
Resonance dispersion curves can be interpreted in a simple way to determine the surface band structure of the metal to within the limit of the present experimental apparatus which will be considerably improved when it is possible to filter digitally the yield curves.

McRae, in order to relate the resonance fluctuations to the required precision, obtained the net-current data in digital form, and used a high-pass digital filter to remove the background due to inelastic and non-resonance elastic scattering. The resonance mechanism derived from the spectra is described elsewhere, (see Section 1-4.3). The essential properties of the resonance peak may be derived by considering the scattering of a plane wave, by a single layer of isotropic (s-wave) atomic scatterer with one atom per unit mesh.

As pointed out above, because of the novel nature of the research, in this laboratory many problems in operating the data processing system were experienced. The data processing system was based on a D.E.C. LSI-11 mini-computer and two similar configurations were used. Initially, the system comprised the LSI-11 micro-processor with a 32k word resident memory; a 16 channel analog to digital converter; key board and monitor and a dual 8" floppy disc drive. The operating system was the D.E.C. RT-11, supplied on disc by Digital software. Spectra from the LIA output were sampled, under programme control, via the analog to digital converter, operating in a Quasi-differential mode, Digital Equipment

Corporation (1979), eliminating Earth loops and spurious noise between the spectrometer and the processor. The samples were then stored on the mass storage medium of floppy discs to allow later processing by the technique of digital filtering, Bogner and Consstantindes (1975), Peled and Lin (1976), and Golo and Rader (1974).

The filtering action is basically a convolution about a sample X_n, of X(n-H) to X(n+H), where H is the filter order. The D.F. (Digital filtering) coefficients were determined from the routine developed by McClellan et al. (1973). The coefficients are user-determined by setting the parameters of filter band edges, filter order and the pass band/stop band ripple ratio. This gives the great advantage over active digital filters of flexibility - to redesign a particular filter it is simply a matter of redefining the input parameters of the filter programme.

Before attempting to filter original antimony spectra, McRae's unfiltered results for Ni were first processed to check the validity of the technique on the raw data. This was accomplished by manually digitising the unfiltered curves, and then filtering these samples with the same type of high pass filter that McRae used. The filtered output was very similar to that of McRae's, although the signal/noise (S/N) was much inferior, due to the crude method of sampling. Thus the validity of the technique was established and original spectra sampling was attempted with the initial system described. Spectra were sampled at a rate of 50 samples/second, giving 10,000 samples per spectra.

These samples were then filtered, using both a high pass filter of order 29 and high pass filter of order 45, and the filter output was stored on disc. At this stage, the first of many problems arose, this being the lack of availability of a compatible graph plotter. A normal X-Y recorder is not suitable without a great deal of custom interface hardware and software, and to purchase a suitable graph plotter was beyond the means of the group. A simple line printer, or Visual Display Unit plot is wholly unsatisfactory, it being based on a grid of only 72 x 134 units, thus providing a grossly approximative curve.

It was decided, therefore, to attempt to transfer the data from disc to the University of Keele's mainframe G.E.C. 4082 series computer, giving access to a sophisticated graph plotter. The only transfer medium available was punched paper tape produced from a Data Dynamics Type 33 teletype, which, via a special systems routing could be read by the G.E.C. 4082. Unfortunately, the Type 33 teletype was never designed for long paper tape output, and since it took approximately 1½ hours to record one spectrum onto the tape, the output was always erroneous in places.

To solve this problem, the system was reconfigurated to interface directly with the G.E.C. 4082, allowing sampled data to be stored directly on to the 4082 disc store. To accomplish this, a new operating system software package was written by Knox (1980), which allowed the LSI-11 processor to communicate directly with the 4082 hard disc, and the LSI-11 effectively became a programme controlled data acquisition point. Once sampled and stored, the data

could be processed by the faster and more powerful G.E.C. 4082 mainframe.

After configuring the system and spending some time on "de-bugging" the operating system and the sampling routines, original spectra were sampled at the relatively slow rate of 10 samples/second and stored. However, on plotting these samples, it was discovered that the S/N ratio had deteriorated dramatically, and on investigation the cause was found to lie on the analog to digital converter circuit board. The sampled signal had a maximum magnitude of 1 V, and was often in the millivolt region. The specification of the converter was quoted by the manufacturer to be $\pm$ 0.04 millivolts, but in fact samples were found to vary over $\pm$ 10 millivolt range. This was confirmed by sampling a continuous signal from an accurate DC calibration source. It was not possible to eradicate this entirely random fluctuation by filtering and all structure present on the spectra was comprehensively lost. Consequently, the analog to digital converter board was returned to the manufacturer for repair, and at the time of writing, has only just been returned. Rather than lose the spectra irrevocably, they were simultaneously recorded on a Bell and Howell 3000 4 channel analog tape recorder and stored on standard cassette tapes. This was carried out by connecting the output of the LIA through a potential divider to one of the four tape recorder inputs. It should be noted that the tape must be replayed from the output of the same channel. As soon as the converter board is re-installed and tested these tapes will be used as the source of original data. Sampling and processing will be carried out as originally intended, and it is hoped that filtered results

will be produced in the near future.

However, interpretation of the unfiltered spectra is carried out by taking into account the possible experimental and theoretical approximations, which are clarified in the next section.

4-4.1 Analytical Technique

The calculation of the structure of crystal surfaces is very complicated, McRae and Caldwell (1967). There is some uncertainty that surface structure arises from an ideal surface, based on the following considerations:

a) The structural problem

b) Approximations in band structure calculations.

a) The structures of group V elements (As, Bi and Sb) are only slightly distorted from the simple cubic. Hence, it is reasonable to say that in materials with average valence 5, the simple cubic structure is favoured, much as the diamond and closely related hexagonal structures are favoured by materials with average valence 4, Jona (1967). The net restult of the distortion is that each atom has three equidistant nearest neighbours, Fig. 4-23. The next-nearest neighbours lie in the adjacent layer, and it is the bond between the layers that are broken when a crystal of Sb is cleaved. It is more convenient , however, for the present discussion, to focus attention on the pseudo-cubic character of this structure. Fig. 4-24a depicts a perspective view of the pseudo-cubic cell, and Fig. 4-24b shows how the truly rhombohedral cell

Fig. 4-23

The layer structure of Sb and Bi. Solid lines represent (shorter) intra-layer b
dashed lines represent (longer) inter-layer bonds, Jona (1967)

Jona (1967)

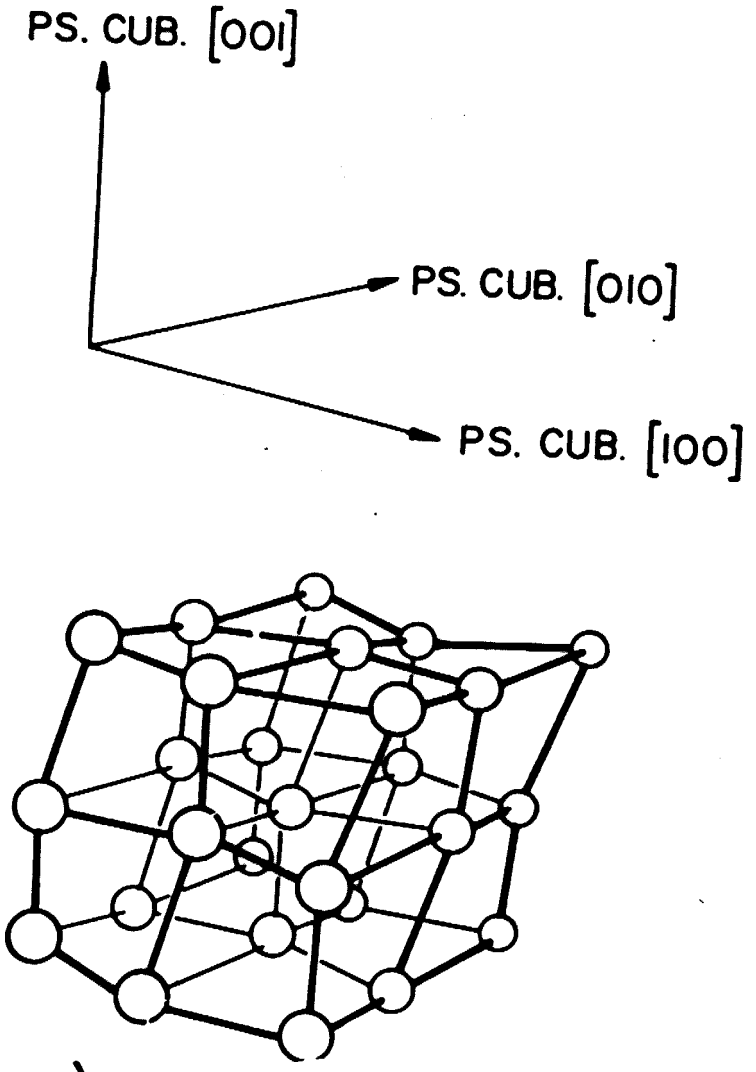

a) Pseudo-cubic cell of Sb or Bi.

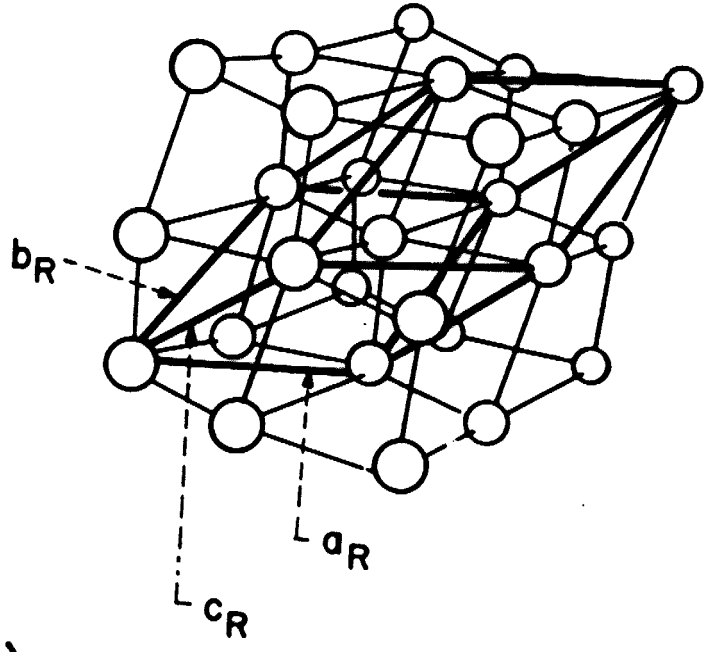

b) Rhombohedral unit cell (heavy lines) inserted into the pseudo-cubic cell of fig.a)

Fig.4-24

fits into the former.

b) Calculation of the band structure is carried out in a fashion similar to that described by McRae and Caldwell (1978) for Ni, and a more complete description appears in Section 2-3.

The nearly-free-electron approximation was used in the calculation, and it must be born in mind that there are a number of factors that may cause inaccuracy in interpretation.

Using this approximation, the $E(k_{||})$ against $\underline{k}_{||}$ function for an Sb crystal with lattice unit a_o = 3.13 Å was calculated. The calculation is derived from the relation

$$E(k_{||}) = \tfrac{1}{2}(k_{||} + 2\pi g)^2$$

as given in Section 2-3.4. The value for a_o is taken from Appendix 4, and is the average of AM and AN. Obviously, this will give rise to some error in the calculation, since it assumes a simple unit lattice with average side 3.13 Å. Since the unfiltered data is subject to considerable error, it was thought that as a first approximation, it should be fitted to this approximated structure.

Surface resonance band structure, derived from Figs. 4-17 to 4-20 and Appendix 5, is plotted as Fig. 4-21. Fig. 4-22 exhibits the scatter of the data in the case of three sets of spectra. Fig. 4-21, however, gives the average of all ten sets of results. The energies plotted are those of identified minima from the figures. The agreement between the calculated and observed energies is encouraging since it is unfiltered data that is plotted. This is supported by

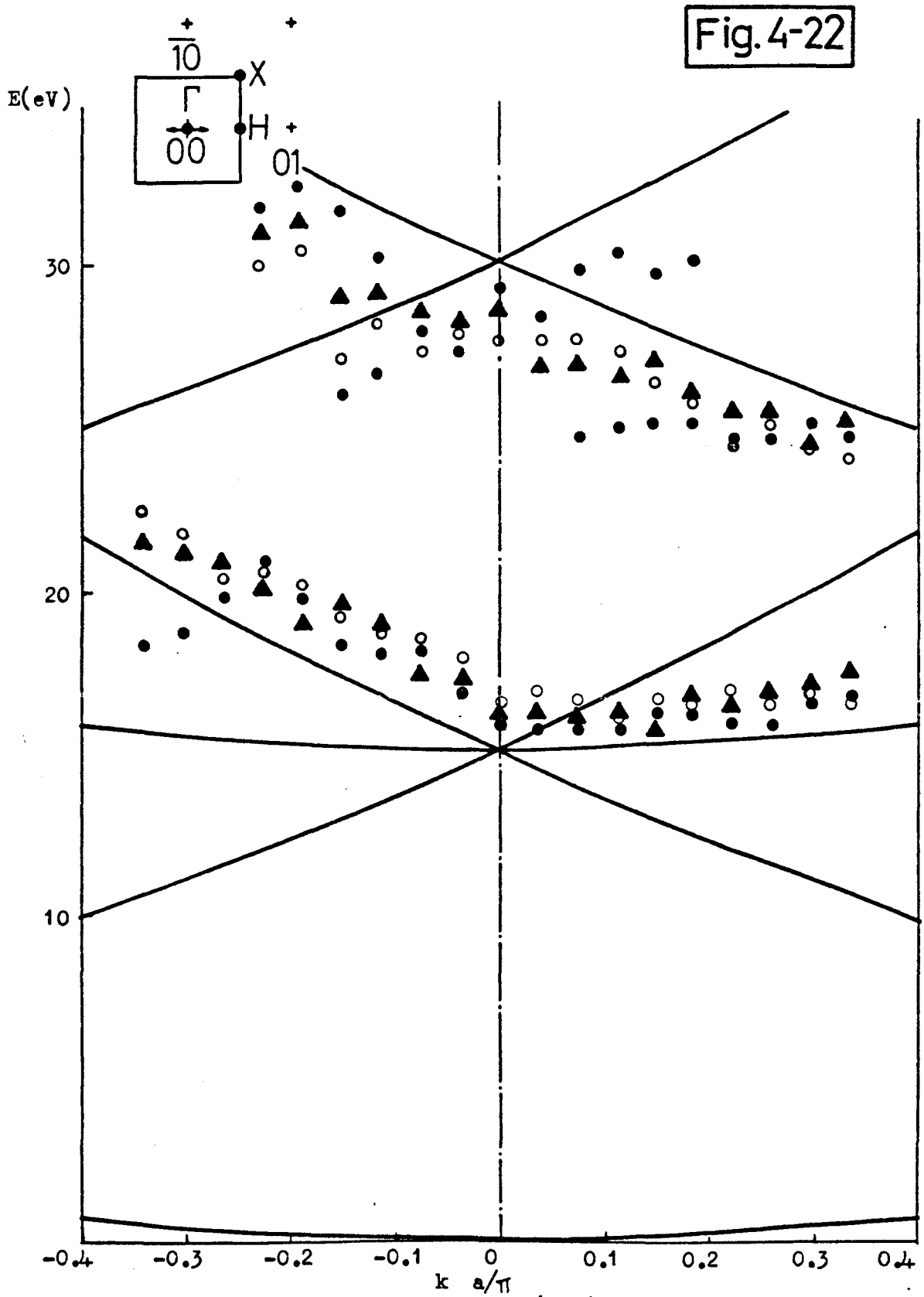

Surface resonance band structure for Sb(100). The experimental points refer to minima taken from three unfiltered spectra. The symbols o, ●, ▲ refer to experimental minina of each of the above spectra. The positions of the observed resonances are fitted by the 2D-free electron approximation with a binding energy of 2.1 eV. For notations see Fig. 4-21 caption.

Fig. 1-11, which shows the similar disparity if one takes McRae's unfiltered results and fits them to the band structure for Ni. Consequently, the preliminary results prove encouraging for further work and the applications of digital filtering techniques to the original curves should prove particularly interesting.

Chapter 5

Conclusions and Suggestions for Future Work

Secondary electron emission spectroscopy provides powerful techniques for the investigation of chemical composition and atomic geometry of surfaces. Electron induced Auger and characteristic energy loss spectroscopy were employed in the present work as surface chemical probes and their analysis proved very successful. However, due to some experimental effects, principally connected with the retarding grid optics, some sources of error were inevitable.

As pointed out in the text, the ideal geometry of the retarding grids is spherical, but this is impossible to achieve in practice. Because of the condition that the target be both at the centre of the grids and demountable, the spherical geometry was attempted by the joining of two hemispheres. The two halves were located by wire pins, thus giving rise to equatorial distortion. Wright (1974) suggested an aluminium disc, grooved to accept the grids, but found it to be unsuccessful in practice. To improve on the original design, a fundamental reassessment of the complete apparatus would have been necessary, and due to time considerations was considered impracticable.

Further, the need for the electron gun, projection lamp, and target holder to project into the inner grid space, necessitated the provision for holes in each grid. Such apertures, although relatively small in comparison to the

grid surface area, are a major source of error, manifested principally as;

a) A proportion of the collector current due to the transmission of unanalysed secondaries through the holes.

b) Interference of the equipotentials of the holes with the collector potential.

c) A loss of homogeneity of grid potential.

Another source of extraneous secondaries was the presence of solids in the grid space (e.g. viewing mirror, see Section 3-2). Secondaries reflected from such inclusions can reach the target and produce further unwanted secondaries, so they were reduced to a minimum number and physical size.

Due to the fact that the chamber itself forms the collector, the necessary addition of welded access ports (see Plate 1) and the need to float the chamber at a positive voltage (in the case of AES and CEEL at 90 V) results in two design disadvantages:

a) The distortion of the collector's spherical geometry, introduces errors analogous to those caused by the grid imperfection.

b) The collector was exposed to the atmosphere, and because it was not earthed, stray radio and electromagnetic signals interfered with true signals from the Sb target. Subsequent signal discrimination by electronic filters then attenuates the true signals. If the collector should accidently short to earth, (in the presence of a voltage on the collector), then damage to associated electronic equipment is probable (on one occasion the Brookdeal

oscillator was damaged).

An attempt was made to shield the collector (see Section 3-2.10) using an aluminium cover, but was not very successful.

Since the target was mounted directly on the manipulator, with no insulation, the application of high potentials to record the yield spectra made the actual manipulator live. Surface resonances are critically dependent on the angle of primary incidence, so that as well as stray field pick-up, the apparatus had the dangerous disadvantage of floating at high voltages. Variation of the target, with respect to the incident beam, was subsequently carried out with great care. Again, due to time limitations, the adaptions necessary to remove this hazard were not undertaken.

As was stated earlier, the optimum position of the target is at the centre of the spherical grids, but this proved difficult to ensure. Due to the ratio of length to diameter of the target support rod (600 mm to 4 mm), some eccentricity at the target end was inevitable. This was minimised at 0.3 mm (see Section 4-1), but may still have been large enough to have an appreciable effect on surface structure spectra. Clearly, the shortening of the rod, or the inclusion of a bearing supporting the rod at some distance from the manipulator would further reduce this problem.

With regard to Auger spectra, the characteristics of the electron beam can be considered to have marked effects. Prolonged exposure of one area of the surface can lead to

electron beam effects, such as desorption of impurities from the bulk. However, with the Sb sample, no such effects were noticed. Also, the fact that the focussed beam was surrounded by a faint diffused "corona", (see Section 3-3), may have an effect on the accuracy of Auger spectra. This can be fairly easily reduced by the addition of a narrow tube to the electron gun collimator to reduce the "free space" distance the beam travels before striking the target. One disadvantage of this, however, is that focussing of the beam becomes more difficult due to the decrease in solid angle the beam can traverse.

From the vacuum point of view, although powerful pumps (with respect to the system volume) were used, the pumping speed was slow since the chamber was coupled to the pumps by a relatively narrow and long (40 mm diameter x 700 mm) tube. Approximately seven days were required to obtain a base pressure of 3×10^{-10} Torr., a very sensitive mass spectrometer confirming the absence of any leaks. As before, the design of the system prevented any effective solution to the problem without resorting to a major rebuild.

In spite of the difficulties mentioned, AES and CEEL spectra of Sb were observed for different primary energies, modulation voltages, and primary angles with respect to the surface normal. They were found to be in excellent agreement with the results of recent workers with each CEEL spectrum being composed of a combination of surface and bulk plasmons.

In the low energy region of SEE yield spectra, fine

structures were detected, and are partially attributed to electronic surface resonances. An attempt was made to interpret these features in the mode described by McRae and Caldwell (1978). Due to computational difficulties, it was not possible to filter the spectra before the time of writing, so experimental data has been extracted from unfiltered spectra which inevitably has considerably increased errors. In fact, it was only just practical to effect calculations, and as a consequence, data is displaced on the calculated surface band structure diagram. However, this displacement is only small and general agreement between experiment and theory is reasonably satisfactory considering the above restriction. This gives confidence for further work to be carried out in this area.

The position of Sb atoms in surface resonance studies is critical, with crystal orientation and the presence of foreign atoms having a marked effect on the results. Consequently, special care should be exercised when mounting the sample, particularly when lattice directions with respect to the overall surface (i.e. the "two dimensional surface lattice") are unknown. Crystal orientation can be defined by X-ray diffraction, but some inaccuracy in the result is expected due to the unsatisfactory mounting of the sample, and the fact that the azimuthal angle can not be finely adjusted without in situ LEED optics which were not incorporated in the present system.

Obviously the purity of the surface under examination should be maximised, and can be monitored by AES. However, AES is not sensitive enough to analyse a few foreign atoms or any reconstruction on the surface, both of which can

effect surface resonance spectra. It is therefore preferential to use LEED , in conjunction with AES, to comprehensively monitor the surface allowing the detection of any fault on the surface. Although the grid optics of the system would support LEED with only minor detection modifications, observation of the diffraction pattern would not be practicable in the present system, due to the enclosed and small nature of the chamber. To use LEED, a redesigned chamber would be necessary, which was unfortunately unfeasible in the present work.

Appendix 1

The following procedures are recommended for chemically cleaning materials to be employed in ultra-high vacuum systems, Varian (1962).

TITANIUM

1. Solvent degrease - Tricholoroethylene or equivalent. Three stages, liquid dip, vapor, drain and dry.
2. Hot alkali dip - Approximately two minutes depending on condition.
3. Hot tap water rinse .
4. Hydrofluoric acid pickle - (3.6% by volume of 48% concentrated hydrofluoric acid in distilled water at room temperature).
5. Cold tap water rinse .
6. Cyanide dip - (At room temperature, suggested preparation 17.31 oz. potassium cyanide and 3.47 oz. potassium hydroxide to 1 gal. water).
7. Cold tap water rinse.
8. De-ionized water rinse - (NaCl less than 1 p.p.m.).
9. Methanol rinse - Use electronic grade methanol. Use for titanium only. Change when water content is more than 80% by volume.
10. Warm air dry - In clean, filtered, fume-free air at approximately 65°C.
11. Optional - Air bake at 150° to 400°C. for 30 minutes to 1 hour, depending on the mass of the part.

STAINLESS STEEL

1. Solvent degrease - Trichloroethylene or equivalent. Three stages, liquid dip, vapor, drain and dry.
2. Hot alkali dip - Approximately 2 minutes depending on condition.
3. Hot tap water rinse.
4. Hydrochloric acid dip - (Solution 1:1 HCl (Tech) in water at 70°C.)
5. Cold tap water rinse.
6. Nitric - Hydrofluoric acid dip - 97 volume % conc. HNO_3; 3 volume % conc. HF. Dip until surface gases slightly. Increase rate of attack. Handle with all caution and respect due hydrofluoric acid.
7. Cold tap water rinse - repeat twice.
8. De-ionized water rinse, cold (NaCl less than 1 p.p.m.) - repeat twice.
9. Methanol rinse - Use electronic grade.
10. Warm air dry - In clean, filtered, fume-free air at approximately 65°C.
11. Optional - Air bake at 150° to 400°C. for 30 minutes to 1 hour depending on the mass of the part.

Appendix 2

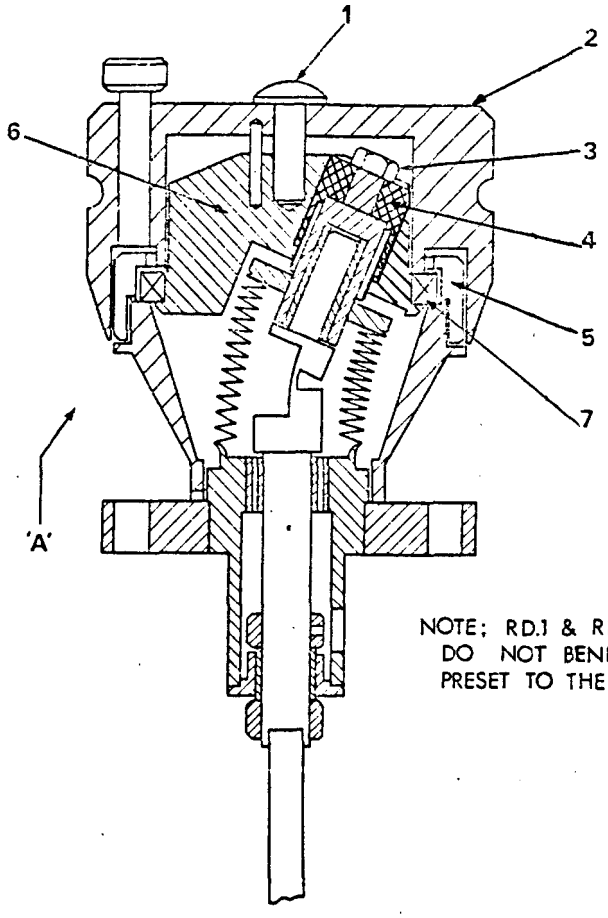

Fig. 7. RD.1 Rotary Motion Drive

COMPONENT REMOVAL PROCEDURE FOR BAKE OUT.

1. Remove Screw, Item 1.
2. Remove Drive Wheel, Item 2.
3. Remove Nut, Item 3 and Thrust washer, Item 4.
4. Unscrew Bearing Retaining Ring, Item 5.
5. Remove Bearing Housing, Item 6, complete with Main Bearing, Item 7, in direction of arrow 'A'

NOTE: If necessary, lubricate Bearings, Item 4 and 7, with V.G. Lubricant.

NOTE; RD.1 & RD.2
DO NOT BEND BELLOWS ASSEMBLY AS THIS IS PRESET TO THE CORRECT ANGLE.

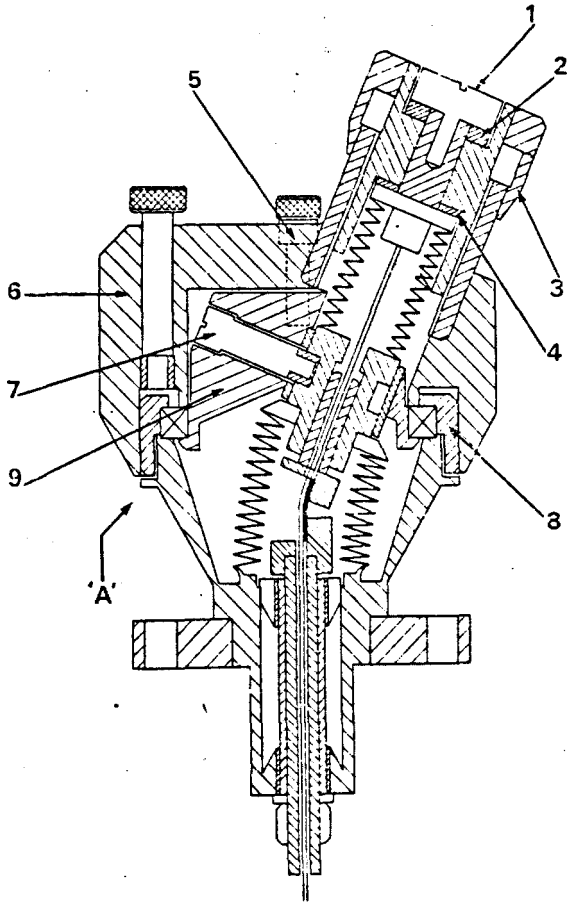

Fig. 8. RD.2 Rotary Motion Drive

COMPONENT REMOVAL PROCEDURE FOR BAKE OUT.

1. Remove top Bellows Retaining Screw, Item 1.
2. Remove Micrometer Screw Assy., Item 3 and Bottom Thrust Washer, Item 4.
3. Remove the two 2BA cap head Screws, Item 5, holding Drive wheel to Bearing Housing.
4. Lift Drive Wheel, Item 6.
5. Remove 2 Pivot Screws, Item 7.
6. Unscrew Bearing Retaining Ring, Item 8.
7. Remove Bearing Housing, Item 9, complete with Main Bearing, in direction of arrow 'A'.

NOTE: If the Drive Unit is of the completely non-magnetic type, the Main Bearing will be a Fluorosint Ring.
If steel Ball Race is fitted in place of Fluorosint Bearing, lubricate with V.G. Lubricant.

Sb Energy levels and electron population in the subshells

Orbital	Coghlan & Clausing (1971)			Bearden & Burr (1967)	
	Population	Z Energy eV	Z+1 Energy eV	Z Energy eV	Z+1 Energy eV
K	2	30491.00	31814.00	30491.2 ±0.3	31813.8 ±0.3
L_1	2	4699.00	4939.00	4698.3 ±0.3	4939.2 ±0.3
L_2	2	4381.00	4612.00	4380.4 ±0.3	4612.0 ±0.3
L_3	4	4132.00	4341.00	4132.2 ±0.3	4341.4 ±0.3
M_1	2	944.00	1006.00	943.7 ±0.3	1006.0 ±0.3
M_2	2	812.00	870.00	811.9 ±0.3	869.7 ±0.3
M_3	4	766.00	819.00	765.6 ±0.3	818.7 ±0.3
M_4	4	537.00	582.00	536.9 ±0.3	582.5 ±0.3
M_5	6	528.00	572.00	527.5 ±0.3	572.1 ±0.3
N_1	2	152.00	168.00	152.0 ±0.3	168.3 ±0.3
N_{23}	6	99.00	110.00	98.4 ±0.5	110.2 ±0.5
N_{45}	10	32.00	40.00	31.4 ±0.3	39.8 ±0.3
O_1	2	7.00	12.00	6.7 ±0.5	11.6 ±0.6
O_{23}	3	2.00	2.00	2.1 ±0.4	2.3 ±0.5

Appendix 3

Appendix 4

SEE Yield Spectra

Spectra recorded under different conditions at variable electron beam currents.

It will be noted that on some sets individual spectra for some angles of beam incidence are missing. This was due to the instrumental malfunctioning at that particular angle only.

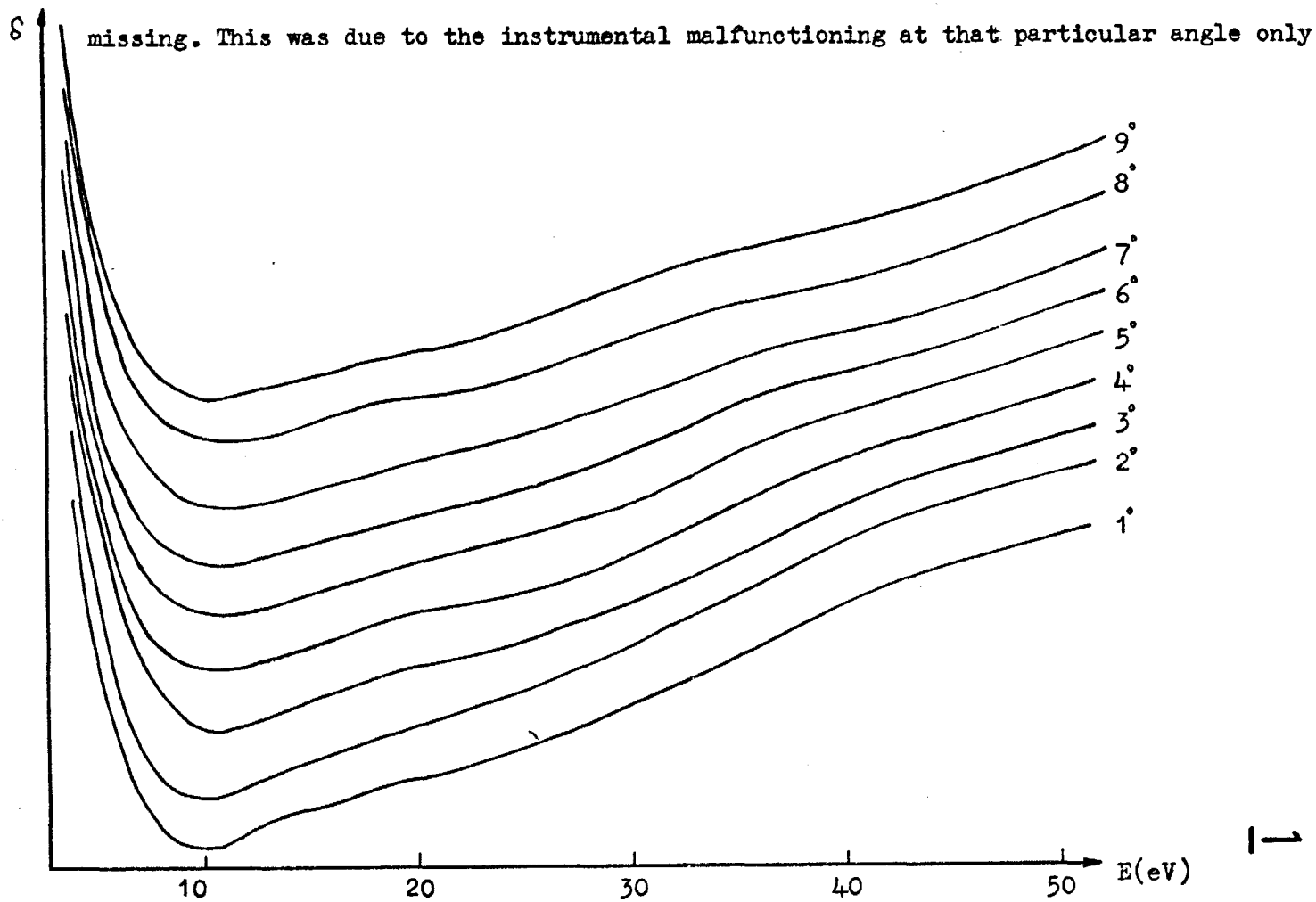

Raw SEE yield electron-reflection data for Sb(100). For notations see Fig. 4-21 caption.

Appendix 5

1 Continued

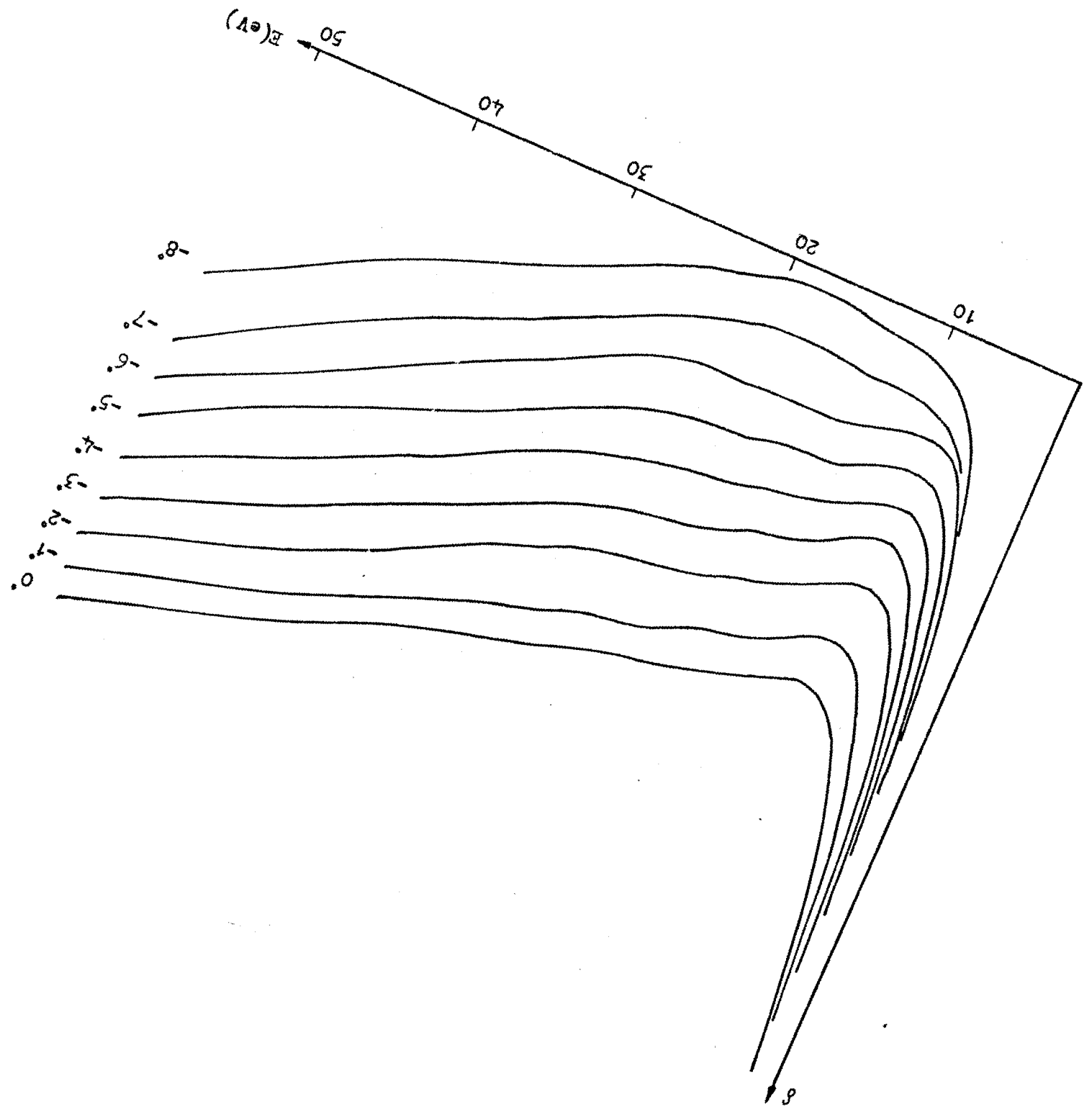

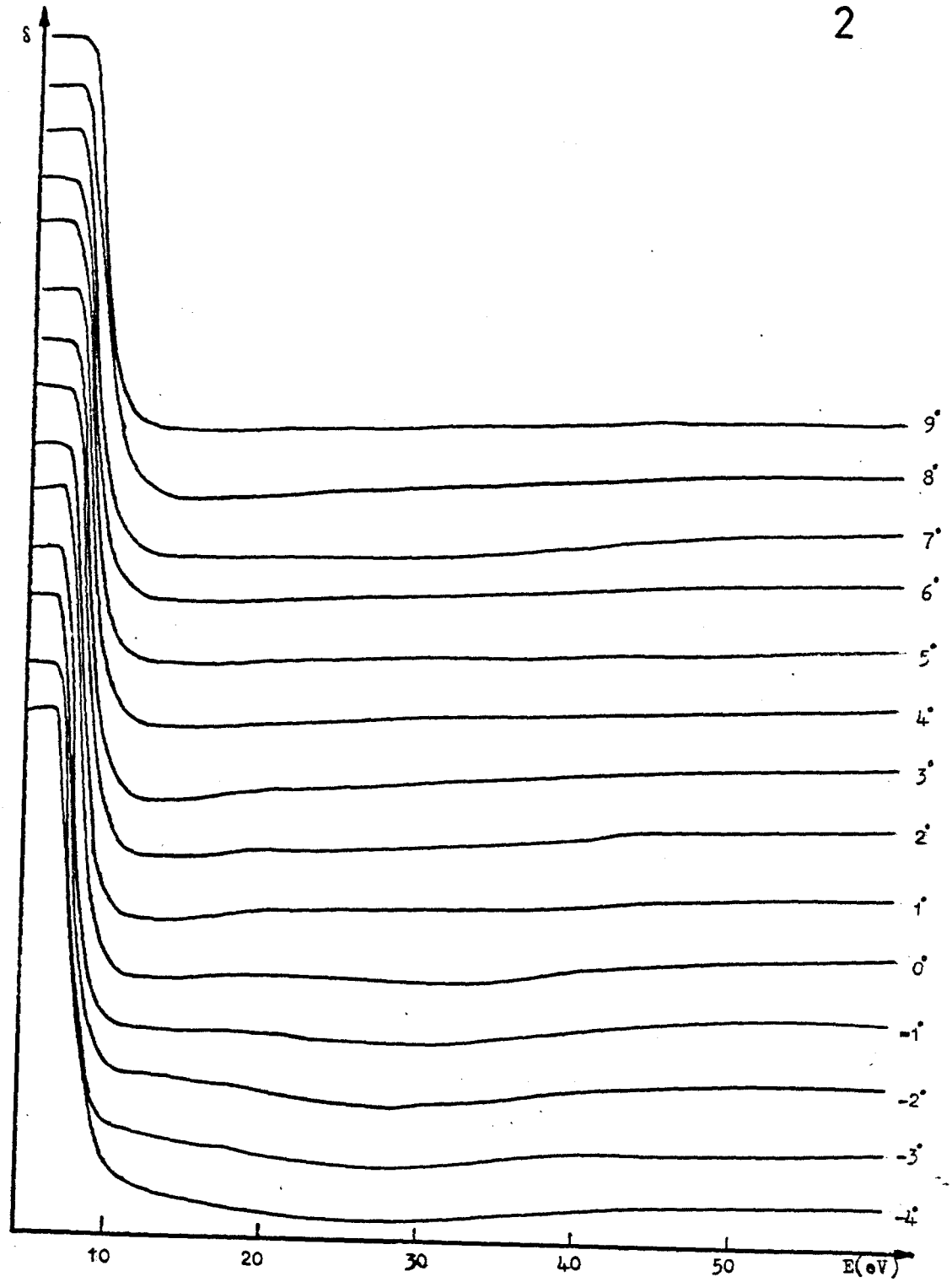
δ
9°
8°
7°
6°
5°
4°
3°
2°
1°
0°
-1°
-2°
-3°
-4°
10
20
30
40
50
E(eV)

2 Continued

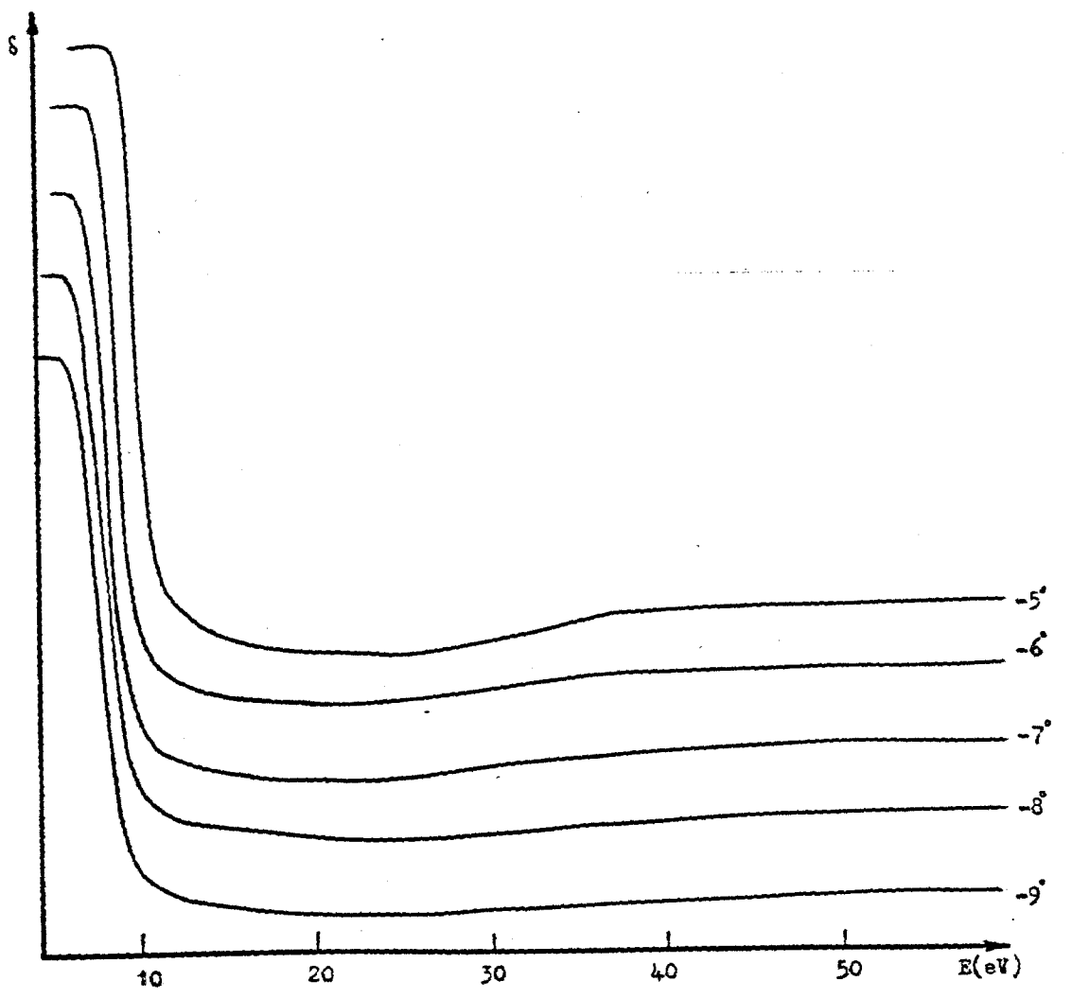

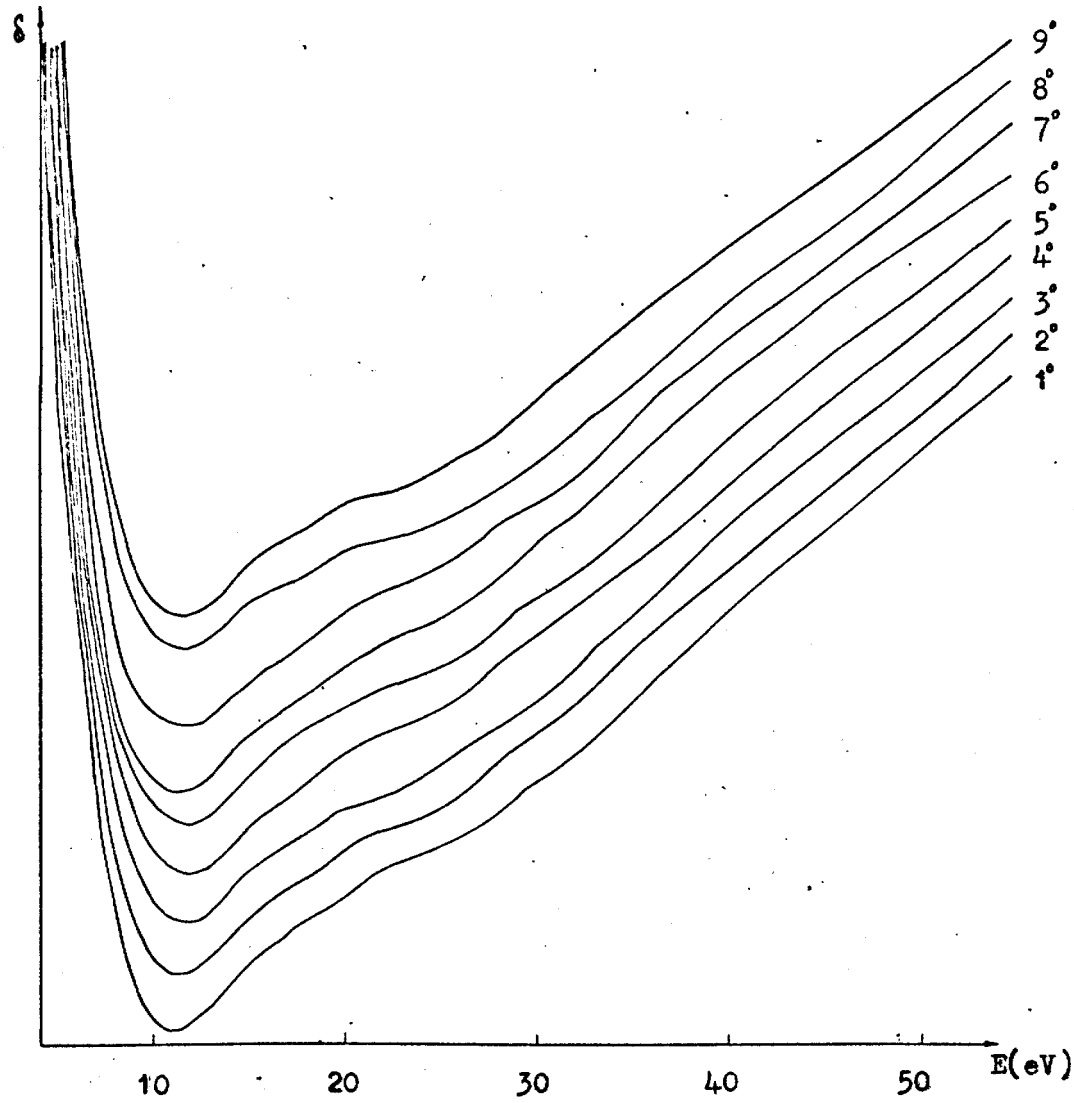
S
9°
8°
7°
6°
5°
4°
3°
2°
1°
10
20
30
40
50
E(eV)

3 Continued

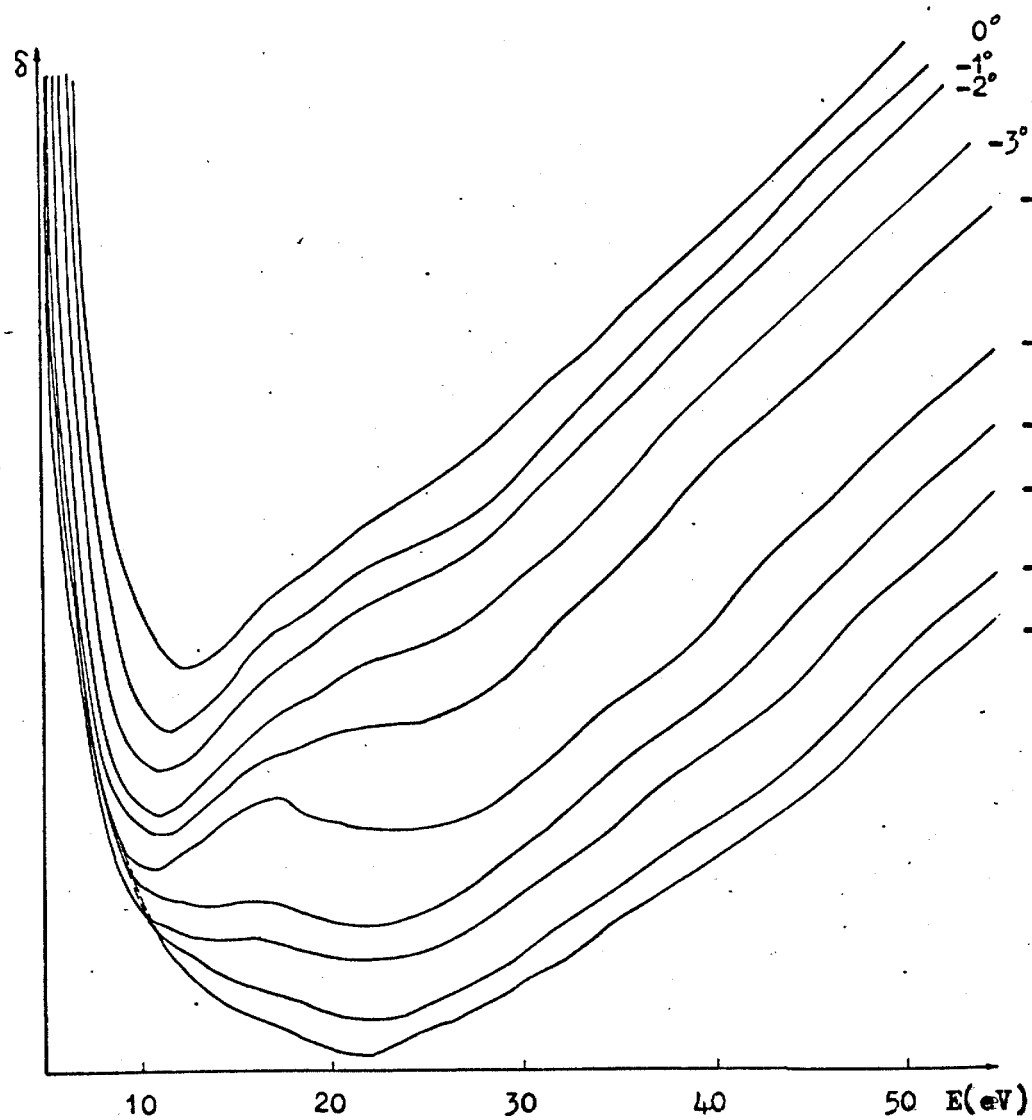

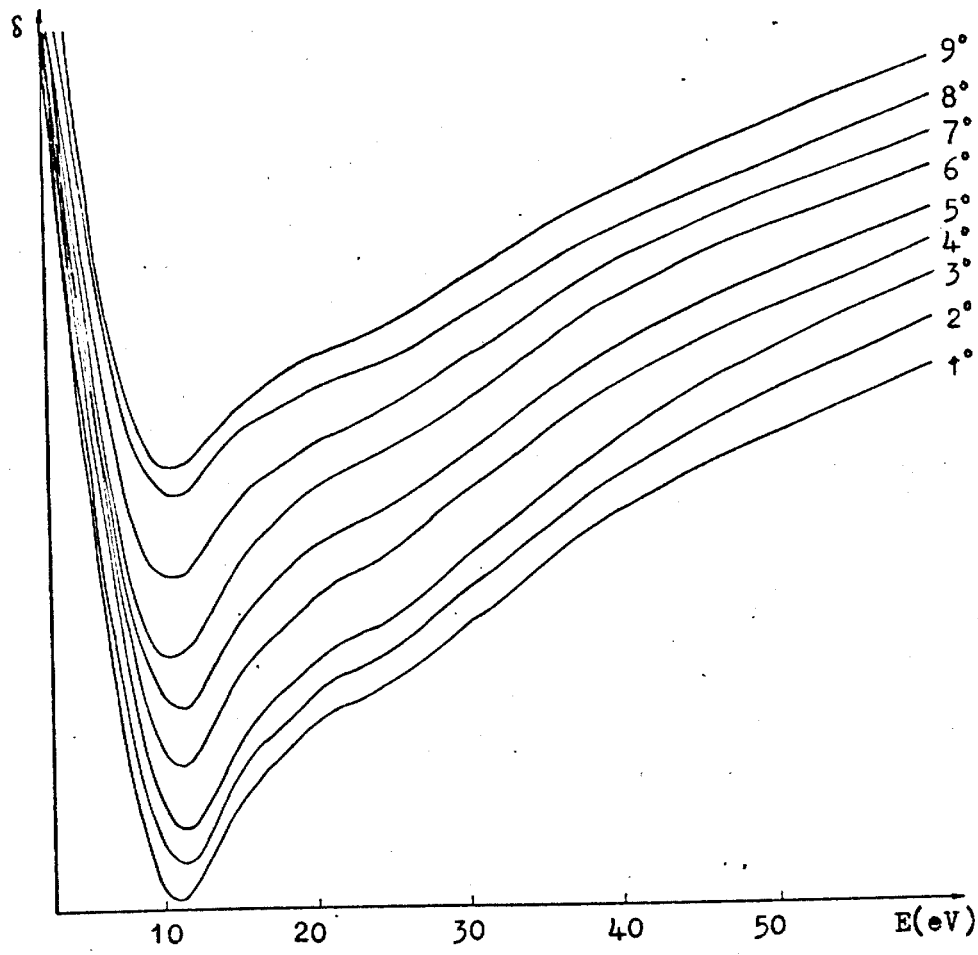
δ
9°
8°
7°
6°
5°
4°
3°
2°
1°
10
20
30
40
50
E(eV)

4 Continued

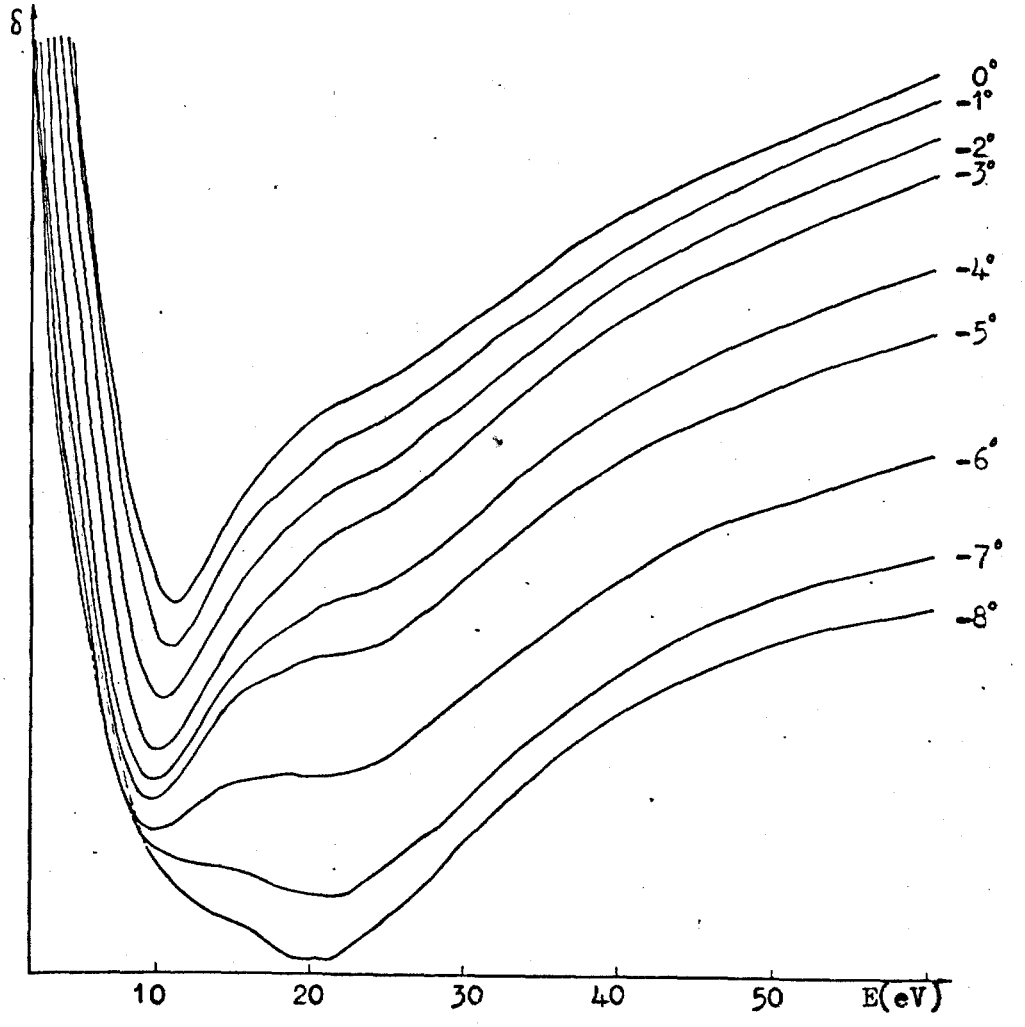

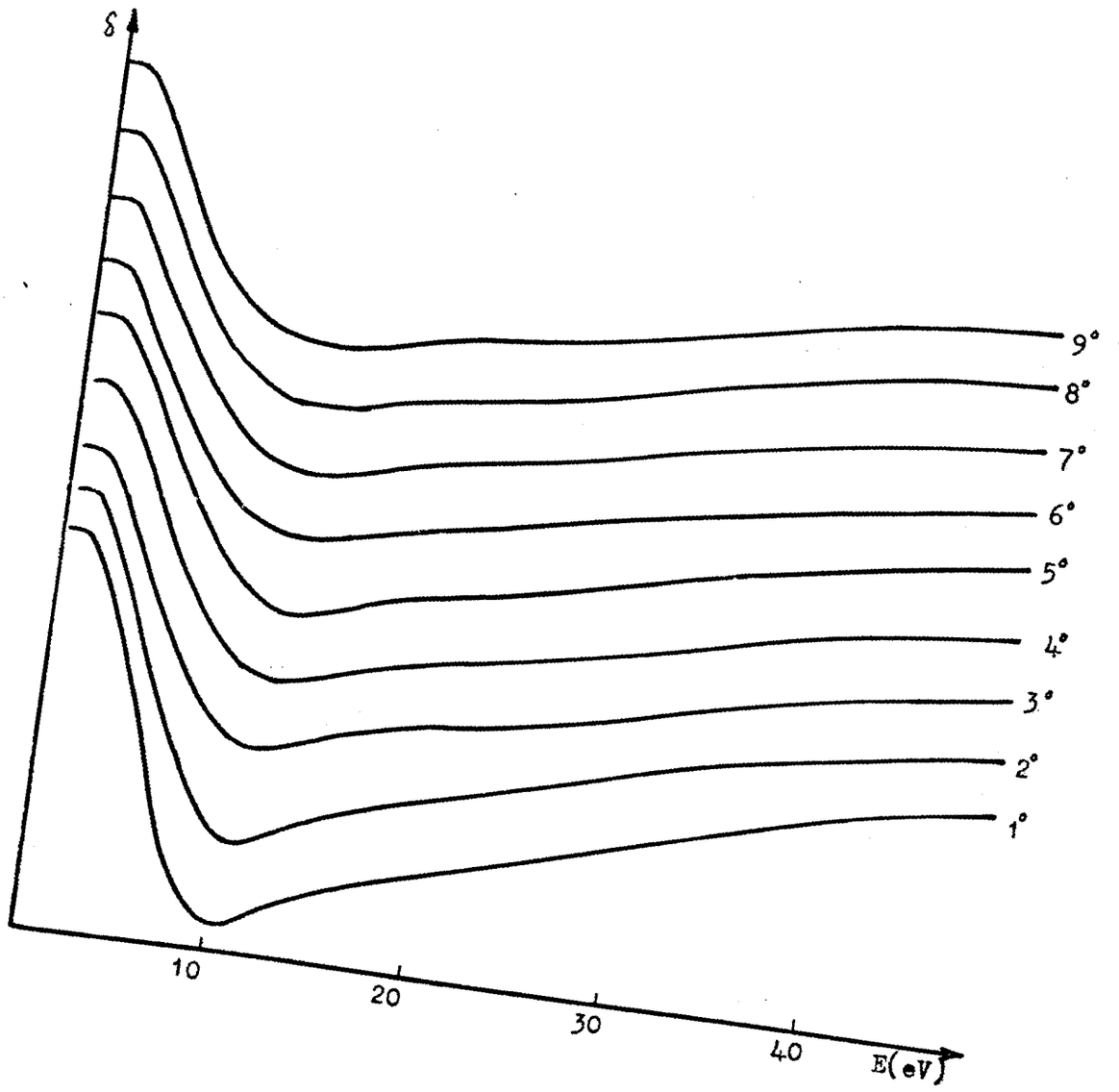
δ
9°
8°
7°
6°
5°
4°
3°
2°
1°
10
20
30
40
E(eV)

5 Continued

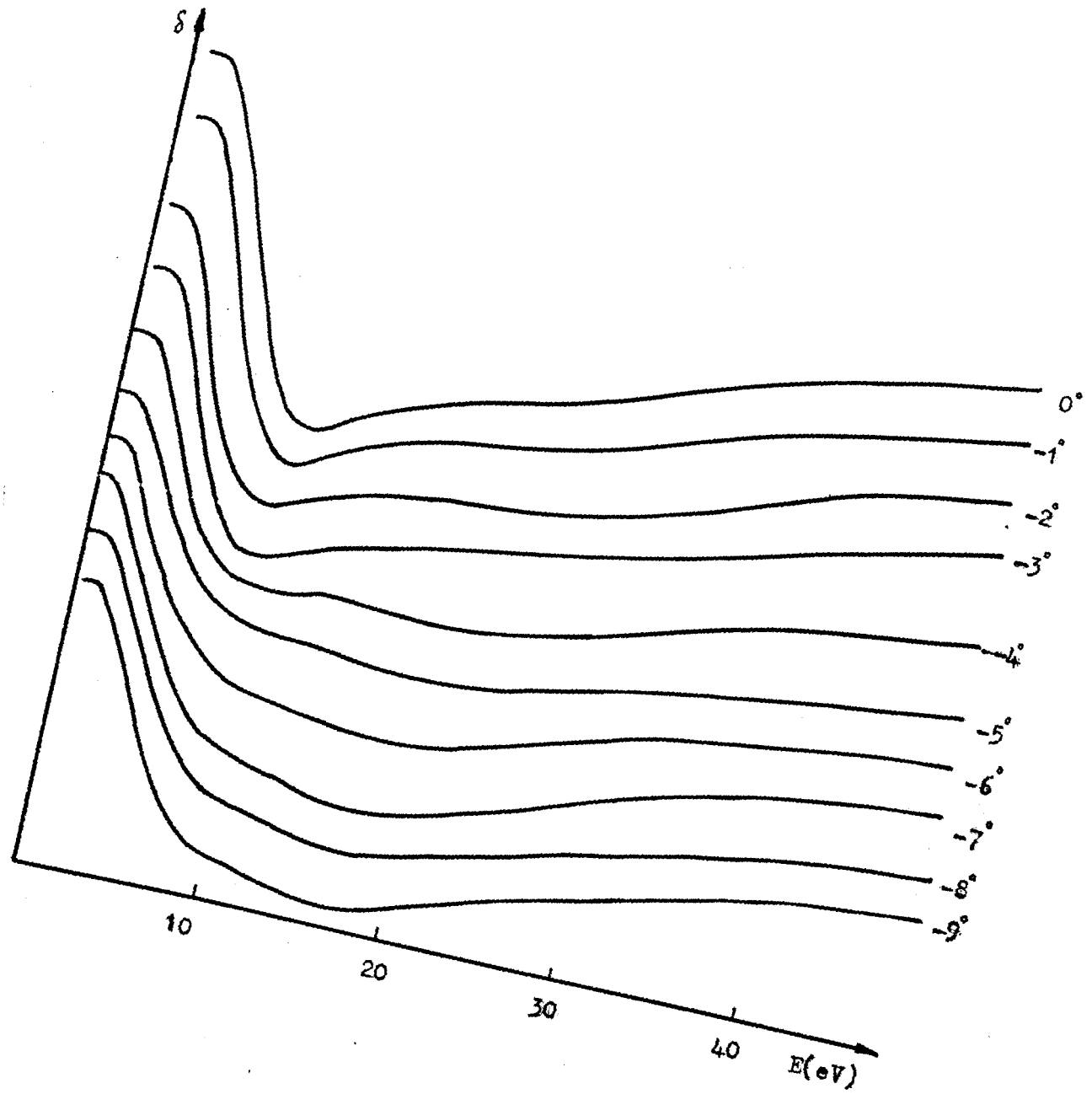

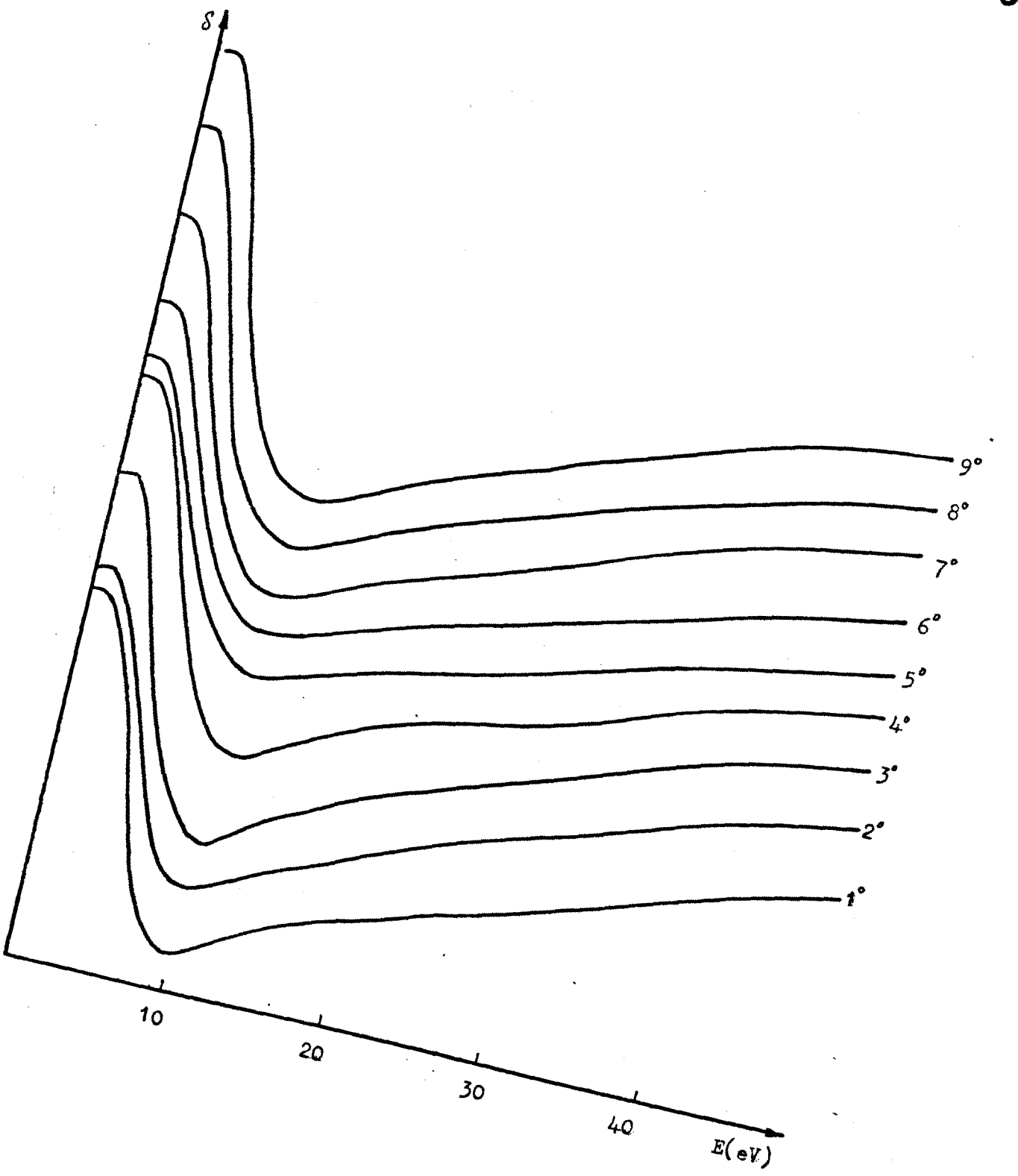
δ
9°
8°
7°
6°
5°
4°
3°
2°
1°
10
20
30
40
E(eV)

6 Continued

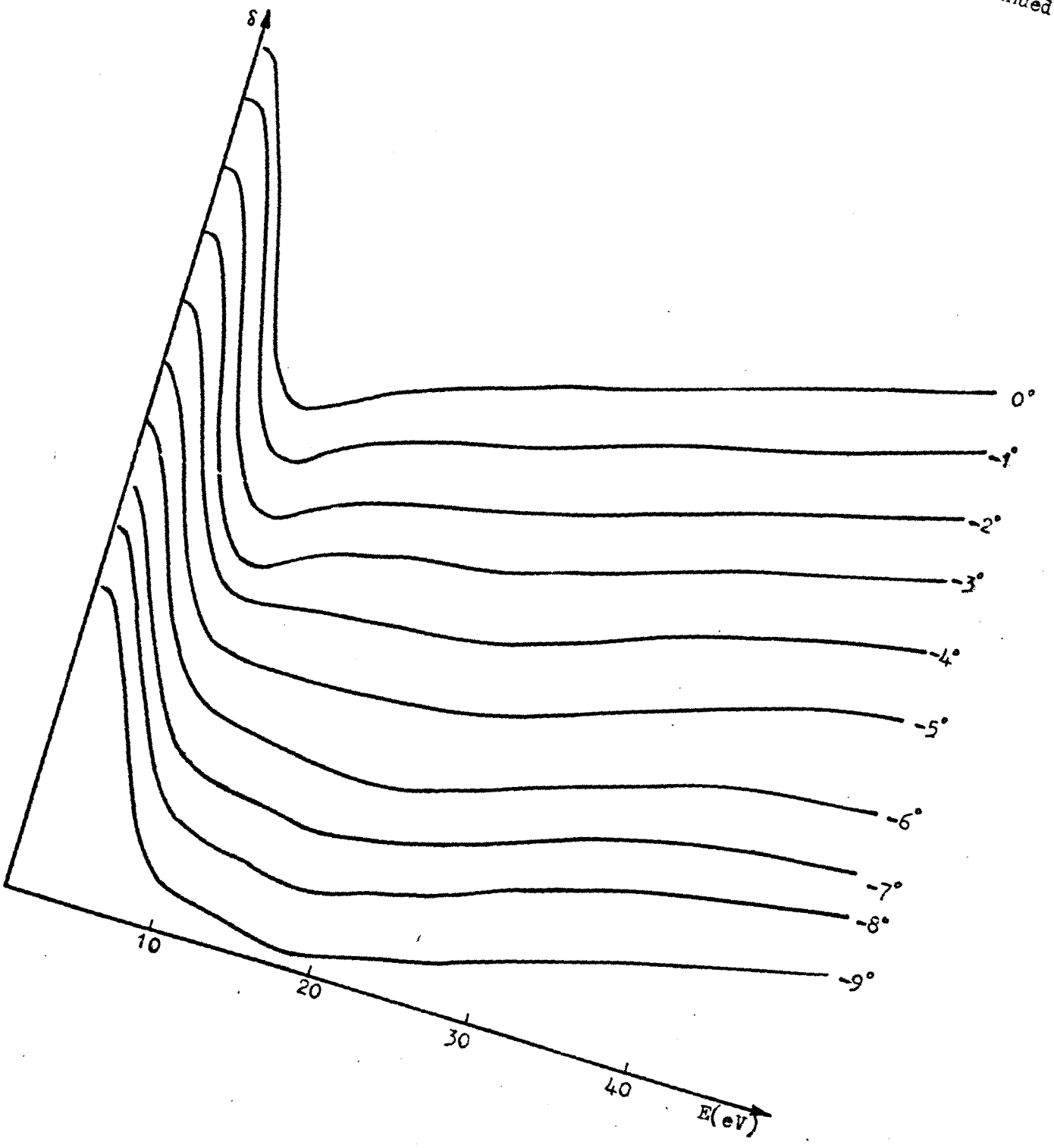

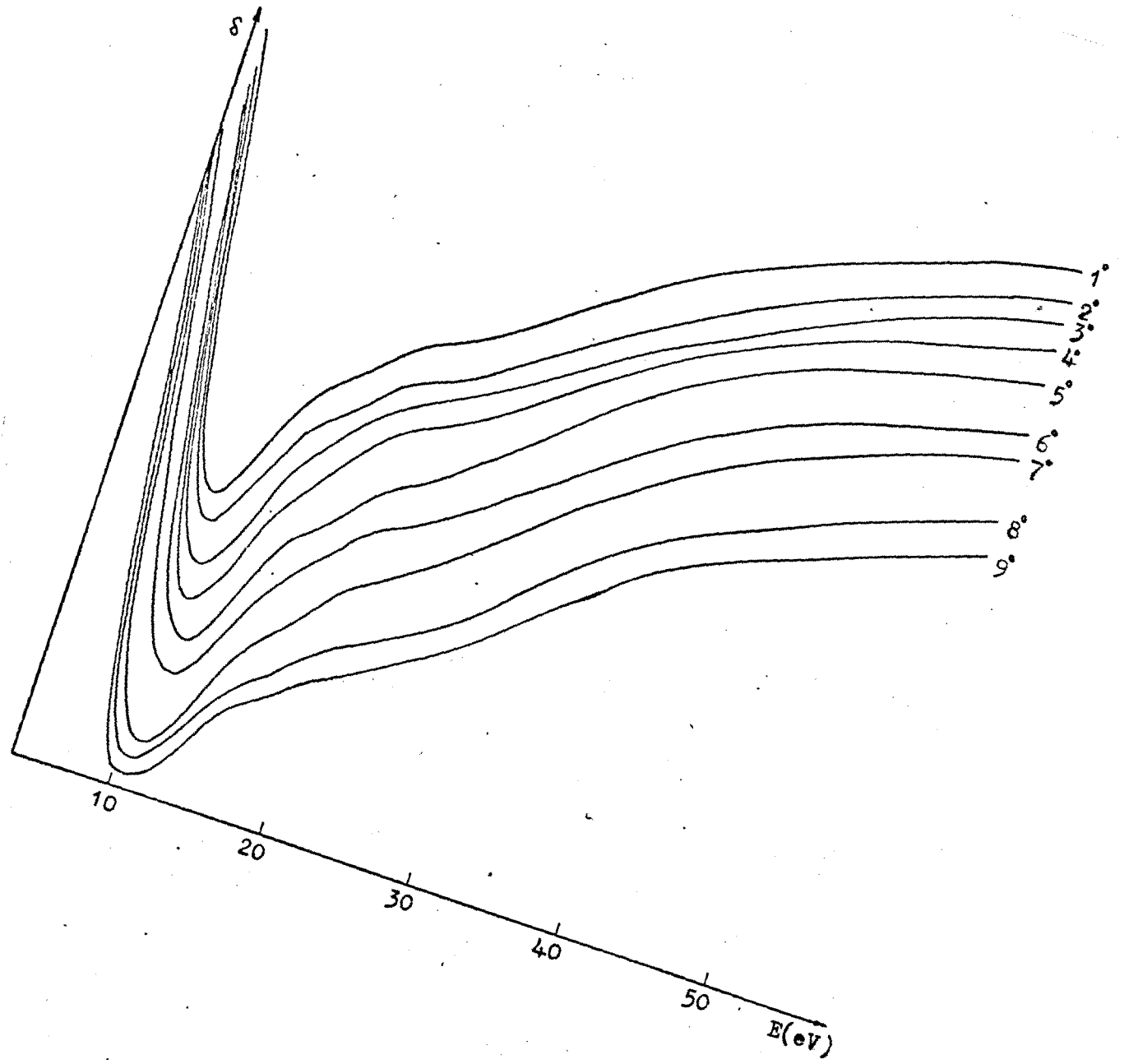
δ
1°
2°
3°
4°
5°
6°
7°
8°
9°
10
20
30
40
50
E(eV)

7 Continued

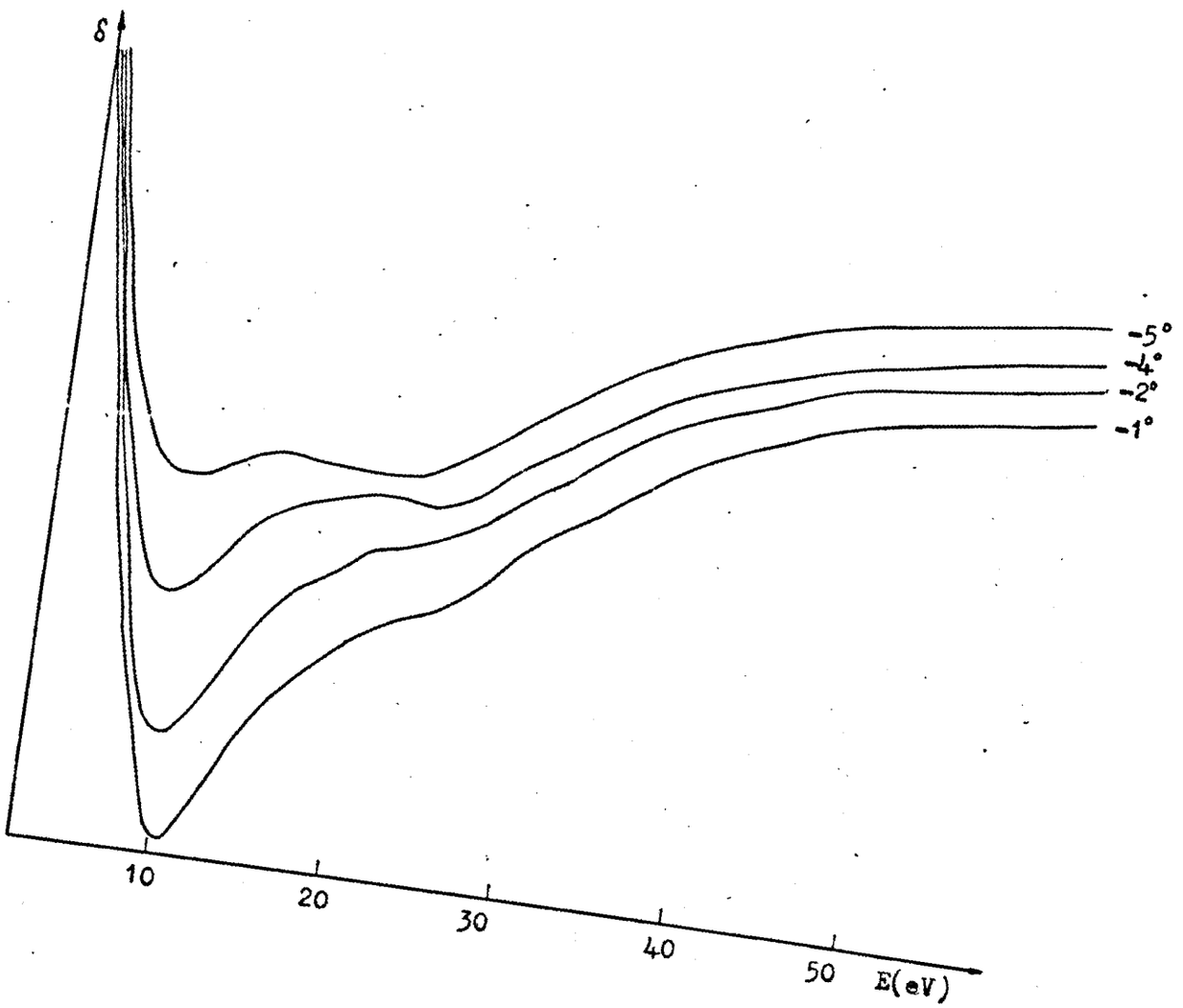

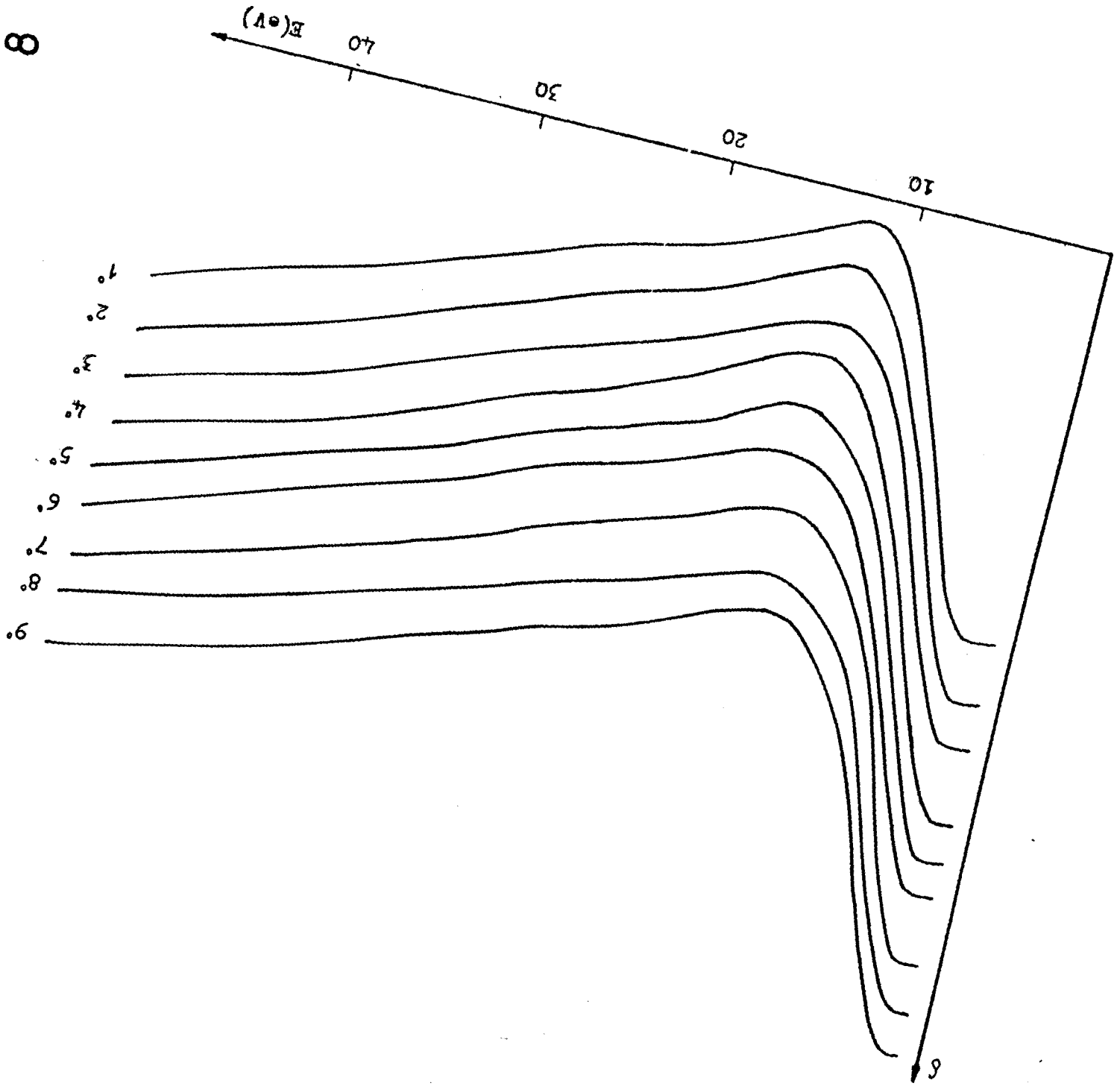
E(eV)
40
30
20
10
1°
2°
3°
4°
5°
6°
7°
8°
9°

8 Continued

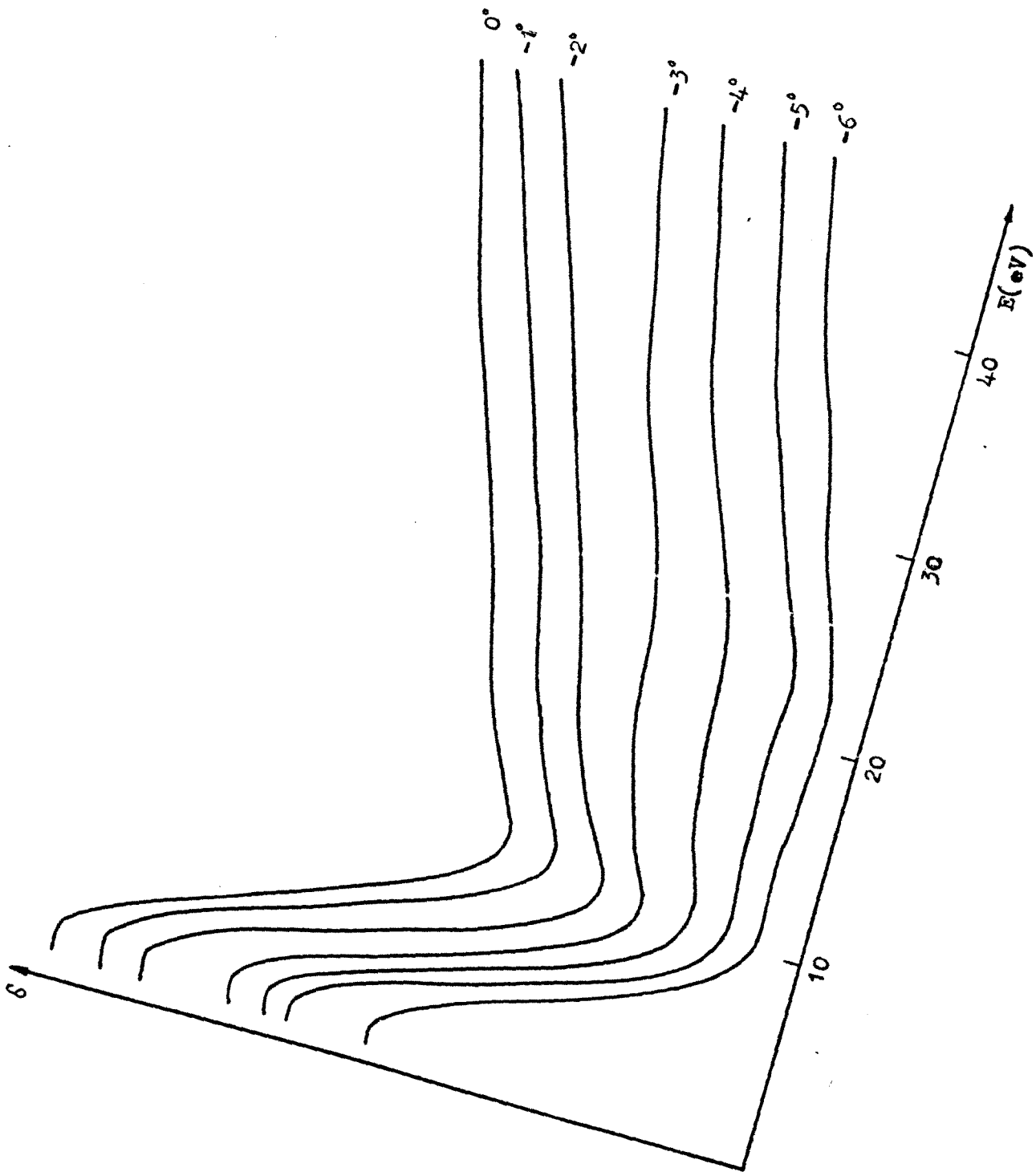

REFERENCES:

AHEARN A.J. (1931), Phys. Rev., 38, 1858

AKSELA S. (1971), Z. Physik, 244, 268

ALFORD N.A., BARRIE A., DRUMMOND I.W. and HERD Q.C. (1979) Surf. & Interface Anal., 1, 36

APPELBAUM J.A. and HAMANN D.R.(1976) Rev. of Mod. Phys., 48, 479

APPELT G. and HACHENBERG O.(1960), Ann. Phys., (7), 6, 67

ASTON F.W. (1919), Phil. Mag., 38, 710

AUGER P. (1925), Compt. Rend, 180, 65

AUSTIN L. and STARKE H. (1902), Ann. Phys., 9, 271

BARODY E.M. (1950), Phys. Rev., 78, 780

BARODY E.M. (1956), Phys. Rev., 101, 1679

BARTNING B. (1972), Opt. Commun., 4, 404

BEARDON J.A. and BURR A.F. (1967), Rev. Mod. Phys., 39, 125

BEILBY G. (1921), Aggregation & Flow of Solids, McMillan, London.

BEST P.E. (1975), Phys. Rev. Letters, 34, 674

BLAUTH E. (1957) Z Physik, 147, 288

BOGNER R.E. and CONSSTANTINDES A.G. (1975), "Introduction to Digital (Filters)", J. Willey

BOHM D. and PINES D. (1953), Phys. Rev., 92, 609

BRONSHTEIN I.M. and DOLININ S.S. (1968), Sov. Phys. Solid St., 9, 2133

BURHOP E.H.S. (1952), "Auger and Other Radiation-less Transitions", University Press, Cambridge, England

BRUINING H. (1954), "Physics and Applications of Secondary Electron Emission",Pergamon Press Ltd., London.

BURNS J. (1960), Phys. Rev., 119, 102

CITRIN P.H. (1975), J. Elec. Spectro. & Relate. Phenom., 5, 273

CHANG C.C. (1974), In, "Characterization of Solid Surface", Eds. Kane & Larrabee, Plenum Press, New York

CHATTARJI D. (1976), "The Theory of Auger Transitions", Academic Press, London

CHELIKOWSKY J.R. and COHEN M.L. (1976), Phys. Rev. B13, 826

CHUNG M.F. and EVERHART T.E. (1977), Phys. Rev., B15, 4699

CHUNG M.F. and JENKINES L.H. (1970), Surf. Sci., 22, 479

CHRISTENSEN N.E. and FEUERBACHER B. (1974), Phy. Rev., B10, 2349

CHRISTENSEN N.E. and WILLIS R.F. (1979) J. Phys. C., 12, 167

COGHLAN W.A. and CLAUSING R.E. (1971),"A Catalogue of Calculated Auger Transition for the Elements", Oak Ridge National Laboratory, Oak Ridge, Tennessee, 37830 U.S.A.

COGHLAN W.A. and CLAUSING R.E. (1972), Surf. Sci., 33, 411
COSSLETT V.E. and THOMAS R.N. (1969), Br. J. Appl. Phys., 15, 1283
COSTER D. and KRONIG R. (1935), Physica, 2, 13
CRC (1979), "Hand Book of Chemistry and Physics", CRC Press Inc, Boca Raton, Florida, Ed. 59, E349

DANIELS J., von FESTENBERG C., RAETHER H., and ZEPPENFELD K. (1970), Springer Tracts in Modern Physics, 54, 77
DEKKER A.J. (1958), "Solid State Physics", McMillan & Co. Ltd., London
DEKKER A.J. (1958a), Solid St. Phys , 6, 251
DIELS K. and JAECKEL R. (1966), "Leybold, Vacuum Hand Book", Pergamon Press Ltd., Oxford.
DIEKE G.H. (1963), "Am. Inst. Phys. Hand b"., New York McGraw-Hill, §7, 14
DIGITAL & EQUIPMENT CO. (1979), "Memories & Peripherals", Publishing System.
DIONISIO J.S. and VIEU C. (1975), J. Elect. Spectro. & Relate. Phenom., 5, 173
DIONNE G.F. (1975), J. Appl. Phys., 46, 3347
DOBRETSOV L.N. and MATSKEVICH T.L. (1957), Sov. Phys. Tech. Phys., 2, 663
DRAWIN H.W. (1961), Z. Physik, 164, 513

EASTMAN D.E., HIMPSEL F.J. and KNAPP J.A. (1978), Phys. Rev. Letters, 40, 1514

FALICOV L.M. and LIN P.J. (1966), Phys. Rev., 141, 562
FEUERBACHER B. and CHRISTENSEN N.E. (1974), Phys. Rev., B10, 2373
FLORIO J.V. and ROBERTSON W.D. (1969), Surf. Sci., 18, 398
FRASER W.A., FLORIO J.V., DELGASS W.N. and ROBERTSON W.D.(1973), Rev. Sci. Instrum., 44, 1490
FREDERIKSE H.P.R. (1963), "Am. Inst. Phys. Hand.", New York, McGraw-Hill, § 9, 158
FRÖHLICH H. (1932), Ann. Physik, 13, 229
FROITZHEIM H. (1977), "Electron Spectroscopy for Surface Analysis" , Springer-Verlag, Berlin

GALLON T. (1972), J. Phys. D., 5, 822
GALLON T. and MATTHEWS J.A.D. (1970), Phys. State. Sol., 41, 343
GAUTHE B. (1959), C.R. Acd. Sic., Paris, 242, 2634
Phys. Rev., 114, 1265
GEHRTS A. (1911), Ann. Phys. Lpz., 36, 995
GEIGER J. (1962), A. Naturforsch, 17a, 696
GEIGER J. and STICKEL W. (1969), Phys. Lett., 28A, 629

GOLD B. and RADER C.M. (1974), "Digital Processing of Signals", McGraw-Hill

GOTO K. and ISHIKAWA K. (1972), J. Appl. Phys., 43, 1559

GOTO K. and ISHIKAWA K. (1973), J. Appl. Phys, 44, 132

GRANT J.T., HAAS T.W., and HOUSTON J.E. (1973), Phys Lett., 45A, 309

GRANT J.T., HAAS T.W., and HOUSTON J.E. (1974), Surf. Sci., 42, 1

HAAS T.W., GRANT J.T. , and DOOLEY G.J. (1970), Phys. Rev. B., 1, 1449

HAAS T.W., SPRINGER R.W., HOOKER M.P. and GRANT J.T. (1974) Phys. Lett., A47, 317

HACHENBERG O. and BRAVER W. (1959), Adv. in Electronic and Electron Phys., 11, 413

HARRIS L.A. (1968), J.Appl. Phys., 39, 1419

HARRIS L.A. (1968a) J.Appl. Phys., 39, 1428

HARRIS P.R. (1972), "Ph.D. Thesis", University of Keele

HARRISON W.A. (1966), "Pseudopotentials in the Theory of Metals" Benjamin, New York

HARROWER G.A. (1956), Phys. Rev., 102, 340

HAYAKAWA K. and MIYAKA S. (1974), J. Appl. Phys. Suppl. 2 Pt.2, 625
Acata. Cryst., A30, 374

HENRICH V.E. (1973), Rev. Sci. Instr., 44, 456

HENRICH V.E. (1975), Sur. Sci., 49, 675

HOLLIDAY J.E. and STERNGLASS E.J. (1959), J. Appl. Phys., 30, 1428

HUCHITAL D.A. and RIGDEN J.D. (1972), In "Electron Spectroscopy", Ed. Shirley, North Holland Publishing Co.

JENKINS L.H. and CHUNG M.F. (1972), Surf. Sci., 33, 159

JOHNSON J.B. (1925), Phys. Rev. (2), 26, 71

JOHNSON J.B. and McKAY K.G. (1954), Phys. Rev., 93, 668

JONA F. (1967), Surf. Sci., 8, 57

JONES R.C. (1959), Pro. IRE, 47, 1481

JONES R.O. (1975), "Surface Physics of Semiconductors and Phosphors", Eds. Scott C.G. and Read C.E., Academic Press, London.

JONES. R.P. (1963), "Ph. D. Thesis", University of Keele

JONKER J.L.H. (1954), Philips Res. Rept., 9, 391

KANAYA K. and KAWAKATSU H. (1972), J. Phys. D., 5, 1727

KANEFF W. (1960), Ann. Physik, (7), 6, 82

KANTER H. (1961a), Phys. Rev., 121, 677

KANTER H. (1961b), Phys. Rev., 121, 681

KAVEI G. (1978), "M.Phil. Thesis", University of Southampton

KITTEL C. (1976), "Introduction to Solid State Physics, 5th Ed.", J. Wiley, London.

KNOX J. (1980), Private Communication, Computer Centre, Keele University
KOBAYASHI K.L.I., SHIRAKI Y., and KATAYAMA Y. (1979), Surf. Sci., 77, 449
KOLLATH R. (1956), "Handbuch der Physik", Ed. Flügge S., Springer, Berlin, 21, 232
KORTOV V.S. and SLESAREV A.I. (1975), Sov. Phys. Solid St., 17, 591
KRANERT W., LEISE K.H., and RAETHER H. (1944), Ann. Physik, 122, 248
KRANERT W. and RAETHER H. (1943), Ann. Physik., 43, 520
KUNZE C. (1960), Ann. Physik., 7, 89

LANDER J.J. (1953), Phys. Rev., 91, 1382
LANGMUIR I. (1924), Frank. Inst. J., 196, 751
LAUZIER J., de BERSUDER L., and HOFFSTEIN V. (1971), Phys. Rev. Lett., 27, 735
LEDER L.B. (1956), Phys. Rev., 103, 1721
LEDER L.B. and MARTON L. (1954), Phys. Rev., 95, 1345
LEDER L.B. and SIMPSON J.A. (1958), Rev. Sci. Instr., 29, 571
LEMONIER J.C., THOMAS J., and ROBIN M. (1973), J. Phys. E., (6), 6, 553
LIN P.J., and PHILLIPS J.C. (1966), Phys. Rev., 147, 469

MARCUS H.L. (1977), J. Met., 29, 20
MARSHALL J.E. (1952), Phys. Rev., 88, 416
MARTON L. (1967), "Methods of Experimental Physics"., Vol 4, Part A, Academic Press
McCLELLAN J.H., PARK T.W., and RABINER L.R.(1973), IEEE Trans., Audio Electroacoust., Au21, 506
McGUIRE E.J. (1972a), J. Phys. Chem. Solids., 33, 577
McGUIRE E.J.. (1972b), Phys. Rev. A, 5, 1052
McRAE E.G. (1971), Surf. Sci., 25, 491
McRAE E.G. (1978), Phys. Rev., B, 17, 907
McRAE E.G. (1979a), J. Vac. Sci. Technol., 16, 654
McRAE E.G. (1979), Rev. Mod. Phys., 51, 541
McRAE E.G., ABERDAM D., BAUDOING R., and GAUTHEIR Y. (1978) Surf. Sci., 78, 518
McRAE E.G. and CALDWELL C.W. (1967), Surf. Sci., 7, 41
McRAE E.G. and CALDWELL C.W. (1976), Surf. Sci., 57, 63
McRAE E.G. and CALDWELL C.W. (1978), Surf. Sci., 74, 285
McRAE E.G. and WHEATLEY G.H. (1972), Surf. Sci., 29, 342
MEDVEDEV V.K. and SMEREKA T.P. (1975), Sov. Phys. Solid State, 16, 1046
MEYER F. and VRAKKING J.J. (1975), Surf. Sci., 47, 50
MICHEL R., GASTALDI J., ALLASIA C, JOURDAN C., and DERRIEN J. (1980), Surf. Sci., 95, 309
MORGULISU N.D. and DJATLOWITZKAJA B.T. (1940), J. Techn. Phys. USSR, 10, 657

MUSKET R.G. and BAUER W. (1972), Appl. Phys. Lett., 20, 455
MUSKET R.G. and FERRANTE J. (1970), J. Vac. Technol, 7, 14

NAMBA Y., MORI T., and SAITO J. (1979), J. Vac. Soc. Jpn., 21, 352
NEAVE J.H., FOXON C.T., and JOCE A.B. (1972), Sur. Sci., 29, 411
NOZIERES P. and PINES D. (1958), Phys. Rev., 109, 1062
NOZIERES P. and PINES D. (1966), "Theory of Quantum Liquids", Benjamin, U.S.A.

ODA O. and RHEAD G.E. (1980), Surf. Sci., 92, 467
ONO S. and KANAYA K. (1979), J. Phys. D., 12, 619

PALMBERG P.W. (1968), Appl. Phys. Lett., 13, 183
PALMBERG P.W. (1972), In, "Electron Spectroscopy", Ed. Shirley D.A., North Holland Publishing Co., Amsterdam.
PALMBERG P.W. (1975), J.Elec. Spectro. & Relate. Phenom., 5, 691
PALMBERG P.W., BOHN G.K., and TRACY J.C. (1969), Appl. Phys. Lett., 15, 254
PALMBERG P.W. and RHODIN T.N. (1968), J. Appl. Phys., 39, 2425
PALMBERG P.W., RIACH G.E., WEBER R.E. and MacDONALD N.C. (1972), "Handbook of Auger Electron Spectroscopy", Physical Electronic Ind., Inc., Edina, Minnesota
PARK R.L. (1975), Phys. Today, AP28, 52
PAYLING R., ROBERTS R.H., O'NEILL M. and RAMSEY J.A. (1979), J. Electron. Spectro & Relat. Phenom., 15, 151
PELED A. and LIN B. (1976), "Digital Signal Processing", J. Wiley, International Ed.
PELLERIN F. and Le GRESSUS C. (1979), Surf. Sci., 87, 203
PINES D. (1956), Rev. Mod. Phys., 28, 184
PINES D. (1960), Physica, 26 Suppl., 103
PINES D. (1964), "Elementary Excitations in Solids", Benjamin, New York.
PINES D. and BOHM D. (1952), Phys. Rev., 85, 338
(1953), Phys. Rev., 92, 609
PLUMMER E.W., GADZUK J.W., and PENN D.R. (1975), Phys. Today, AP28, 63
POTTER R.E. and EISENMAN W.L. (1962), Appl. Optics, 1, 567
POWELL C.J. (1960), Proc. Phys. Soc., 76, 593
POWELL C.J., ROBINS J.L. and SWAN J.B. (1958), Phys. Rev., 110, 657
POWELL C.J. and SWAN J.B. (1959), Phys. Rev., 115, 869
PROPST F. and LÜSCHER (1963), Rev. Sci. Instrum., 34, 574
PRUTTON M. (1975), "Surface Physics", Oxford Univ. Press
PURCELL E.M. (1938), Phys. Rev., 54, 818

RAETHER H. (1965), Springer Tracts Mod. Phys., 38, 84

RAETHER H. (1980), Springer Tracts Mod. Phys., 88, 1

RAIMES St. (1961), "The Wave Mechanics of Electrons In Metals", North Holland Pub. Co.

RASHKOVSKII S.F. (1958), Radio Eng. Electro., 3, 97

RITCHIE R.H. (1957), Phys. Rev., 106, 874

RUDBERG E. (1930), Pro. Roy. Soc. London, A123, 111

RUDBERG E. and SLATER J.C. (1936), Phys. Rev., 50, 150

SEAH M.P. (1979), Surf. and Interface Analy., 1, 91

SERVIER K.D. (1972), "Low Energy Electron Spectrometry", J. Wiley, London

SIMON R.E. and WILLIAMS B.F. (1968), IEEE Trans. Nucl. Sci.,A15, 167

SINGH S. (1976), "Ph.D. Thesis", University of Keele

SMITH J.R., GAY J.G. and ARLINGHAUS F.J. (1980), Phys. Rev., B21, 2201

SMITHELLS C.J. (1955), "Metal Reference Book", Butterworths London.

SOEZIMA Y. (1949), J. Sci. Res. Inst., 44, 63

STAIB P. (1972), Phys. Lett. , A41, 3

STRAUSSER Y.E. and UEBBING J.G. (1970), "Varian Chart of Auger Energies", Varian, England

STREN E.A. and FERRELL R.A. (1960), Phys. Rev., 120, 130

SUEOKA O. (1965), J. Phys. Soc. Japan., 20, 2203

SULEMAN M. (1971), "Ph. D. Thesis", University of Keele

SULEMAN M. and PATTINSON E.B. (1971), J. Phys. F. , 1, L21

SULEMAN M. and PATTINSON E.B. (1980), J. Phys. F., 13, 693

TAYLOR N.J. (1969), Rev. Sci. Instrum., 40, 792

THOMAS G.E. and WEINBERG C. (1979), Rev. Sci. Instrum., 50, 497

THOMAS S. and PATTINSON E.B. (1969), J. Phys. D., 2, 1539

(1970), J. Phys. D., 3, 349

THORNE A.P. (1974), "Spectrophysics", Chapman and Hall, London

THRAP L.N. and SCHEIBNER E.J. (1967), J. Appl. Phys., 38, 3320

TINOFEEW P.W. and LUNKOWA J. (1940), J. Techn. Phys. USSR, 10, 20

TRACY J.C. and BURKSTRAND J.M. (1974), Crit. Rev. Solid State Sci., 4, 381

Van der ZIEL A. (1973), Phys. Rev., 92, 35

VARIAN (1962), "Instruction Manual for (VI-5, VI-6 and VI-8)

WATANABE H. (1954), J. Phys. Soc. Japan, 9, 920

WATANABE H. (1956), J. Phys. Soc. Japan, 11, 112

WEBER R.E. and PERIA W.T. (1967), J. Appl. Phys., 38, 4355

WHETTEN N.R. (1966), Appl. Phys. Lett., 8, 135

WILLIS R.F. and CHRISTENSEN N.E. (1978), Phys. Rev. B, 18, 5140

WILLIS R.F., FEUERBACHER B., and CHRISTENSEN N.E. (1977), Phys. rev. Letters., 38, 1087

WILLIS R.F., FITTON B., and PAINTER G.S. (1974), Phys. Rev. B., 9, 1926

WOOLDRIDGE D.E. (1939), Phys. Rev., 56, 562

WRIGHT B. (1974), "Ph. D. Thesis", University of Keele